IAEA-TECDOC-1334

Intercalibration of in vivo counting systems using an Asian phantom

Results of a co-ordinated research project
1996–1998

INTERNATIONAL ATOMIC ENERGY AGENCY

January 2003

FOREWORD

Radioactive materials are used in many industries, and, whenever unsealed radioactive sources are present, intakes of radionuclides by workers can occur. Adequate radiation protection of workers is an essential requirement for the safe and acceptable use of radiation, radioactive materials and nuclear energy. Guidance on the application of the requirements of the International Basis Safety Standards for Protection against Ionizing Radiation and for the Safety of Radiation Sources (BSS) to occupational protection is given in three interrelated Safety Guides: Occupational Radiation Protection (RS-G-1.1); Assessment of Occupational Exposure due to Intakes of Radionuclides (RS-G-1.2); Assessment of Occupational Exposure due to External Sources of Radiation (RS-G-1.3) published in 1999 and further guidance is given in Safety Reports.

Uranium, thorium and transuranic elements such as plutonium and americium are encountered throughout the nuclear fuel cycle and in industry. Radionuclides of these elements have a significant potential for internal radiation exposures when they are ingested or inhaled. As a result, the dosimetry services responsible for internal dose assessment must be capable of detecting such radionuclides deposited in the body in very low quantities. The detection problem is made more difficult because several of these radionuclides (e.g. $^{238, 239}$Pu, ^{241}Am, and ^{235}U) decay with the emission of low energy photons that are difficult to detect by direct measurement or in vivo methods. A variety of sophisticated detection systems has been developed to address this problem. In addition, complex anthropomorphic phantoms have been fabricated to provide for highly realistic detector calibrations. However, the measurement task remains highly challenging. The detection and calibration resources are costly, and relatively few dosimetry services are equipped to undertake these measurement tasks.

This report describes the development of international programmes conducted by the IAEA involving the use of torso phantoms which facilitated the calibration and comparison of national detection systems. More specifically, it describes the use of the so-called Asian Phantom for intercalibrating in vivo counting systems.

The IAEA acknowledges the contributions of H. Spitz, University of Cincinnati, for the preparation of the radioactively labeled foamed plastic organs used for the intercalibration; D. Hickman, Lawrence Livermore National Laboratory, for his assistance in the distribution and use of the MRIPP software; R. Toohey, Radiation Internal Dose Information Center, for co-ordination of the intercalibration programme; and R.V. Griffith, for the compilation of the final report. The IAEA officer responsible for this publication was S. Na of the Division of Radiation and Waste Safety.

EDITORIAL NOTE

CONTENTS

1. INTRODUCTION

1.1. Background

The International Atomic Energy Agency provides services for Member States to improve their radiation protection programmes. To this end, the IAEA has sponsored a number of co-ordinated research projects (CRPs) designed to develop or improve radiation protection procedures, and to assist Member States in implementing such procedures. The detection of inhaled radionuclides that emit only low energy photons (i.e. energies less than 200 keV) is a problem of particular concern to many Member States. Some of the radionuclides that fall into this category are prominent in the nuclear fuel cycle, particularly isotopes of uranium, plutonium, and americium. These radionuclides are primarily alpha emitters with long physical half-lives and are retained in the body for many years. Consequently the effective dose per unit intake of these radionuclides is rather high. In addition, photons are emitted in only a few percent of the alpha decays, and the low energies of the emitted photons results in severe attenuation by overlying soft tissue. Therefore, detection of inhaled activity by external monitoring in vivo is much more difficult than is the case for inhaled fission or activation products, which typically emit copious numbers of high-energy gamma rays (e.g. ^{137}Cs, ^{60}Co).

In the early 1970s, the IAEA sponsored a CRP: The calibration of burdens of inhaled plutonium by external counting) in which three male volunteers of small, medium, and large body stature, respectively, inhaled an aerosol labeled with ^{51}Cr and ^{103}Pd. The 20 keV X ray from ^{103}Pd were intended to simulate the 17 keV X ray from plutonium, while the 320 keV gamma rays from ^{51}Cr provided a much more easily measurable marker that was used to determine the amount of aerosol deposited in the lung. Once the aerosol quantity had been determined, measurement of the 20 keV X ray was used to determine the counting efficiency for plutonium X ray (after correction for the difference in transmission between the 20 keV X ray and 17 keV X ray family). Following administration of the "mock plutonium" aerosol, the volunteers were counted by in vivo counting facilities in Europe and North America.

The results of this CRP showed that most methods in use at the time for calibration of in vivo monitors for low-energy photons were seriously in error [1]. Partially as a result of this CRP, a realistic torso phantom, specifically designed to calibrate in vivo monitoring systems for inhaled low-energy photon emitters, was developed at the Lawrence Livermore National Laboratory in the United States of America [2], with financial support from the US Department of Energy. The phantom was based on the average body size of US male plutonium workers, and provided overlays of muscle-equivalent, adipose-equivalent, or combined muscle-adipose equivalent material to build up the chest wall thickness of the phantom so as to match that of a individual to be monitored. The IAEA subsequently initiated an intercomparison study in 1980 to validate this phantom, in which eight male volunteers, again covering a range of body builds, inhaled an aerosol labeled with ^{92m}Nb, another form of mock plutonium. This radionuclide emits a gamma ray at 934 keV and X ray at around 16 keV (close to another X ray energy emitted by plutonium isotopes.) As in the previous study, the body content could be assessed accurately by measuring the gamma rays, and then the measured counting efficiency for the X ray could be compared to that predicted by the phantom. In general, the phantom was found to give satisfactory calibration results, with predicted counting efficiencies within 20% of those actually observed [3].

The IAEA purchased two phantoms and sponsored a second CRP: Use of a realistic chest phantom for the calibration of counting facilities for the assessment of plutonium and other actinides deposited in lungs, 1983–1988) in which participating laboratories from eleven Member States were given the opportunity to make measurements with one of the phantoms to obtain primary calibrations for their counting systems, or to compare with existing

calibrations. The participants in this CRP represented Argentina, Australia, Belgium, Brazil, China, Finland, Hungary, India, Japan, Sweden, and Switzerland. The participants were provided with simulated lung sets, livers and primary lymph node sets separately loaded with low levels of ^{239}Pu and ^{241}Am. The United States and United Kingdom participated in the CRP to standardize and intercompare the two phantoms. In addition, both phantoms were measured at the IAEA laboratory at Seibersdorf, Austria, where they are now stored. These phantoms are available for use by qualified laboratories of any Member State.

A number of recommendations for further research were developed as a result of the second CRP. Specifically, many specialists in Asian Member States have felt that, because the phantom is based on the stature of western workers, it is not representative of typically smaller Asian worker populations, and is not appropriate for calibration of counting systems used to assess intakes of workers in these populations. Moreover, several States had also requested calibrations for additional radionuclides, such as uranium and thorium, which were not included in the final results of the CRP on International Calibration of Detector Systems for the Measurement of Low Energy Photon Emitters in Vivo, 1986–1988 [4].

1.2. Overview

Between 1996 and 1998 the IAEA organized and conducted a third CRP on intercomparison of in-vivo counting systems using a reference Asian phantom [5] in address these recommendations. The CRP was conducted to:

- assess differences in counting system calibrations introduced by the use of phantoms having western vs. Asian stature;
- provide the participants access to a phantom for calibration of lung counting systems that would not otherwise be available;
- intercalibrate detector systems, geometries, and methods used by the participants for the assessment of radionuclides in the body;
- provide a forum for the exchange of information among participants involved in in-vivo measurements;
- allow some participants the opportunity to compare the JAERI phantom with other phantoms (e.g. the Livermore torso phantom) and existing calibration methods;
- provide a computational calibration using mathematical techniques (the MRIPP computer programme) for comparison with the phantom measurements;
- provide participants with a version of MRIPP containing each facility's detector/measurement system input files necessary for use with the MRIPP programme.

The participants in the third CRP included representatives of dosimetry services from Australia, Bangladesh, Canada, China, India, Japan, the Republic of Korea, Malaysia, the United Kingdom and the USA, as well as the IAEA laboratory at Seibersdorf. Research Coordination Meetings (RCM) were held in Mumbai, India in December 1996 and in Taiyuan, China in November 1998. The CRP was conducted under a protocol developed during the first RCM.

1.3. Phantom and organs

The phantom used in the intercomparison was developed by the Japan Atomic Energy Research Institute (JAERI) in Tokai-mura, Japan to represent a typical Japanese plutonium worker. The organizers felt that the JAERI phantom is 1) sufficiently different in stature from the Lawrence Livermore phantom, and 2) adequately representative of smaller Asian populations to meet the objectives of the intercomparison. This phantom is now manufactured and sold commercially by Kyoto Kagaku Hyohon Co., Ltd, Kyoto, Japan. It was procured by the IAEA and, like the Livermore phantom, is available for use by dosimetry services in IAEA Member States.

Unlike the second CRP, only radioactively loaded lungs were used for the intercalibration. The lungs provided with the phantom were replaced with lungs fabricated using a polyurethane based lung material substitute [2]. Details of the phantom construction and lung fabrication are provided in the next sections.

The radionuclides used in the third CRP were ^{238}Pu, ^{241}Am, natural uranium, uranium with a 3% ^{235}U enrichment, and natural thorium. ^{238}Pu was selected to replace the ^{239}Pu used in the previous CRP to make the problems of shipping somewhat easier. The X ray emission properties of the two isotopes are very similar and it was felt that the substitution would be appropriate. Natural and enriched uranium was included in large part following the recommendations resulting from the earlier CRP recognizing the nuclear fuel cycle applications. Thorium was included because of the widespread exposure to thorium in industry, particularly in the production of gas lantern mantles. A blank lung set was provided for background measurements.

1.4. Detectors

Two classes of detectors were used by the participants in the CRP — high-resolution germanium detectors or low resolution scintillation detectors. The germanium detectors were used individually or in arrays (Figure 1). The high resolution offers the possibility to distinguish between photons that are very close in energy. This is particularly valuable, for example, for measurement of ^{238}Pu with X ray energies of 13.6, 17.1 and 20.3 keV (Figure 2). Low energy spectra obtained with a germanium detector for the ^{241}Am, natural uranium, 3% enriched uranium and natural thorium sources are shown in Figures 3–6.

The scintillation detectors are either traditional cylindrical sodium iodide crystals, or the phoswich dual detectors that were developed specifically for measuring the X ray from ^{238,239}Pu. For this CRP, the sodium iodide (NaI) detectors ranged from smaller 75 mm thick by 75 mm diameter detectors that have been around for decades to 200 mm diameter by 100 mm thick crystals that are still widely used in the nuclear industry to provide sensitive detection of the gamma rays from fission and activation products.

Conventional NaI detectors can not be used very effectively for measurement of low energy photons (< 50 keV) because of the low energy background that is inherent in thick crystals. This has been a particular problem for in vivo measurement of $^{238, 239}$Pu since it is necessary for radiation protection to detect of the order of one X ray count per minute. This problem led to development of the dual crystal phoswich detector in the early 1970s. In phoswich detectors, a thin crystal (few mm thick) of NaI (Tl) is backed by a thicker CsI(Tl) crystal (Figure 7). The light pulses from the two materials have significantly different shapes, and this difference is used as a basis for detection and suppression of photons that have sufficient energy to interact in both detectors.

1.5. Data and reporting

The decay schemes and radionuclide photon emission tables for the radionuclides are reported in detail in Ref. [6]. The major photons used as a basis for the measurements are summarized in Table I. The participants were provided with EXCEL spreadsheets on diskette and hardcopy for each lung set and each photon energy, 13 in all. The spreadsheet format was established during the first RCM. Using EXCEL, the spreadsheets contained data necessary for automatic calculation of counting sensitivities. Participants simply entered the detector or detection system identification, surface area, lower and upper energy limits used for each photon energy, count date, count time, total peak counts, and background. EXCEL made the necessary calculations including source decay corrections. If a participant did not have access to EXCEL, the sheets were submitted in hard copy and the data transcribed by the organizers.

TABLE I. PHOTON ENERGIES USED FOR CRP MEASUREMENTS

Radionuclide	^{238}Pu	^{241}Am	Natural Uranium	Uranium with 3% ^{235}U Enrichment	Natural Thorium
Photon Energy	17.1 keV X ray 20.3 keV X ray 43.5 keV	59.5 keV	63.3 keV (^{234}Th) 185.7 keV (^{235}U)	63.3 keV (^{234}Th) 143.8 keV (^{235}U) 185.7 keV (^{235}U)	209 keV (^{228}Ac) 238 keV (^{212}Pb) 911 keV (^{228}Ac) 2614 keV (^{208}Tl)

Participants were not required to submit results for all lung sets and photon energies. This determination was made individually based on the capabilities of their systems, and operational need to measure the various radionuclides. Some, for example, have no occasion to measure plutonium. The resolution of the counting system was very important in determining the photon energies to be measured. Those with scintillation based systems tended to avoid measurement of the ^{238}Pu X ray, relying on the 43.5 keV photon instead.

1.6. MRIPP

It has been noted that calibration of in-vivo measurement systems for low energy photon emitters presents a particular challenge because of uncertainties related to accurate assessment of the transmission of photons through overlying tissue, and availability of complex phantoms, and well calibrated sources and solutions of radioactive material. The US Department of Energy has funded development of computer software designed to provide the user the ability to conduct computational calibrations that require only point source measurements to establish the detection efficiency of photons emitters distributed in a wide range of body organs and tissues. One objective of the CRP was to evaluate the use of the Magnetic Resonance Image Photon Phantom (MRIPP) for calibration of participants' systems. The software was made available to most participants through the Radiation Shielding Information Center (RSIC) in the USA.

Fig. 1. *Germanium detector array for lung counting (courtesy Australian Radiation Protection and Nuclear Safety Agency).*
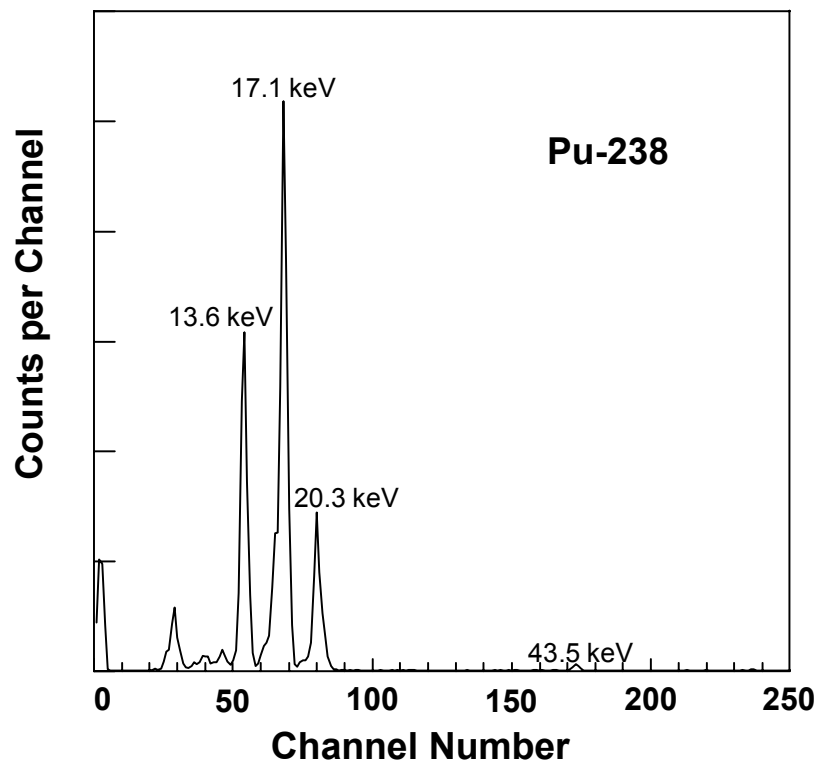
Fig. 2. Germanium detector spectrum of ^{238}Pu.
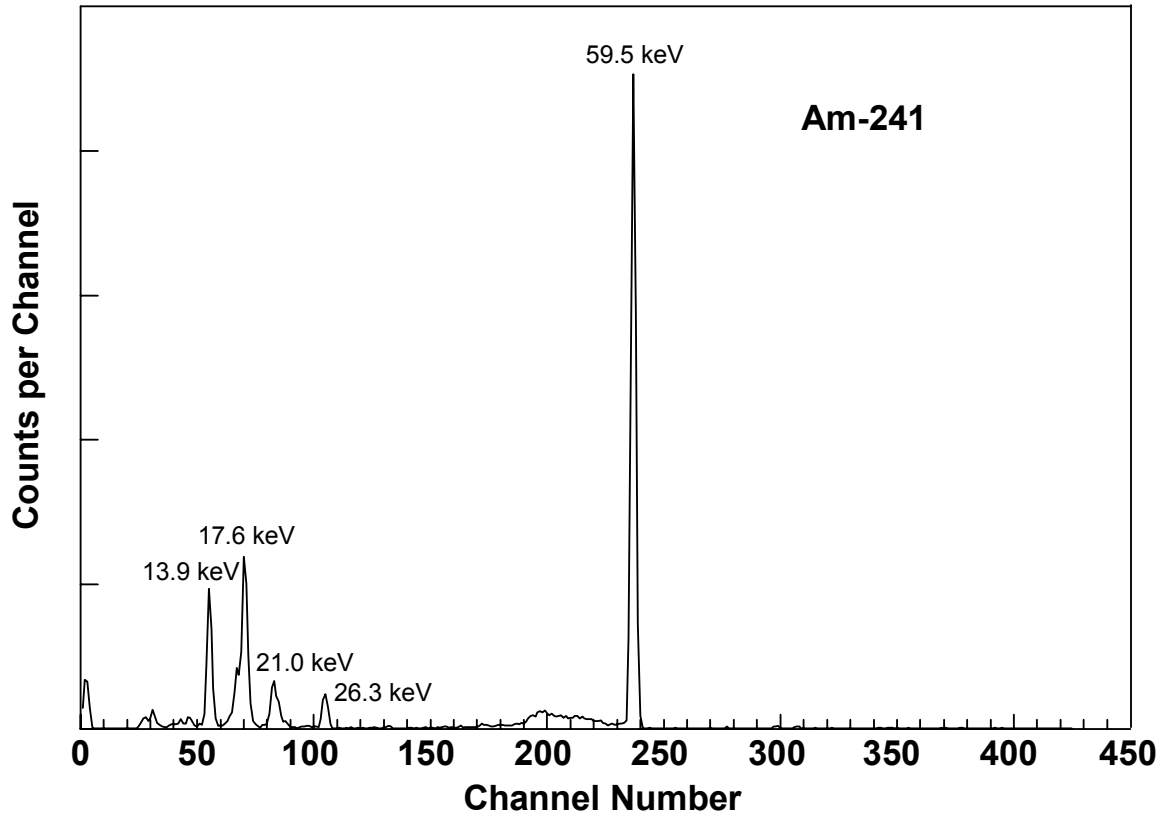
Fig. 3. Germanium detector spectrum of ^{241}Am.
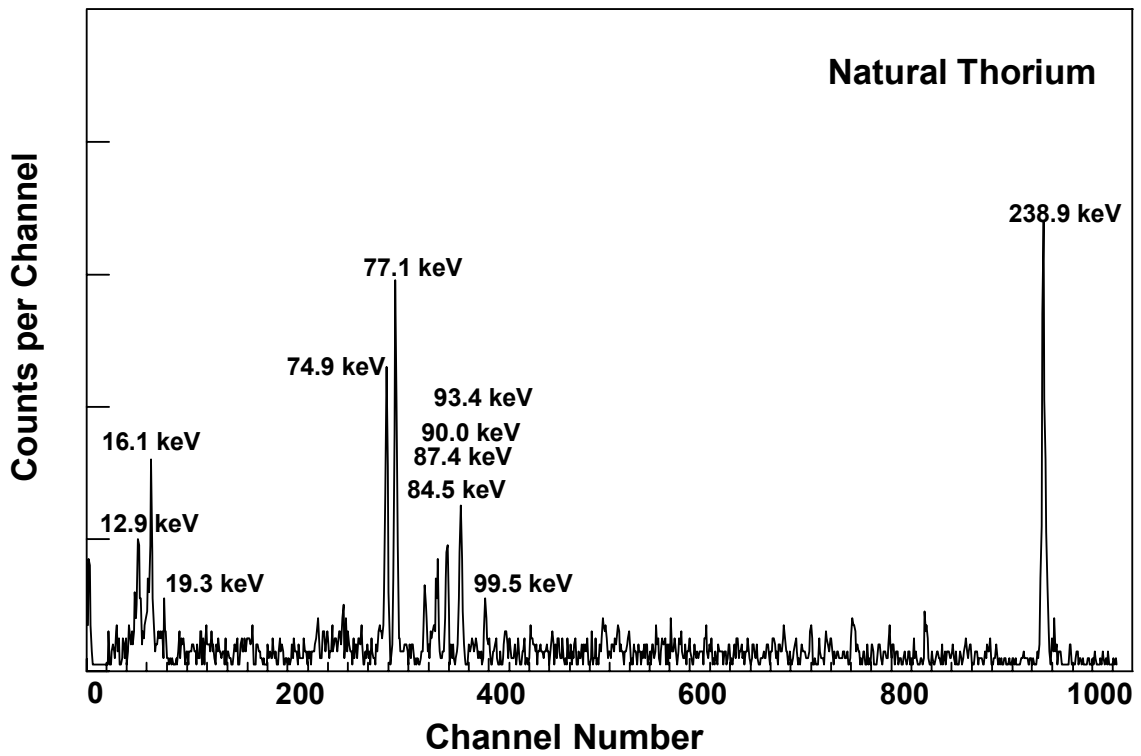
Fig. 4. Germanium detector spectrum of natural thorium.
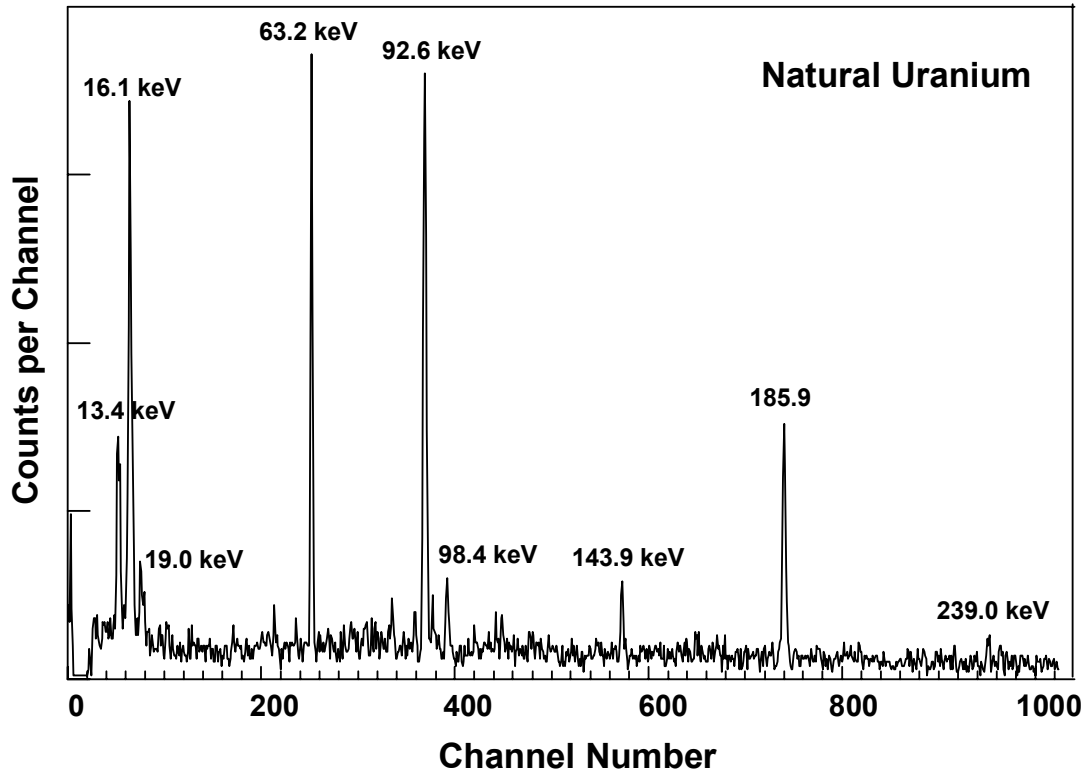
Fig. 5. Germanium detector spectrum of natural uranium.
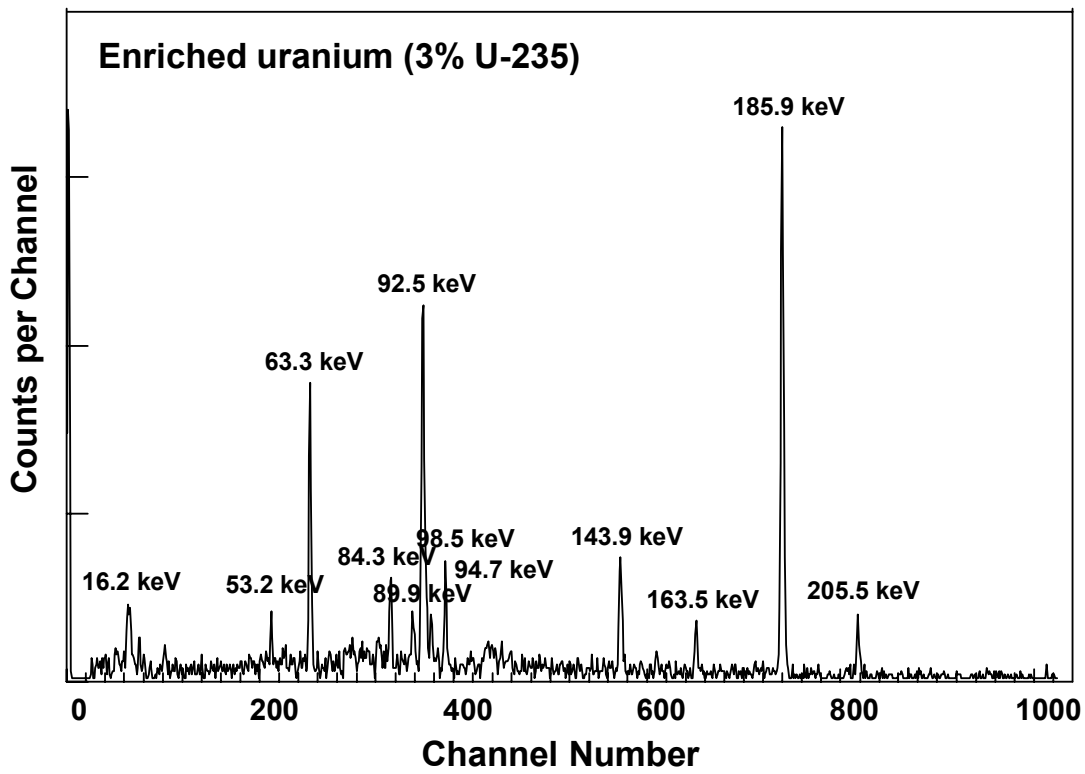
Fig. 6. Germanium detector spectrum of uranium with 3% ^{235}U enrichment.
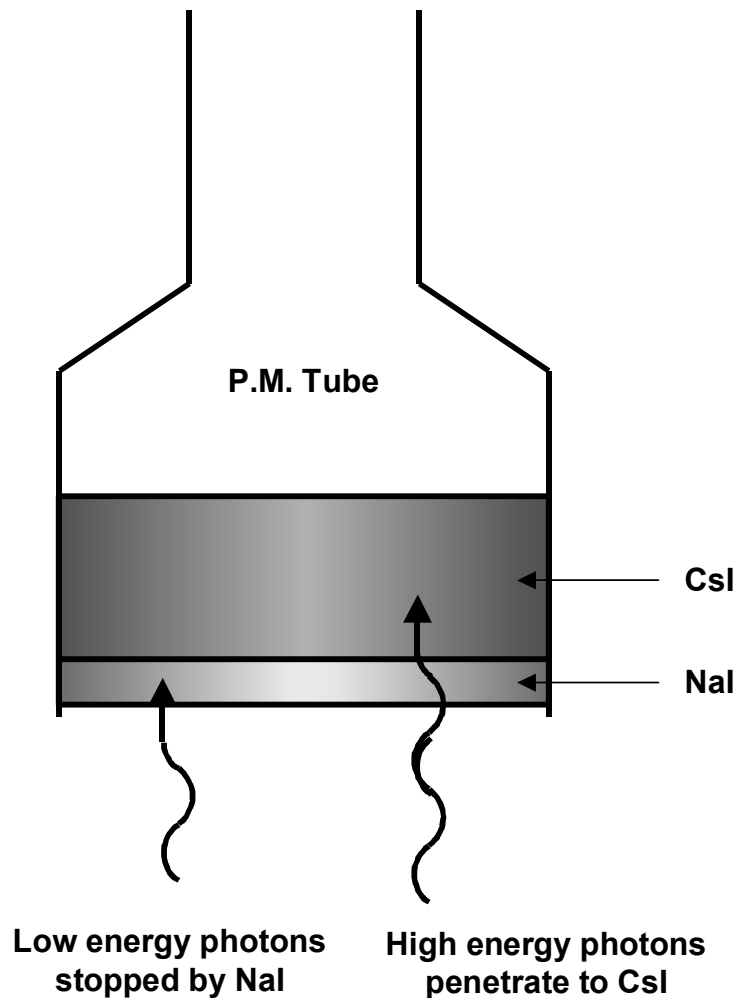
Fig. 7. Cross section diagram of dual crystal (Phoswich) detector.

2. JAPAN ATOMIC ENERGY RESEARCH INSTITUTE PHANTOM

2.1. Summary

The Japan Atomic Energy Research Institute (JAERI) designed a torso phantom for calibration of lung counters [5]. The parameters of the phantom are based on the characteristics of male workers in Japanese plutonium processing facilities. A family of tissue substitutes based on polyurethane and epoxy (for bone substitute) was developed to simulate major body tissues, including lung, for use in the phantom. Tests were performed by JAERI to validate the phantom and tissue substitutes. The phantom is commercially available. The phantom used in this CRP was purchased by the IAEA for intercalibration purposes. Although segmented foamed lungs are provided with the phantom, special polyurethane based foamed lungs, labeled with radioactive material, were fabricated for this CRP.

2.2. Tissue substitutes

2.2.1. Formulation

Tissue substitutes must have the same photon attenuation properties with those of human tissues being simulated. A tissue substitute is general formulated using a base material,

which is an organic compound having elemental composition similar to that of human tissue, and an additive, which is an inorganic compound with higher atomic number, added to the base material to achieve the proper tissue simulation for photon transmission purposes. The amount of additive used depends on the tissue to be simulated (i.e. lung, adipose, muscle, bone). The International Commission on Radiation Units and Measurements (ICRU) [7] has prepared an extensive compilation of the radiation transmission properties of tissues and tissue substitutes.

The researchers at JAERI evaluated the application of a number of possible base materials such as polyethylene, epoxy, polystyrene, Lucite, polyester, phenol resin, polyurethane and cork as base materials for tissue substitutes. The results showed that polyurethane for soft tissue substitutes and epoxy resin for bone substitute are better suited as base materials than the others for the following reasons:

1. It is very easy to vary the elemental composition of the tissue substitute, by mixing various concentrations of additive into the base materials.
2. Polyurethane and epoxy resin are very easy to form into irregular shapes, and its products are not easily deformed, cracked and broken by a mechanical shock.
3. Foamed polyurethane, which has a density of 0.24–0.31 $g \cdot cm^{-1}$, can be used as a lung simulant.
4. Epoxy resin is better suited for a base material of bone substitute, because of its hardness and higher density.

Polyurethane consists basically of two liquid components, part A (polyisocyanate) and part B (polyol). It has the additional advantage that it foams very easily. Epoxy resin consists of a main component and hardener. Table II describes physical data of the base materials. The SZ-50 and EZ-100 are base materials for soft tissue and bone substitutes. The foamed lungs were prepared separately, and their characteristics are described in the next section.

Ester of phosphoric acid (tris chloroethyl phosphate, $(C_2H_4C_{10})_3P0$) was selected as an additive, because this compound is liquid and has relatively lower density (1.43 $g \cdot cm^{-1}$) than calcium carbonate ($CaCO_3$), which has been used in other tissue substitutes. Moreover, it mixes uniformly with the components of polyurethane. Calcium carbonate was used as an additive to the epoxy resin, because of its higher density (2.73 $g \cdot cm^{-3}$). Table III summarizes the tissue substitutes used in the JAERI phantom.

TABLE II. CHARACTERISTICS OF BASE MATERIALS SELECTED FOR TISSUE SUBSTITUTES

		Polyurethane	Epoxy resin
		SZ-50	EZ-100
Density (g cm^{-1})		1.062	1.162
Elemental composition	H	8.49	7.74
weight%			
	C	72.26	71.99
	N	4.49	1.79
	0	14.76	18.49

* Average of measured values.

TABLE III. TISSUE SUBSTITUTES USED IN THE JAERI PHANTOM

Substitutes	SZ-208	SZ-207	SZ-220	SZ-160	EZ-129
Corresponding human tissue	Muscle	Total soft tissue	Muscle + 10% adipose	Cartilage	Bone
Base material	SZ-50	SZ-50	SZ-50	SZ-50U[a]	EZ-100
Amounts of additive (w%)	8.48	6.22	7.35	9.00	29.4
Density (g·cm^{-1})[b]	1.075	1.067	1.069	1.117	1.623

[a] SZ-50U is a hardness type of SZ-50 with a density of 1.074 g cm^{-3}
[b] Average of measured values.

2.2.2. Calculated linear attenuation coefficients

The mass and linear attenuation coefficients for photoelectric interactions and Compton scattering were calculated in the energy range of 8 keV to 1 MeV. The calculations used McMaster's X ray Cross Section Tables [8] and Table 108 in ICRP Publication 23 [9]. Table IV shows the calculated results for the substitutes, corresponding human tissue and water in the energy range of Pu LX ray. For comparison, the coefficients for Griffith muscle (polyurethane + 4.3% $CaCO_3$) [7] and Rando muscle are listed in this table. The accuracy of the calculated coefficients depends principally on the uncertainty in the values of the cross section of elements, inaccuracy of the elemental compositions in the organs and tissues of reference man and the interpolation error.

2.3. Phantom construction and evaluation

2.3.1. Phantom construction

A realistic torso phantom containing an artificial rib cage and four removable simulated organs (lungs, heart, liver and kidneys) has been constructed with the tissue substitutes, and is terminated just above the femoral region. Figure 8 shows the completed torso phantom with chest plate in place, and Figure 9 shows the phantom chest with the torso cover removed to show internal organs. The Table V describes the dimensions of the phantom and simulated model organs. The body size was based on solid plaster cast made from a person who was close to average size of Japanese adult males. The sizes of organs and rib cage were determined from the data for reference Japanese man, X ray film and anatomical charts. Table VI summarizes the substitutes used in each part of the phantom. As noted previously, special solid foamed polyurethane lungs were prepared for this CRP to replace the sectioned lungs originally provided with the phantom (Figure 10).

Chest plates are used to correct the range of chest wall thicknesses, adipose/muscle ratios, and the resulting photon attenuation seen in the chest walls of adult males (Figure 11). The phantom core with no chest plates has a thickness of 15 mm. Two sets of chest plates have been provided with thicknesses of 8 mm and 15 mm. The total chest wall thickness of 2.3 cm using the 8 mm plates was based on ultrasonic measurements of 70 Japanese male subjects. Table VII presents the elemental composition of the base material, SZ-50; additive, muscle, and the JAERI torso phantom components. The adipose/muscle ratios in Table VIII are not the ratios in each chest plate itself, but are the ratios in total chest wall (phantom core + chest plate). 15 mm thick chest plates with the same ratios also have been provided.

TABLE IV. CALCULATED LINEAR ATTENUATION COEFFICIENTS OF TISSUE SUBSTITUTES AND HUMAN TISSUES FOR PU L X RAY SERIES RADIATIONS. $\mu(P)$: ATTENUATION COEFFICIENT FOR PHOTOELECTRIC INTERACTIONS. $\mu(C)$: ATTENUATION COEFFICIENT FOR COMPTON SCATTERING

Tissue or Tissue Substitute		Linear attenuation coefficients (cm^{-1})					
		13.6 keV		17.2 keV		20. 2 keV	
		μ (P)	μ(C)	μ(P)	μ(C)	μ(P)	μ(C)
SZ-50		0.876	0.172	0.403	0.180	0.237	0.187
SZ-208		1.823	0.173	0.873	0.182	0.528	0.189
SZ-207		1.571	0.171	0.748	0.180	0.450	0.186
SZ-220		1.690	0.173	0.808	0.182	0.487	0.188
SZ-160		1.954	0.180	0.937	0.189	0.567	0.196
EZ-100		1.011	0.188	0.466	0.197	0.274	0.204
EZ-129		7.364	0.211	3.666	0.224	2.275	0.233
(Polyurethane+ 4.3% CaC0$_3$)		1.720	0.179	0.824	0.186	0.498	0.190
Alderson Rando Muscle	1)	1.500	0.166	0.700	0.173	0.423	0.175
	2)	1.030	0.167	0.465	0.174	0.279	0.176
Alderson lung		0.232	0.043	0.113	0.045	0.073	0.046
Human tissue							
Muscle		1.851	0.170	0.870	0.179	0.519	0.186
Adipose		0.879	0.157	0.408	0.164	0.243	0.169
Muscle+10% adipose		1.744	0.169	0.819	0.178	0.489	0.184
Muscle+23% adipose		1,627	0.167	0.764	0.176	0.456	0.182
Cartilage		1.961	0.179	0.921	0.188	0.549	0.195
Lung		0.506	0.045	0.238	0.048	0.142	0.050
Bone		7.760	0.192	3.833	0.204	2.367	0.212
Water		1.731	0.164	0.809	0.172	0.480	0.179

TABLE V. DIMENSIONS OF THE JAERI-PHANTOM AND ORGANS

Body parameters		Organ volumes	
Height	1. 68 m	Lungs - right	1,892 cm^3
Weight	63. 5 kg	left	1, 633 cm^3
Chest circumference	0.905 m*	Kidneys - right	151 cm^2
Chest width	0.297 m*	left	154 cm^3
Chest thickness	0. 213 m*	Liver	1, 761 cm^3
		Heart	818 cm^3

* Values for phantom with chest plate in place.

TABLE VI. TISSUE SUBSTITUTES USED IN JAERI PHANTOM

Substitutes used	
Trunk	SZ-220
Kidney	SZ-208
Liver	SZ-208
Cartilage	SZ-160
Trachea	SZ-208
Rib cage	EZ-129
Chest plate	CZ-10879, and others

2.3.2. Phantom evaluation

The phantom was examined, using an X ray Computed Tomographic Scanner, to determine if there are construction flaws such as deformation of rib cage or holes in the soft tissues. Table IX shows the observed CT values, linear attenuation coefficients derived from the CT values, and attenuation coefficients calculated from the elemental composition of each substitute.

2.3.3. Mass attenuation coefficients

The mass attenuation coefficients for the JAERI torso phantom components have been calculated based on the elemental compositions of the tissue substitute formulations. They are presented in Table X. Photon energies of particular interest to this CRP are indicated in bold.

2.3.4. Chest wall thickness

The effective thickness of the tissue layer between the lungs and detector (chest wall thickness) is a critical factor in accurate assessment of the amount of radioactive material in the lung and, consequently, the internal dose. This is primarily true at low photon energies. For 17 keV plutonium photon energies, for example, an error of 1 mm can results in an error of 10% in the assessment. Variations of several centimeters have been observed in the workforce.

In practice, specialized ultrasound measurements are often used to make the thickness determination. Less accurate estimates based on the body characteristics (height, weight, etc,) of the subject have been employed. It should be emphasized that accurate thickness measurements are not required for most applications, but in view of the radiological importance of some low energy photon emitters such as plutonium, this issue had to be addressed.

Thickness measurements were made at 106 points on the phantom core cover and each of the six overlays. The effective chest wall thickness was determined using exponential averaging. The phantom chest wall thicknesses determined using this process are shown in Table XI. The thicknesses indicated for various chest overlays represent the total for the core and overlying plates.

The concept of muscle equivalent chest wall thickness (MEQ-CWT) was introduced to remove adipose fraction as a variable for comparing results and establishing calibration factors [3]. Additional information related to application of this concept to the JAERI phantom has been provided by Kramer and Hauck [10]. The MEQ-CWT is determined from the following relationship:

$$MEQ - CWT = \frac{X[\mu_A A + \mu_M (1-A)]}{\mu_A}$$

where X is the physical chest wall thickness (cm), μ_A is the linear attenuation coefficient for adipose at a given energy (cm^{-1}), A is the adipose mass fraction (%), and μ_M is the linear attenuation coefficient for muscle at a given energy (cm^{-1}). Table XI illustrates the effect of the energy dependence of the MEQ-CWT. It is clearly most pronounced below 50 keV, and for convenience, the value at 17 keV is usually used.

TABLE VII. JAERI PHANTOM ELEMENTAL COMPOSITION TABLE

| Element | Elemental Composition% | | | Elemental Composition with Additive -% | | | | | | | |
| | SZ-50 | Additive | Muscle | Core | Chest Overlay | | | | | | |
					CZ10879	CZ11577	CZ20853	CZ21559	CZ30826	CZ31541	
H	8.49	4.24	10.20	8.18	8.15	8.16	8.26	8.24	8.38	8.32	
C	72.26	25.24	14.30	68.80	68.55	68.64	69.77	69.49	71.04	70.33	
N	44.9		3.40	4.16	4.14	4.14	4.25	4.23	4.37	4.31	
O	14.76	22.42	71.00	15.32	15.36	15.35	15.17	15.21	14.96	15.07	
Cl		37.25	0.10	2.74	2.94	2.87	1.97	2.20	0.97	1.53	
P		10.85	0.20	0.80	0.86	0.84	0.58	0.64	0.28	0.44	
Na			0.10								
S			0.30								
K			0.40								
Additive fraction%				7.35	7.90	7.70	5.30	5.90	2.60	4.10	

TABLE VIII. ADIPOSE FRACTIONS ASSOCIATED WITH JAERI PHANTOM CHEST PLATES

Chest plate materials	Nominal Thickness - mm	Adipose/Muscle Ratio – wt%
CZ – 10879	8	10/90
CZ – 20853	8	20/80
CZ – 30826	8	30/70
CZ – 11577	15	10/90
CZ – 21559	15	20/80
CZ – 31541	15	30/70

TABLE IX. OBSERVED CT VALUES AND LINEAR ATTENUATION COEFFICIENTS

Phantom component or organ	Tissue Substitute	CT value[a]	Linear attenuation coefficients [b] – cm^{-1}	Linear attenuation coefficients [c] – cm^{-1}
Trunk	SZ-220	43.2	0.1986	0.1963
Heart, liver, kidney	SZ-208	47.5	0.1990	0.1994
Cartilage	SZ-160	61.1	0.2020	0.2088
Rib cage	EZ-129	1,115.	0.4027	0.3355

a   CT values = $1,000 (\mu_p - \mu_w)/\mu_w$, where μ_p and μ_w denote linear attenuation coefficients of the phantom material and water, respectively.
b   Derived from the CT values.
c   Calculated from elemental compositions of each tissue substitute at 60 keV.

13

TABLE X. MASS ATTENUATION COEFFICIENTS FOR THE JAERI TORSO PHANTOM CHEST WALL AND OVERLAYS

Energy MeV	Mass Attenuation Coefficients – cm² g⁻¹								
	Skeletal Muscle	Adipose	JAERI Torso Phantom Component						
			Core	Chest Overlay					
				CZ10879	CZ11577	CZ20853	CZ21559	CZ30826	CZ31541
1.00E-02	5.36E+00	3.27E+00	4.63E+00	4.76E+00	4.72E+00	4.12E+00	4.27E+00	3.45E+00	3.82E+00
1.36E-02	2.21E+00	1.39E+00	1.96E+00	2.01E+00	1.99E+00	1.75E+00	1.81E+00	1.47E+00	1.62E+00
1.50E-02	1.69E+00	1.08E+00	1.51E+00	1.55E+00	1.53E+00	1.35E+00	1.40E+00	1.14E+00	1.26E+00
1.71E-02	1.20E+00	7.89E-01	1.08E+00	1.10E+00	1.09E+00	9.68E-01	1.00E+00	8.28E-01	9.06E-01
2.00E-02	8.21E-01	5.68E-01	7.47E-01	7.65E-01	7.59E-01	6.80E-01	7.00E-01	5.91E-01	6.41E-01
2.03E-02	7.94E-01	5.52E-01	7.24E-01	7.41E-01	7.35E-01	6.59E-01	6.78E-01	5.75E-01	6.22E-01
3.00E-02	3.78E-01	3.06E-01	3.56E-01	3.61E-01	3.60E-01	3.36E-01	3.42E-01	3.10E-01	3.25E-01
4.00E-02	2.69E-01	2.40E-01	2.57E-01	2.59E-01	2.59E-01	2.49E-01	2.51E-01	2.38E-01	2.44E-01
4.35E-02	2.50E-01	2.28E-01	2.40E-01	2.42E-01	2.42E-01	2.34E-01	2.36E-01	2.26E-01	2.30E-01
5.00E-02	2.26E-01	2.12E-01	2.19E-01	2.20E-01	2.19E-01	2.15E-01	2.16E-01	2.09E-01	2.12E-01
5.95E-02	2.06E-01	1.98E-01	2.00E-01	2.00E-01	2.00E-01	1.97E-01	1.98E-01	1.94E-01	1.96E-01
6.00E-02	2.05E-01	1.97E-01	1.99E-01	1.99E-01	1.99E-01	1.97E-01	1.97E-01	1.94E-01	1.95E-01
6.33E-02	2.00E-01	1.94E-01	1.94E-01	1.95E-01	1.95E-01	1.92E-01	1.93E-01	1.90E-01	1.91E-01
8.00E-02	1.82E-01	1.80E-01	1.78E-01	1.78E-01	1.78E-01	1.77E-01	1.77E-01	1.76E-01	1.76E-01
1.00E-01	1.69E-01	1.69E-01	1.65E-01	1.66E-01	1.66E-01	1.65E-01	1.65E-01	1.65E-01	1.65E-01
1.44E-01	1.51E-01	1.52E-01	1.48E-01	1.48E-01	1.48E-01	1.48E-01	1.48E-01	1.48E-01	1.48E-01
1.50E-01	1.49E-01	1.50E-01	1.46E-01	1.46E-01	1.46E-01	1.46E-01	1.46E-01	1.46E-01	1.46E-01
1.86E-01	1.39E-01	1.40E-01	1.36E-01	1.36E-01	1.36E-01	1.36E-01	1.36E-01	1.36E-01	1.36E-01
2.00E-01	1.36E-01	1.37E-01	1.33E-01	1.33E-01	1.33E-01	1.33E-01	1.33E-01	1.33E-01	1.33E-01
2.09E-01	1.34E-01	1.35E-01	1.31E-01	1.31E-01	1.31E-01	1.31E-01	1.31E-01	1.31E-01	1.31E-01
2.24E-01	1.31E-01	1.32E-01	1.28E-01	1.28E-01	1.28E-01	1.28E-01	1.28E-01	1.28E-01	1.28E-01
2.39E-01	1.28E-01	1.29E-01	1.25E-01	1.25E-01	1.25E-01	1.25E-01	1.25E-01	1.25E-01	1.25E-01
3.00E-01	1.18E-01	1.19E-01	1.15E-01	1.15E-01	1.15E-01	1.15E-01	1.15E-01	1.15E-01	1.15E-01
4.00E-01	1.05E-01	1.06E-01	1.03E-01	1.03E-01	1.03E-01	1.03E-01	1.03E-01	1.03E-01	1.03E-01
5.00E-01	9.60E-02	9.70E-02	9.41E-02	9.41E-02	9.41E-02	9.42E-02	9.42E-02	9.43E-02	9.43E-02
6.00E-01	8.87E-02	8.97E-02	8.70E-02	8.70E-02	8.70E-02	8.71E-02	8.71E-02	8.72E-02	8.72E-02
8.00E-01	7.79E-02	7.87E-02	7.64E-02	7.64E-02	7.64E-02	7.65E-02	7.65E-02	7.66E-02	7.65E-02
9.11E-01	7.33E-02	7.40E-02	7.18E-02	7.18E-02	7.18E-02	7.19E-02	7.19E-02	7.20E-02	7.19E-02
1.00E+00	7.01E-02	7.08E-02	6.87E-02	6.87E-02	6.87E-02	6.88E-02	6.87E-02	6.89E-02	6.88E-02

1.02E+00	6.93E-02	7.00E-02	6.80E-02	6.79E-02	6.80E-02	6.80E-02	6.80E-02	6.81E-02	6.81E-02
1.25E+00	6.27E-02	6.33E-02	6.14E-02	6.14E-02	6.14E-02	6.15E-02	6.15E-02	6.16E-02	6.15E-02
1.50E+00	5.70E-02	5.76E-02	5.59E-02	5.59E-02	5.59E-02	5.60E-02	5.59E-02	5.60E-02	5.60E-02
2.00E+00	4.90E-02	4.94E-02	4.80E-02	4.79E-02	4.79E-02	4.80E-02	4.80E-02	4.81E-02	4.80E-02
2.04E+00	4.84E-02	4.88E-02	4.74E-02	4.74E-02	4.74E-02	4.74E-02	4.74E-02	4.75E-02	4.75E-02
2.61E+00	4.23E-02	4.27E-02	4.14E-02	4.14E-02	4.14E-02	4.15E-02	4.15E-02	4.15E-02	4.15E-02
3.00E+00	3.93E-02	3.96E-02	3.84E-02	3.84E-02	3.84E-02	3.85E-02	3.85E-02	3.85E-02	3.85E-02
4.00E+00	3.37E-02	3.38E-02	3.29E-02	3.29E-02	3.29E-02	3.29E-02	3.29E-02	3.29E-02	3.29E-02
5.00E+00	3.00E-02	3.00E-02	2.92E-02	2.92E-02	2.92E-02	2.92E-02	2.92E-02	2.92E-02	2.92E-02
6.00E+00	2.74E-02	2.72E-02	2.66E-02	2.66E-02	2.66E-02	2.66E-02	2.66E-02	2.66E-02	2.66E-02
7.00E+00	2.55E-02	2.52E-02	2.47E-02	2.47E-02	2.47E-02	2.47E-02	2.47E-02	2.46E-02	2.46E-02
8.00E+00	2.40E-02	2.37E-02	2.32E-02	2.32E-02	2.32E-02	2.32E-02	2.32E-02	2.31E-02	2.31E-02
9.00E+00	2.29E-02	2.24E-02	2.20E-02	2.20E-02	2.20E-02	2.20E-02	2.20E-02	2.19E-02	2.20E-02
1.00E+01	2.19E-02	2.14E-02	2.11E-02	2.11E-02	2.11E-02	2.10E-02	2.10E-02	2.10E-02	2.10E-02

TABLE XI. EFFECTIVE CHEST WALL THICKNESSES FOR JAERI PHANTOM AND
OVERLAYS

	Chest Wall Thickness – cm						
	Overlay						
Core	CZ10879	CZ20853	CZ30826	CZ11577	CZ21559	CZ31541
Measured						
1.99	2.79	2.79	2.79	3.49	3.49	3.49
Photon Energy - MeV	MEQ-CWT						
0.017	1.79	2.53	2.44	2.35	3.16	3.05	2.93
0.020	1.81	2.56	2.47	2.39	3.20	3.07	2.98
0.043	1.91	2.69	2.66	2.63	3.36	3.33	3.29
0.060	1.93	2.71	2.70	2.69	3.39	3.37	3.36
0.063	1.94	2.72	2.71	2.70	3.40	3.39	3.38
0.143	1.94	2.73	2.73	2.72	3.41	3.41	3.41
0.185	1.95	2.73	2.74	2.74	3.41	3.43	3.43
0.208	1.95	2.73	2.73	2.34	3.41	3.41	3.41
0.238	1.94	2.72	2.72	2.72	3.41	3.41	3.41
0.911	1.95	2.73	2.73	2.74	3.42	3.42	3.42
2.614	1.95	2.73	2.73	2.73	3.42	3.42	3.42

FIG. 8. JAERI phantom.

Fig. 9. JAERI phantom with cover removed.

16

FIG. 10. Natural uranium lung sets for JAERI phantom.

FIG. 11. Chest overlays for JAERI phantom.

3. FABRICATION OF RADIOACTIVELY LABELED LUNGS

3.1. Summary

The University of Cincinnati (UC) fabricated thirteen sets of simulated lungs for use in the JAERI calibration phantom using molds supplied by Lawrence Livermore National Laboratory (LLNL). The lung phantoms were fabricated using the tissue substitutes formulated at UC which are based on the specifications for the lungs used in the LLNL torso calibration phantom. Each lung set was prepared in duplicate and detailed certificates were provided with each phantom to document the content of radioactive material and the formulation used in fabrication of the lung. A set of 5 sources of radioactive material sealed in Plexiglas was also prepared using the same radioactive solutions as those used to prepare the lung phantoms. All of the lung sets, sources, and documentation were shipped to Livermore National Laboratory for use in the IAEA intercomparison programme.

3.2. Description of research

The chemical formulation used at the University of Cincinnati (UC) to fabricate the lung phantoms for the IAEA is equivalent to the original Livermore lung tissue substitute [2]. It was developed from the elemental composition of hydrogen, carbon, nitrogen, oxygen, magnesium, calcium, and tin listed for Griffith Lung in ICRU publication No. 44 (1989) [7]. Raw materials, including polyurethane, calcium carbonate ($CaCO_3$), and catalyst were selected to produce a final reacted polyurethane having an elemental composition consistent with the Griffith Lung [11, 12]. Table XII lists the elemental composition of the constituents of the UC lung tissue substitute.

TABLE XII. ELEMENTAL COMPOSITION OF LUNG PHANTOM MATERIALS (WEIGHT PERCENT)

	H	C	N	O	Ca	Mg	Sn
Polyurethane	8.443	63.509	4.436	23.52	0	0.11	0
Calcium Carbonate	0	12.00	0	47.96	40.04	0	0
Catalyst	7.9	48.6	0.39	16.9	0	0	26.20

Solid polyurethane has a density of 1.06 g cm^{-3} and attenuation characteristics similar to tissue. These characteristics can be readily modified through the addition of $CaCO_3$ (to increase the effective Z) to simulate more dense tissue. A foaming polyurethane (CPR-1940D) was used to simulate the lung tissue substitute material based upon the attenuation properties and to achieve a density in the range of 0.25–0.30 g cm^{-3}. The reaction is catalyzed by the addition of a small amount of stannous octoate, Dabco T-9 consisting of 90% stannous octoate, 0.1% t-butyl catechol, and 9.9% 2-ethyl hexanoic acid. Ref. [12] reproduced the exact formulation for the original LLNL lung tissue substitute. Comparison of the densities of human tissue with the polyurethane substitutes is given in Table XIII.

Molds for casting the Asian phantom lungs were provided to the University of Cincinnati by the Lawrence Livermore National Laboratory. The molds are of the same two piece construction as the Livermore phantom lungs, with each side having a void volume roughly 50% of the total. The molds are produced from silicone rubber material and are very durable. The intricate shape of the JAERI lung phantoms make the casting process very difficult because the polyurethane material must flow into all the deep crevices before

foaming begins. The two-part molds have to be filled, closed, latched, and positioned quickly and in such a manner to insure that the material expands uniformly into all the nooks and crannies of the mold and that the CO_2, formed during the foaming process, escapes. Any CO_2 trapped in the mold can produce a large void in the final cast.

Table XIV provides an empirical formulation for the materials used in the production of the lung phantoms as described in the original Livermore procedures. The polyurethanes represent a mixture composed of 8.443% hydrogen, 63.5% carbon, 4.463% nitrogen, 23.52% oxygen, and 0.11% magnesium. The foaming is a result of the release of carbon dioxide during the reaction of water and the isocyanate group. The reaction between the two polyurethanes is catalyzed by the addition of a small amount of stannous octoate catalyst.

TABLE XIII. DENSITIES OF HUMAN TISSUES AND POLYURETHANE SUBSTITUTES

Organ	Human tissue [8] g cm^{-3}	Polyurethane Substitute g cm^{-3}
Skeletal Muscle	1.04	1.09
Adipose	0.92	-
Lung (inflated)	0.26	0.26

TABLE XIV. FORMULATION FOR LIVERMORE LUNG TISSUE SUBSTITUTE MATERIAL TO MAKE A 100 g BATCH [12]

Material	Quantity (g)
Polyurethane CPR 1940-D/B	52.85
Concentrate[a]	18.50
H_2O[b]	0.24
Polyurethane CPR 1940-D/A	28.16
Catalyst T-9[c]	4.5 drops

[a] Formulated to produce a 6.2% content of $CaCO_3$ in a small quantity of CPR 1940-DIB.
[b] Water controls the final density of the foam.
[c] The quantity of the catalyst is adjusted to give a workable reaction rate.

The concentrate is made of 66.67% CPR 1940-D/B and 33.33% $CaCO_3$ with the purpose of insuring that the $CaCO_3$ powder is fully and uniformly incorporated into the polyurethane. The concentrate represents a thixotropic mixture that is easily added to the formulation just prior to the foaming process and insures that the $CaCO_3$ remains suspended during foaming.

The quantity of material required for each lung phantom depends upon the volume of the lung and its density. The volume of each lung for the Asian phantom has been reported as 1,892 cm^3 for the large lung and 1,633 cm^3 for the small lung [5]. However, the lung molds provided to UC by Livermore had volumes of 2,028 ± 13.6 cm^3 and 1,680 ± 17 cm^3 for the large and small lung, respectively. The mass of material used to fabricate each lung was adjusted to produce a phantom having a density of 0.26 g cm^{-3}. Prior to producing lungs containing radioactive material, a set of sample blank lungs were submitted to Livermore to determine whether the size of the phantoms would be adequate to fit into the JAERI thorax phantom.

The procedure for fabricating a lung phantom involves initial preparations to insure that all materials are present in sufficient quantities to complete the process. The $CaCO_3$ is dried for several hours at 1,100 °C until no weight loss is detected and then stored in a desiccator to cool before use. The molds are cleaned using a lint free cloth dampened with a 50/50 mixture of acetone and toluene and then preheated to 35–38 °C in an oven for at least 30 minutes prior to use. Immediately before use, the interior of the molds are sprayed with a mold release agent.

First, the concentrate is prepared by adding a quantity of 1940-D/B to a pre-weighed beaker followed by the addition of a quantity of dry $CaCO_3$. The concentrate is mixed by hand for 2 minutes and stored until needed in a desiccator. Second, a quantity of 1940-D/B is added to a pre-weighed paper bucket to which is added a quantity concentrate, distilled water, catalyst, and radioactive solution. The contents of the bucket are mixed for two minutes using a drill fitted with a paint stirring blade. Immediately after mixing, without removing the stirrer, a quantity of 1940-D/A is added to the bucket and the total contents are vigorously stirred for 10 seconds. The material is quickly poured into the appropriate half of the mold and the weight of the residual materials in the bucket is quickly determined at the same time as the mold is sealed, clamped, and properly positioned for foaming. After 1 hour, the mold is opened and the residual materials in the bucket are re-weighted to determine the weight loss of CO_2 due to foaming. The lung is removed from the mold, trimmed, cleaned and weighted.

Analysis of the quality of the simulated organ is performed by observing the physical characteristics of the lung and calculating its density and formulation. The density and elemental content are automatically calculated using Excel and the information contained on the data form. The first page of the data form contains fabrication measurements, the second page gives the final corrected activity of the phantom, and the third page lists the quality assurance information on the elemental content of the phantom and its density. The corrected activity reported on the data form represents the final activity contained in the phantom lung accounting for the loss of mass due to foaming and release of CO_2.

TABLE XV. ACTIVITY CONTENT OF POINT SOURCES

Isotope	Activity (kBq)
Natural Uranium (^{238}U)	0.47
3% Enriched Uranium (^{238}U)	1.00
^{241}Am	1.59
^{238}Pu	6.97
^{232}Th	0.10

3.3. Results

The work under this project included fabrication of a total of twelve lung sets containing radioactive material, a blank lung set, and a set of calibration sources made using the same solutions that were used to fabricate the lung phantoms. Table XV lists the activity in each of the point sources. Each point source was fabricated from a small rectangular piece of Plexiglas into which a flat-bottomed hole was drilled. The thickness of the remaining Plexiglas in the bottom of the hole was measured. The activity was deposited into the hole and covered with an epoxy resin to seal in the radioactive material. Table XVI lists the activity contained in each phantom lung set.

TABLE XVI. ACTIVITY CONTENT OF LUNG PHANTOMS FABRICATED AT THE UNIVERSITY OF CINCINNATI

Identification Number	Primary Isotope	Activity (Bq)
IAEA-5U-L4	^{238}U (3% ^{235}U enriched)	840
IAEA-5U-S4		710
IAEA-5U-L5		840
IAEA-5U-S5		730
IAEA-5U-Ll		610
IAEA-5U-L2		610
IAEA-L-PU3	^{238}Pu	22,500
IAEA-S-PU3		18,300
IAEA-L-PU5		21,800
IAEA-S-PU5		20,500
IAEA-L-PU8		2,700
IAEA-S-PU8		1,900
IAEA-L-PU9		2,600
IAEA-S-PU9		2,400
IAEA-L-AM1	^{241}Am	270
IAEA-S-AM1		220
IAEA-L-AM2		230
IAEA-S-AM2		190
IAEA-8U-L1	^{238}U	640
IAEA-8U-S1		520
IAEA-8U-L2		450
IAEA-8U-S2		410
IAEA-L-TH5	^{232}Th,	67
IAEA-S-TH5		53
IAEA-L-TH7		63
IAEA-S-TH7		62
JAERI-19A-LL	Blank	0
JAERI-19A-SL		0

3.4. Comparative lung set measurements

Following measurements performed by the intercalibration participants, the phantom and duplicate lung sets were returned to the Lawrence Livermore National Laboratory for comparative measurements using a four germanium detector array in a fixed geometry. The bottom sections of the right and left lung molds were used to hold the lungs in a reproducible geometry for counting. Four detectors in two transverse rows with one row of two detectors in the inferior and another row of two detectors in the superior position, transversely centered, and positioned approximately 25 cm from the anterior-posterior center of the lung using the mold surface as a reference.

Operational use of the LLNL counting facility constrained the time available for measurements. Typical measurement times were 3600 to 7200 seconds (1 to 2 hours) for each lung. The results are presented in Table XVII. Lungs sets used in the intercalibration are identified in bold. Although the measurements normalized to the reference activity values are within 8% for lung pairs, comparison of right and left lung duplicates showed differences of up to 17.3% for the high level ^{238}Pu lungs. This could be the result of errors in the comparison measurements, assay of the original stock solution used to make the lungs, the amount of stock solution actually used in the lungs, or non-uniform distribution of the radioisotopes in the lungs. It is currently planned that one set of lungs be destructively analyzed in the future to provide verification of the reference values for that set, and additional assay information for the remaining lungs.

TABLE XVII. SUMMARY OF COMPARATIVE DUPLICATE LUNG SET COUNTS USING A GERMANIUM DETECTOR ARRAY

Radionuclide	Lung Set	ID	Count Time (s)	Reference Activity Bq	Photon(s) Used keV	Counts	Error (1s)	Counts per Bq	% diff
Am-241	Left	**IAEA-S-AM1**	**7200**	**217**	**60**	**6287**	**79**	28.9	**–10.5%**
		IAEA-S-AM2	7200	192	60	6131	78	32.0	
	Right	**IAEA-L-AM1**	**7200**	**271**	**60**	**6235**	**79**	23.0	**–4.4%**
		IAEA-L-AM2	7200	228	60	5468	74	24.0	
	Total					total cps		Cps/Bq	
		AM1		**488**		**1.74**		3.57E-03	**–7.8%**
		AM2		419		1.61		3.84E-03	
Pu-238	Left	**IAEA-S-PU8***	**10800**	**1,900**	**13,17,&20**	**7611**	**87**	4.00	**12.6%**
Low Level		IAEA-S-PU9*	10800	2,410	13,17,&20	8446	92	3.51	
	Right	**IAEA-L-PU8**	**14400**	**2,720**	**13,17,&20**	**12493**	**112**	4.59	**–8.3%**
		IAEA-L-PU9	14400	2,590	13,17,&20	12843	113	4.97	
	Total					total cps		Cps/Bq	
		PU8		**4,630**		**1.57**		3.41E-04	**1.5%**
		PU9		5,000		1.67		3.35E-04	
Pu-238	Left	**IAEA-S-PU3**	**10800**	**18,400**	**13,17,&20**	**69613**	**264**	3.78	**17.3%**
High level		IAEA-S-PU5	10800	20,500	13,17,&20	64345	254	3.14	
	Right	**IAEA-L-PU3**	**7200**	**22,500**	**13,17,&20**	**38927**	**197**	1.73	**–15.2%**
		IAEA-L-PU5	7200	21,800	13,17,&20	43452	208	2.00	
	Total					total cps		Cps/Bq	
		PU3		**40,800**		**11.85**		2.90E-04	**2.3%**
		PU5		42,300		11.99		2.84E-04	
U-nat	Left	**IAEA8US1**	**10800**	516	**185**	**2708**	**52**	5.24	**0.1%**
		IAEA8US2	10800	408	185	2138	46	5.24	
	Right	**IAEA8UL1**	**10800**	641	**185**	**2548**	**50**	3.97	**1.3%**
		IAEA8UL2	10800	453	185	1777	42	3.92	
	Total					total cps		Cps/Bq	
		8U1		1,160		**0.487**		4.21E-04	**-0.1%**
		8U2		861		0.363		4.21E-04	
U-235 (3%)	Left	**IAEA-5U-S4**	**7200**	729	**185**	**4472**	**67**	6.14	**0.9%**
		IAEA-5U-S5	7200	725	185	4411	66	6.08	
	Right	**IAEA-5U-L4**	**5400**	836	**185**	**2986**	**55**	3.57	**0.7%**
		IAEA-5U-L5	5400	951	185	3377	58	3.54	
	Total					total cps		Cps/Bq	
		5U4		1,560		**1.174**		7.49E-04	**1.6%**
		5U5		1,680		1.238		7.38E-04	
Th-232	Left	**IAEA-S-TH5**	**7200**	53.3	**238**	**979**	**31**	18.38	**7.7%**
		IAEA-S-TH7	7200	62.5	238	1060	33	16.95	
	Right	**IAEA-L-TH5**	**7200**	66.6	**238**	**962**	**31**	14.43	**5.5%**
		IAEA-L-TH7	7200	63.3	238	864	29	13.65	
	Total					total cps		Cps/Bq	
		TH5		120		**0.270**		2.25E-03	**5.5%**
		TH7		126		0.267		2.12E-03	

4. MAGNETIC RESONANCE IMAGE PHOTON PHANTOM (MRIPP)

4.1. Introduction

Calibration of detectors and detector systems for in vivo measurements traditionally has depended on the use of phantoms intended to simulate the portion of the human body to be measured for radioactive material. These phantoms may simulate tissues, organs, sections of the body, or the body as a whole. They are constructed in a way that permits distribution of radioactive sources or radioactive material throughout the volume to be simulated. The International Commission on Radiation Units and Measurements (ICRU) [13] has prepared a detailed review of such phantoms.

A large number of calibration phantoms has been designed and constructed. Their complexity depends primarily on the radionuclides of concern and expected deposition sites. Phantom designs range from very simple objects to highly anthropomorphic reproductions of part or all of the body. The cost of phantoms such as the one used in this CRP may be US $50 000 or more.

Although calibration phantoms provide the possibility for direct measurement, their use has a number of disadvantages as well. In addition to being potentially very expensive, they require the use of radioactive sources, or radioactive material. The necessary radionuclides may not be readily available, may be expensive, and may present handling concerns, particularly if liquid solutions are involved. Moreover, the benefit of such calibration is limited by the available radionuclides and fixed phantom design so that application of the data to people of various statures, having deposition sites that are different from the phantom, or containing additional radionuclides is limited. These disadvantages are all particularly important for many developing IAEA Member States that have limited financial and technical resources.

The Magnetic Resonance Image Photon Phantom (MRIPP) provides a new way to calibrate in vivo measurement systems. It was developed, under a contract from the US Department of Energy, to augment or replace tissue equivalent phantoms by using a calculational approach to in vivo measurement system calibrations. MRIPP provides simulations of a database of people with varying size, gender, and body proportions, and could potentially be very useful for internal dosimetry programmes in many Member States.

4.2. Overview

A whole body counter generally consists of a place for the person (lying down, sitting, or standing), and one or more detectors that can be placed in contact with the person, or at some measured distance. MRIPP provides a method of calibrating WBCs in which the physical simulation of a person with a deposition of a nuclide is replaced with a computer simulation. The physical phantom is replaced with a set of magnetic resonance images called MRI phantoms. And finally, a computer simulation of photon transport models emission and detection.

The main computer screen for MRIPP is shown in Figure 12. Use of MRIPP begins with development of a schematic description of the detector system. The size and elemental composition of the sensitive volumes (detection elements such as NaI) are entered into the appropriate spaces on the first MRIPP data screen (Option 1). Two sensitive volumes are allowed so that phoswich detectors can be modeled. The detector window, side cladding and shielding are specified in the second screen (Option 2). The thickness and composition of the entrance window is particularly important, for example for low energy photons. MRIPP requires the use of a source measurement to obtain a relative calibration, thus ancillary features such as photomultiplier tubes are not important in the photon interaction process and are not modeled.

The use of multiple detector arrays is accommodated in the third and fourth steps (Options 3 and 4). Each detector within an array is characterized in the first two steps, and the geometrical relationship of the detectors in the assembly is simulated step 3. Specification of the array shielding, if any, is described in step 4. Once the detectors or detector arrays have been geometrically defined, a calculation is performed using a simulated point source (Option 5). The user mathematically describes the geometry of the source that is to be used for the relative calibration measurement, then provides the information necessary to represent the spatial relationship of the source and detector or detector array.

When the source-detector geometry is established, it is necessary to run the calculation that simulates the point source counting process (Option 5). This step is intended to provide mathematical simulation of a measurement with a real source. The ratio of the phantom calculation (to be described) to the source calculation becomes the Efficiency Correction Factor (ECF). The measured point source efficiency is multiplied by the ECF to establish the phantom counting efficiency, ie the calibration. Since the calculations are done through the MCNP Monte Carlo code, the user selects the number of photons to be generated. The statistical uncertainty in the result decreases with the number of histories run. The default setting is 10^6 photons. However, it many be necessary to increase this number if the source-detector distance is large (≥ 50 cm).

After the point source calculation is complete, the result is retained in a reference file for comparison with subsequent phantom calculations involving the same detector and source. The phantom calculations begin by opening "Viewit" (Option 6). It is here that the mathematical phantom to be used for calibration is selected. There are a number of such phantoms in the library. These are based on MRI scans of physical phantoms or human volunteers. Once a phantom has been selected by number, a detailed list of physical characteristics is presented. This allows the user to select the phantom most closely matching the requirements of the calibration.

For this CRP, four mathematical or voxel phantoms were prepared from MRI scans. These represent the JAERI phantom core with organs, and the core plus 8 mm thick overlays CZ10879, CZ20853, CZ30826 with 10%, 20% and 30% adipose mass fraction respectively. It was not possible to develop voxel phantoms for the phantom with the thicker overlays. It is these four voxel phantoms that are used for the CRP.

When a phantom has been selected, a 3-dimensional plane representation of the phantom appears (Figure 13). The source organs are selected using the cursor. The cursor can be moved either by the mouse or the keyboard. However, experience suggests that the keyboard offers finer control of cursor placement. After selecting the source organs (lungs in the case of this CRP), it is necessary to establish a reference point on the surface of the phantom using the cursor. Lung counting typically uses the notch at the top of the sternum or the bottom tip of the sternum as reference positions when placing detectors on human subjects. It is important to select a reference that can be located reproducibly on the subject or phantom during actual measurement. Users of MRIPP can be extremely precise in specifying the reference point by observing the optional slice-by-slice input of the phantom as the 3-dimensional plane is being read into the computer.

After selection of a reference point, the user defines the detector position relative to the reference point. MRIPP uses an X, Y, Z coordinate system with the X axis lateral across the chest, the Z axis longitudinal along the body lie and Y is normal to the plane of the body or the counting bed; in addition, detectors can be tilted in planes with X and Z axes. Although preliminary detector position is established with the cursor, the next step within MRIPP is used to refine the settings of the detection orientation (Option 7). The reference point on the phantom, which is established in VIEWIT, can not be changed at this point.

The final step (Option 8) is to complete the phantom calculation. The user can, and should, review the planar view of the detector-phantom-geometry as provided. As in the

FIG. 12. MRIPP menu screen.
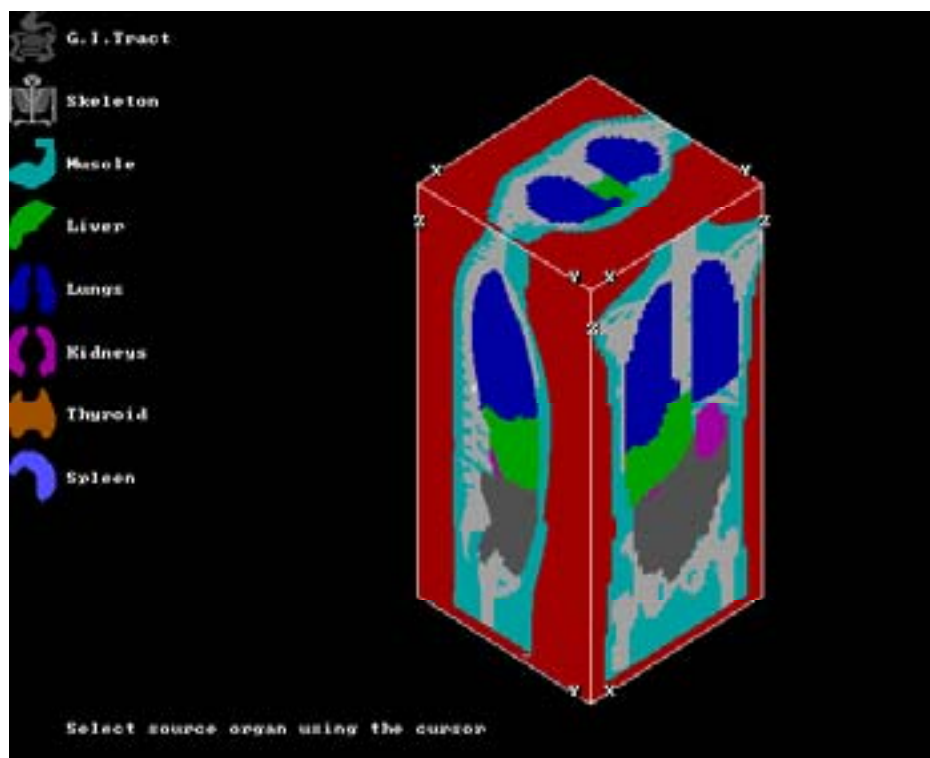
FIG. 13. 3D phantom representation for selection of source organs and detector positioning.

simple source calculation, the number of photons to be generated determines the statistical uncertainty of the result. While 10^6 photons are likely to be sufficient above 50 keV, the losses incurred in the photon interaction process are such that as many as 5×10^6 or more may be need at energies below 20 keV in order to obtain reliable statistics. When the calculation is complete, the resulting ECF is found in the file EFICENCY.OUT, together will the estimate of the 1 σ standard error. As indicated previously, ECF represents the ratio of the phantom (subject) counting efficiency to that of a source counted in a standard geometry. It remains for the user to make a measurement of the efficiency of the source that was modeled into MRIPP and multiply the ECF by the measured efficiency

The calculation time depends largely on the computer speed. A P.C. with a minimum 100 MHz processor is highly recommended. The higher the processor speed, the faster the computations. Additional requirements are memory with at least 20 MB conventional memory free and 100 MB of free disk space. For complicated or very large whole body counters, more memory or more disk space may be required. However, considering the advances in personal computer technology since development of MRIPP, these requirements are no longer a serious limitation.

5. RESULTS OF THE CO-ORDINATED RESEARCH PROJECT

5.1. Detection system efficiency measurements

The levels of radioactive material in the lung sets provided for the intercalibration were similar to those that could be expected following significant internal contamination of workers in the nuclear industry and certain non-nuclear industrial applications such as the manufacture of mantles for gas lanterns. However, they were low enough to cause problems for a few of the participants in accurate quantification. In fact, one participant was unable to provide meaningful results. The problem was, of course, most acute at lower energies, particularly the X ray from ^{238}Pu. This is illustrated in Figure 14, which presents the low energy spectra from the point source that was distributed with the phantom, and that from the ^{238}Pu loaded lungs in the JAERI phantom with a 15 mm thick, 20% adipose overlay (MEQ CWT – 3.22 cm). The effect of the attenuation of the 13.6, 17.1, and 20.3 keV X ray is quite apparent.

Fifteen detection systems were used in the intercalibration, including five germanium detector systems, five phoswich systems, and five sodium iodide detector based systems. However, only four germanium and four phoswich based systems were used for most or all of the lung set – chest overlay combinations. The participants detection systems are described in Annex I, and the results of the measurements are presented in Annex II. Since this was intended to offer the participants an opportunity to compare the efficiencies of their counting systems, the results include measurement of the counts per photon for each detection system. The participants provided measurements of the surface areas of their detectors or detector arrays to establish the efficiency in terms of counts per square centimeter of detector surface area per photon so that the efficiencies of the systems could be compared.

Table XVIII presents the average efficiencies for four of the germanium detector based systems (participants A, C, N and O). These results are also represented in Figure 15. Figure 16 shows the efficiency as a function of energy for the JAERI phantom core. Equivalent data for four phoswich systems (participants D, F, G and M) are given in Table XIX, and plotted in Figure 17. Because of the importance of the low energy region, Figure 18 compares the average germanium detector efficiencies with those for the phoswich detectors.

TABLE XVIII. AVERAGE EFFICIENCIES FOR 4 GERMANIUM BASED DETECTOR SYSTEMS – COUNTS•CM^2•PHOTON^{-1}

Photon energy keV	Muscle equivalent chest wall thickness - cm						
	1.91	2.47	2.58	2.68	3.09	3.22	3.36
17	3.59E-06	1.53E-06	1.36E-06	1.06E-06	6.69E-07	5.24E-07	4.47E-07
20	1.34E-05	6.97E-06	6.74E-06	5.86E-06	4.17E-06	3.55E-06	3.19E-06
43	1.02E-04	7.34E-05	7.23E-05	6.64E-05	5.21E-05	5.17E-05	5.29E-05
60	1.52E-04	1.10E-04	1.10E-04	1.10E-04	8.77E-05	8.60E-05	8.86E-05
63 (Ave.)	1.26E-04	9.16E-05	9.03E-05	8.89E-05	6.99E-05	7.11E-05	7.06E-05
143	1.33E-04	9.58E-05	9.45E-05	9.23E-05	7.71E-05	7.80E-05	7.77E-05
185 (Ave.)	1.11E-04	8.48E-05	8.11E-05	8.22E-05	6.69E-05	6.89E-05	6.79E-05
209	7.76E-05	5.17E-05	5.79E-05	5.97E-05	4.49E-05	5.02E-05	4.68E-05
238	7.36E-05	5.54E-05	5.75E-05	5.55E-05	4.43E-05	4.74E-05	4.58E-05

TABLE XIX. AVERAGE EFFICIENCIES FOR 4 PHOSWICH BASED DETECTOR SYSTEMS – COUNTS•CM^2•PHOTON^{-1}

Photon energy keV	Muscle equivalent chest wall thickness - cm						
	1.91	2.47	2.58	2.68	3.09	3.22	3.36
17	5.80E-06	2.88E-06	2.52E-06	2.20E-06	1.50E-06	1.29E-06	1.12E-06
43	1.56E-04	1.24E-04	1.23E-04	1.30E-04	1.04E-04	1.02E-04	1.03E-04
60	2.30E-04	1.90E-04	1.90E-04	1.85E-04	1.61E-04	1.62E-04	1.59E-04
63 (nat U)	6.07E-04	5.35E-04	5.33E-04	5.23E-04	4.80E-04	4.78E-04	4.73E-04
63 (3% U^{235})	9.47E-04	8.57E-04	8.46E-04	8.36E-04	7.78E-04	7.73E-04	7.67E-04
185 (nat U)	1.50E-04	1.25E-04	1.27E-04	1.21E-04	1.07E-04	1.10E-04	1.08E-04
185 (3% U^{235})	4.34E-04	3.36E-04	3.35E-04	3.35E-04	2.85E-04	2.86E-04	2.91E-04

The results in Figures 15, 17 and 18 have been fitted with the exponential:

$$Y = Be^{AX}$$

Where Y is the efficiency and X is the MEQ-CWT in cm. The coefficients are summarized in Tables XX and XXI. These tables illustrate the importance of chest wall thickness at lower energies with increased magnitude of the value of A. However, some of the chest wall thickness dependence is due to detector placement. The detectors are normally placed as close to the chest as possible to obtain the best counting geometry.

TABLE XX. PARTICIPANT AVERAGE MEQ-CWT DEPENDENT COEFFICIENTS –
GERMANIUM BASED SYSTEMS

Energy	A	B
17	−1.43032	5.333E-5
20	-0.9743	8.241E-5
43	-0.4856	2.497E-4
60	-0.3888	3.051E-4
63 (Natural U)	-0.4175	2.698E-4
63 (3% Enriched ^{235}U)	-0.4064	2.610E-4
63 (Average)	-0.4121	2.654E-4
143	-0.3708	2.533E-4
185 (Natural U)	-0.3362	2.007E-4
185 (3% Enriched ^{235}U)	-0.3485	2.067E-4
185 (Average)	-0.3448	2.052E-4
209	-0.3253	1.342E-4
238	-0.3332	1.341E-4

TABLE XXI. PARTICIPANT AVERAGE MEQ-CWT DEPENDENT C COEFFICIENTS –
PHOSWICH BASED SYSTEMS

Energy	A	B
17	−1.117	4.642E-5
43	-0.2996	2.719E-4
60	-0.2593	3.701E-4
63 Natural U	-0.1748	3.673E-4
63 3% Enriched U-235	-0.14878	1.246E-3
185 Natural U	-0.2316	2.280E-4
185 3% Enriched U-235	-0.2830	7.108E-4

The relatively poor resolution of the phoswich detectors makes comparison of the efficiency results somewhat complicated. The 17 keV results include contributions from the 20.3 and even 13.6 keV photons associated with the ^{238}Pu decay. The 63 and 185 keV results may also include contribution from other photons. The results do suggest a somewhat higher efficiency for the phoswich-based systems. This may well be the result of the relative position of the sensitive areas of the germanium detectors used in the arrays compared with that achieved with individual detectors having larger dimensions. Of course, overall sensitivity includes background considerations, which were not explored in this intercalibration, and the vastly superior resolution of the germanium based systems play an important role.

It is also interesting to note the wider difference in efficiencies reported for the phoswich systems compared with the germanium-based systems. This is likely the result of difference in spectral interpretation and background subtraction used by different participants. Again, resolution has an impact on this analysis.

5.2. Minimum Detectable Activity (MDA)

A detailed discussion of determination of MDA is beyond the scope of this report. More comprehensive coverage of this topic has been developed by the Health Physics Society [14]. However, select results can be used to give an indication of system performance.

A number of formulations have been developed for determination of MDA depending on the application [1]. For purposes of comparison, the following simplified equation can be used:

$$MDA = \frac{4.65 S_b + 3}{KT}$$

Where S_b is the background standard deviation, K is efficiency in counts per second per Bequerel, and T is count time. Table XXII presents the results of sample MDA calculations for ^{238}Pu using the 17 keV Xray. In the case of the participants using phoswich detectors, the 17 keV x-rya region is used. The values of K are based on the efficiencies reported for the 15cm, 20% adipose overlays. The assumed counting time is 3600 seconds. Equivalent values of MDA for ^{241}Am are shown in Table XXIII.

Table XXIV provides some indication of the effect of the condition of background measurement on MDA. Participants C and O reported background count rates in the region of interest with and without the phantom present. For the 17 keV region, there is little difference in the background, and little difference in the MDA values. At 60 keV, however, the background with the phantom in place is about twice that for the detector only. The result if about a 30% increase in MDA. Of course, the background contribution from a human subject will be even greater, resulting in a further increase in MDA.

The effect of chest wall attenuation is most important at low energies. Table XXV illustrates this point for two germanium and two phoswich systems. The range of MDA under these condition can be as much as a factor of 10.

TABLE XXII. CALCULATED MDA FOR ^{238}PU USING 17 KEV X RAY

Participant	Detector	Region of Interest keV	K cps per Bq	Detector Area cm^2	Background cps	MDA Bq
A	LEGe	16–18.2	1.70E-08	154	8.88E-02	9.14E+03
C	LEGe	16.7–18.1	3.62E-08	156	2.79E-02	2.44E+03
D	Phoswich	13–25	1.15E-07	253	1.95E-01	1.21E+03
F	Phoswich	14–25	5.55E-08	324	1.30E-01	1.60E+03
M	Phoswich	12–27	1.01E-07	253	1.13E-01	1.05E+03
N	LEGe	15.22–18.42	2.82E-08	80	4.90E-02	7.98E+03
O	LEGe	16.1–18.1	2.68E-08	120	3.10E-02	4.50E+03

TABLE XXIII. CALCULATED MDA FOR ^{241}AM USING 60 KEV X RAY

Participant	Detector	Region of Interest keV	K cps per Bq	Detector Area cm^2	Background cps	MDA Bq
A	LEGe	58.4–61	2.33E-05	154	5.66E-02	5.37E+00
C	LEGe	58.9–60.6	3.30E-05	156	4.78E-02	3.46E+00
D	Phoswich	45–70	6.31E-05	253	1.19E-01	1.73E+00
F	Phoswich	32–76	5.62E-05	324	6.78E-01	3.55E+00
M	Phoswich	43–73	7.81E-05	253	2.80E-01	2.12E+00
N	LEGe	57.22–61.02	3.15E-05	80	9.35E-02	9.73E+00
O	LEGe	58.5–60.5	3.50E-05	120	3.53E-02	3.67E+00

TABLE XXIV. EFFECT OF BACKGROUND MEASUREMENT CONDITIONS ON MDA

Participant	Nuclide	Photon energy keV	K cps per Bq	Background Condition	Background cps	MDA Bq
C	^{238}Pu	17.1	3.62E-08	Detector & Phantom	2.79E-02	2.44E+03
			3.62E-08	Detector only	2.98E-02	2.52E+03
O			2.68E-08	Detector & Phantom	3.10E-02	4.50E+03
			2.68E-08	Detector only	3.34E-02	4.66E+03
C	^{241}Am	59.5	3.30E-05	Detector & Phantom	4.78E-02	3.46E+00
			3.30E-05	Detector only	3.30E-02	2.90E+00
O			3.50E-05	Detector & Phantom	3.53E-02	3.67E+00
			3.50E-05	Detector only	1.84E-02	2.70E+00

TABLE XXV. MDA AS A FUNCTION OF CHEST WALL THICKNESS FOR ^{238}PU USING THE 17 KEV X RAY

Phantom Overlay		Participant							
		C		D		M		O	
		LEge		Phoswich		Phoswich		LEGe	
ID	MEQ-CWT cm	K cps per Bq	MDA Bq	K cps per Bq	MDA Bq	K cps per Bq	MDA Bq	K cps per Bq	MDA Bq
None	1.91	1.93E-07	4.57E+02	5.22E-07	2.65E+02	4.704E-07	2.26E+02	2.03E-07	5.95E+02
CZ30826	2.47	9.01E-08	9.81E+02	2.56E-07	5.41E+02	2.261E-07	4.70E+02	8.13E-08	1.48E+03
CZ20853	2.58	7.87E-08	1.12E+03	2.16E-07	6.41E+02	1.991E-07	5.34E+02	8.10E-08	1.49E+03
CZ10879	2.68	6.27E-08	1.41E+03	1.92E-07	7.22E+02	1.682E-07	6.32E+02	5.13E-08	2.35E+03
CZ31541	3.09	4.22E-08	2.09E+03	1.19E-07	1.17E+03	1.174E-07	9.05E+02	3.85E-08	3.14E+03
CZ21559	3.22	3.62E-08	2.44E+03	1.15E-07	1.21E+03	1.013E-07	1.05E+03	2.68E-08	4.50E+03
CZ11577	3.36	2.93E-08	3.01E+03	9.88E-08	1.40E+03	8.349E-08	1.27E+03	2.16E-08	5.59E+03

5.3. Estimated activities

An estimation of activity was left optional to the participants. Only the four participants that depended solely on germanium based systems provided activity estimates for most or all lung set – chest overlay combinations. This may be because these participants use commercial detection and software systems, and the activity estimates are provided with relative ease. However, results were reported for one phoswich system (participant C) for selected lung sets measured in the phantom core. Tables showing these results are found in

Annex II. The averaged ratios of participant estimated activity to the reference values results are shown in Figure 19.

Figures 19a and 19b indicate that, at 17 keV, the activity estimates made by participants with germanium detector systems depends on MEQ-CWT, so that the effect of chest wall thickness is not completely taken into account. The increased scatter for the low level ^{238}Pu lungs (Figure 19b), particularly at 43 keV indicates the problems encountered with estimates at this low level. The ^{241}Am estimates (Figure 19c) are consistently about 25% about the reference value for this lung set. This suggests that there may either be an error in the reference value, or the ^{241}Am may not be uniformly distributed through the lung volume. This is supported by the close agreement between estimated and reference values for the 63 keV photons from the natural and 3% enriched ^{235}U lung sets (Figures 19e and 19d). Figures 19 d, 19e and 19f show good agreement between the estimated and reference values for natural thorium, natural uranium and enriched uranium.

5.4. MRIPP

Evaluation of the use of the Magnetic Resonance Image Photon Phantom (MRIPP) for calculation calibration of the participants counting systems was an important aspect of the intercalibration. Copies of the MRIPP software were distributed to most of the participants on CD ROM.

In addition, it was planned that calculations be made using system descriptions and detector specifications provided to the organizers by the participants. The detector configurations provided by the participants are shown in the Country Reports: Description of Participants' Facilities. Point sources of each radionuclide used in the lungs were shipped with the phantom. Participants were instructed to count these in a fixed, well defined position using the same detection system that was used to measure the phantom. It was intended that this data be used to normalize the MRIPP calculations for the participants' systems and compare with the participants' results. For various reasons including lack of adequate counting data, inadequate geometry description and long calculation times, only MRIPP results for only three phoswich detectors are presented here.

The calculation times depend heavily on photon energy and geometry. While the 10^6 photon histories required for the point source calculation may only take 15 to 20 minutes, 5×10^6 histories may be required for 17 keV photons in the phantom lung. This is because many of the photons are lost in interactions with simulated body tissues, and don't reach the detector. As a result, several hours may be required for the low energy photon calculations. However, the time required does drop significantly with increase in energy. Although it is possible to perform calculations with photons of several energies, scattered photons are added to the tallies for lower energy photons so that their results are invalid. Therefore, the calculations need to be conducted one energy at a time.

Calculations for three participants' detectors are shown Tables XXVI–XXXI. These are all single phoswich detectors. However, calculations can be performed for germanium arrays. Participant D reported making measurements with a single detector separately over each lung and summing the results. Table XXVI shows the results of calculations for each lung. The number of photon histories required to achieve the indicated 1 standard deviation error drops significantly with energy from 5×10^6 for 17.1 keV to 1×10^6 for 63 keV. The result, of course, is a drastically reduced computation time. The results for each lung measurement are then summed and compared with the measured results as shown in Table XXVII.

TABLE XXVI. MRIPP MEASUREMENT RESULTS FOR PARTICIPANT SYSTEM D (SINGLE PHOSWICH)

	Right Lung			Left Lung		
Energy - keV	17.1	43	63	17.1	43	63
Number of Photons	5×10^6	2×10^6	1×10^6	5×10^6	2×10^6	1×10^6
	MRIPP correction factors[a]					
Core	4.29×10^{-3}	0.0779	0.0897	3.33×10^{-3}	0.0658	0.0770
1 σ Error	2.40%	0.70%	0.90%	2.70%	0.8%	1.0%
Core + 8 mm 10% adipose	6.92×10^{-4}	0.054	0.0652	5.45×10^{-4}	0.0466	0.0569
1 σError	5.90%	0.90%	1.10%	6.60%	1.0%	1.2%
Core + 8 mm 20% adipose	7.49×10^{-4}	0.0542	0.0654	5.92×10^{-4}	0.047	0.0572
1 σError -%	5.60%	0.90%	1.10%	6.4	1.0%	1.2%
Core + 8 mm 30% adipose	$8.09 10^{-4}$	0.0547	0.0656	6.37×10^{-4}	0.0473	0.0573
1 σ Error -%	5.40%	0.90%	1.10%	6.1	1.0%	1.2%

a) Phantom counts per photon/point source counts/photon.

A similar comparison of MRIPP calculation with measured results for participant F and participant G are shown in Tables XXVIII and XXIX. These three tables show differences of up to a factor of 4, with the MRIPP predictions being consistently lower. The differences decrease with increasing energy. The relationship between the MRIPP results and measurements for the 8mm overlays tends to be nearly constant. Both values increase slightly with increased adipose content due to slightly reduced attenuation coefficients. At this point, the differences can not be explained. One additional point illustrated in Table XXVII is the ratio of the right to left side MRIPP correction factor, ie detection efficiency. This is consistent with the measured values of about 1.1 in the report of the Japanese National Institute of Radiological Sciences (Figure 2). Tables XXX and XXXI illustrate the effect of performing MRIPP calculations with multiple photon energies. The data in table XXX were obtained by running separate calculations for the 43 and 63 keV photons, and comparing the results with single calculations performed with both photon energies.

When both photon energies are used, the scattered 63 keV photons contribute about 4 to 8 percent to the lower energy 43 keV photon tallies. This effect is much more striking for even lower energies. Calculations were made with single 17, 20, 60 and 63 keV photons and with the four energies together (Table XXXI). The scatter of the higher energies photons represent as much as 90% of the 17 keV tallies, and increase the 20 keV tallies two fold

TABLE XXVII. COMPARISON OF MRIPP RESULTS WITH MEASUREMENT RESULTS FOR PARTICIPANT SYSTEM D

	Right/Left Lung Efficiency			JAERI Efficiency/Point Source Efficiency				
	17 keV	43 keV	63 keV	17 keV	43 keV		63 keV	
	MRIPP	MRIPP	MRIPP	MRIPP	MRIPP	Measured	MRIPP	Measured
Core	1.29	1.18	1.16	0.00384	0.0723	0.22	0.0838	0.096
Core + 8 mm 10% adipose	1.27	1.15	1.14	0.000624	0.0506	0.19	0.0614	0.081
Core + 8 mm 20% adipose	1.26	1.15	1.14	0.000676	0.0509	0.18	0.0616	0.079
Core + 8 mm 30% adipose	1.27	1.15	1.14	0.000729	0.0513	0.18	0.0618	0.084

TABLE XXVIII. COMPARISON OF MRIPP RESULTS WITH MEASUREMENT RESULTS FOR PARTICIPANT SYSTEM F

	JAERI Efficiency/Point Source Efficiency						
	17 keV		20 keV	60 keV		63 keV	
	MRIPP	Measured	MRIPP	MRIPP	Measured	MRIPP	Measured
Number of Photons	5×10^6	-	2.5×10^6	1×10^6	-	1×10^6	-
Core	6.47×10^3	8.7×10^{-3}	2.25×10^{-2}	0.197	0.43	0.201	0.28
1 σ error	2.0%	-	1.3%	0.7%	-	0.7%	-
Core + 8 mm 10% adipose	9.46×10^4	3.4×10^{-3}	6.25×10^{-3}	0.136	0.35	0.139	0.24
1 σ error	5.3%	-	2.5%	0.8%	-	0.8%	-
Core + 8 mm 20% adipose	1.03×10^3	3.8×10^{-3}	6.65×10^{-3}	0.137	0.36	0.140	0.25
1 σ error	5.1%	-	2.5%	0.8%	-	0.8%	-
Core + 8 mm 30% adipose	1.12×10^3	4.5×10^{-3}	7.06×10^{-3}	0.137	0.36	0.140	0.25
1 σ error	4.9%	-	2.4%	0.8%	-	0.8%	-

TABLE XXIX. COMPARISON OF MRIPP RESULTS WITH MEASUREMENT RESULTS FOR PARTICIPANT SYSTEM G

	JAERI Efficiency/Point Source Efficiency						
	17 keV		20 keV	60 keV		63 keV	
	MRIPP	Measured	MRIPP	MRIPP	Measured	MRIPP	Measured
Number of Photons	5×10^6	-	2.5×10^6	1×10^6	-	1×10^6	-
Core	6.50×10^{-3}	0.010	2.25×10^{-2}	0.197	0.39	0.200	0.35
1 σ error	2.0%	-	1.3%	0.7%	-	0.7%	
Core + 8 mm 10% adipose	9.50×10^{-4}	4.2×10^{-3}	6.25×10^{-3}	0.136	0.33	0.139	0.30
1 σ error	5.3%	-	2.5%	0.8%	-	0.8%	-
Core + 8 mm 20% adipose	1.07×10^{-3}	4.5×10^{-3}	6.65×10^{-3}	0.137	0.33	0.140	0.31
1 σ error	5.0%	-	2.5%	0.8%	-	0.8%	-
Core + 8 mm 30% adipose	1.12×10^{-3}	5.2×10^{-3}	7.06×10^{-3}	0.137	0.34	0.140	0.31
1 σ error	4.9%	-	2.4%	0.8%	-	0.8%	-

TABLE XXX. COMPARISON OF RESULTS FOR PARTICIPANT SYSTEM D WITH SINGLE AND DUAL PHOTON ENERGY CALCULATIONS (43 AND 63 KEV)

	JAERI Efficiency/Point Source Efficiency							
	Right Lung				Left Lung			
	43 keV		63 keV		43 keV		63 keV	
	Single energy	Dual energies	Single energy	Dual energies	Single energy	Dual energies	Single energy	Dual energies
Core	0.0779	0.0817	0.0897	0.0900	0.0658	0.0686	0.0770	0.0774
Core + 8 mm 10% adipose	0.0540	0.0582	0.0652	0.0645	0.0466	0.0444	0.0569	0.0494
Core + 8 mm 20% adipose	0.0542	0.0586	0.0654	0.0648	0.047	0.0498	0.0572	0.0571
Core + 8 mm 30% adipose	0.0547	0.0592	0.0656	0.0651	0.0473	0.0501	0.0573	0.0574

TABLE XXXI. COMPARISON OF RESULTS FOR PARTICIPANT SYSTEM G WITH SINGLE AND MULTIPLE PHOTON ENERGY CALCULATIONS (17, 20, 60 AND 63 keV)

| | JAERI Efficiency/Point Source Efficiency | | | | | | | |
| | 17 keV | | 20 keV | | 60 keV | | 63 keV | |
	Single Energy	Multiple Energies	Single Energy	Multiple Energies	Single Energy	Multiple Energies	Single Energy	Multiple Energies
Core	6.50×10^3	1.61×10^2	2.25×10^2	3.05×10^2	0.197	0.216	0.200	0.201
Core + 8 mm 10% adipose	9.50×10^4	9.37×10^3	6.25×10^3	1.33×10^2	0.136	0.153	0.139	0.139
Core + 8 mm 20% adipose	1.07×10^3	9.43×10	6.65×10^3	1.37×10^2	0.137	0.154	0.140	0.139
Core + 8 mm 30% adipose	1.12×10^3	9.46×10^3	7.06×10^3	1.40×10^2	0.137	0.155	0.140	0.140
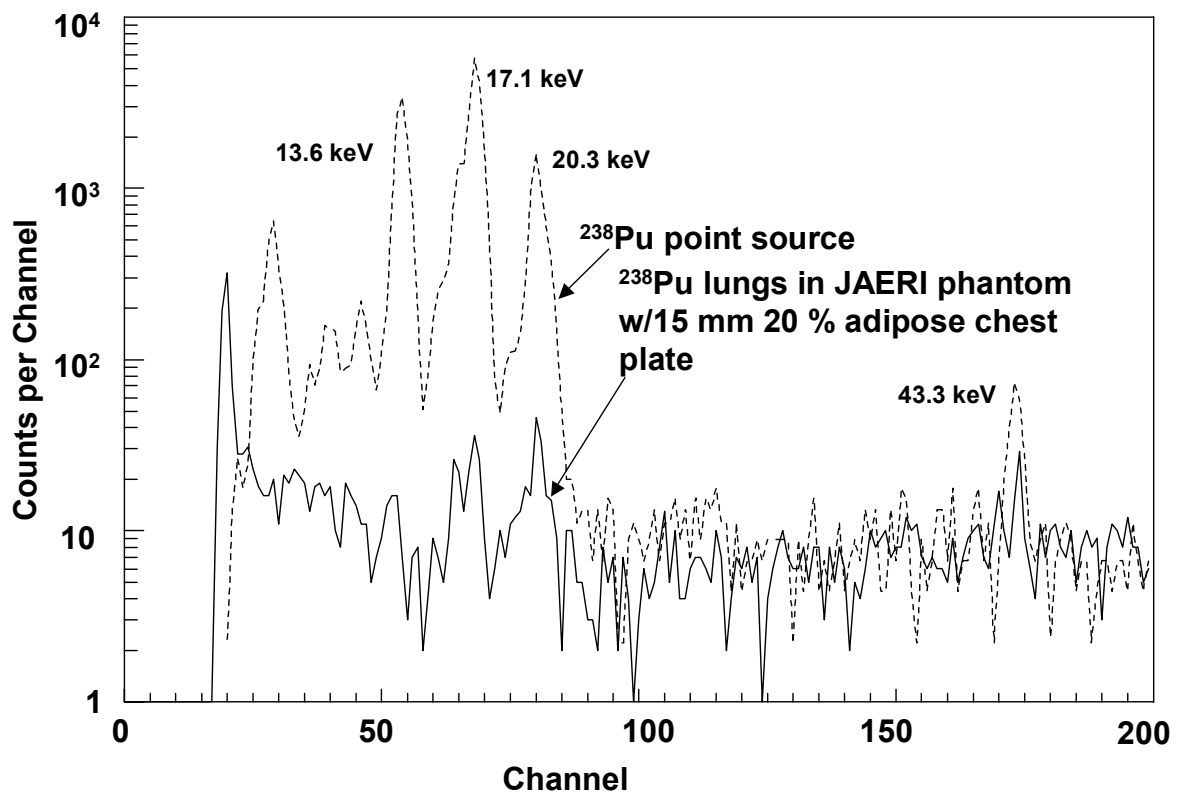
FIG. 14. Comparison of spectra for a ^{238}Pu point source and a ^{238}Pu loaded lung set in phantom, using a germanium detector array.
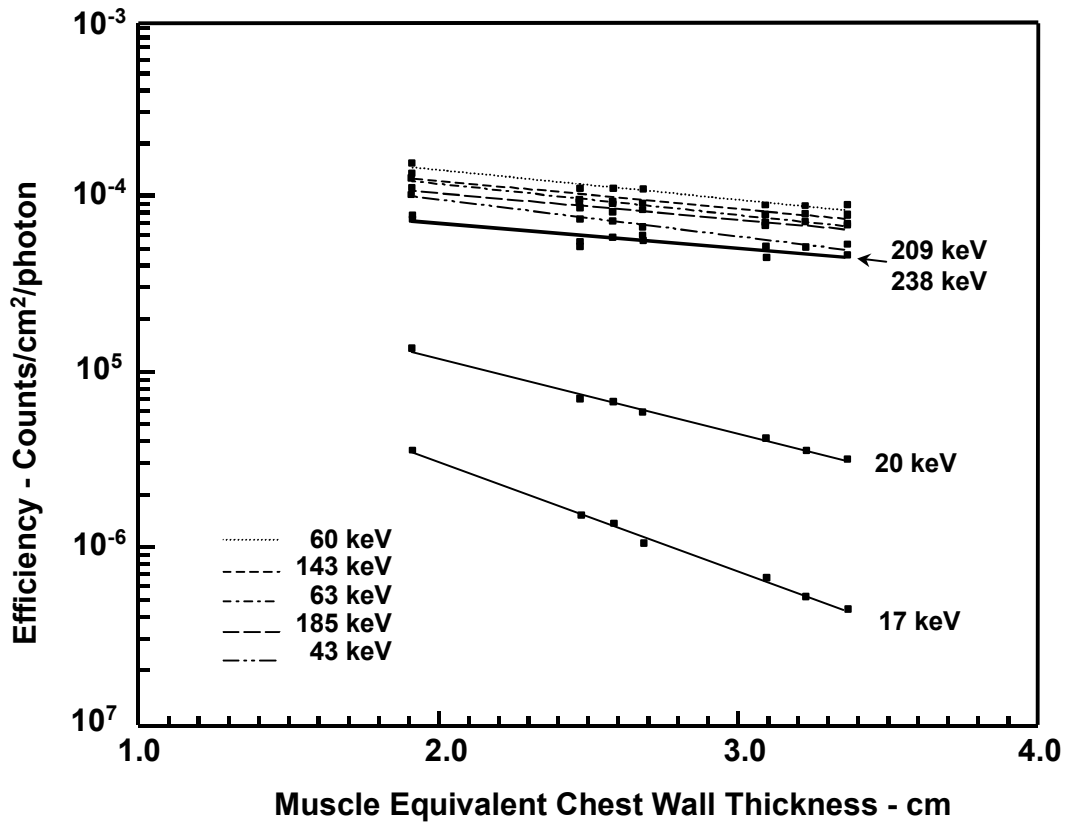
FIG. 15. *Average detection efficiencies for participating germanium detector systems.*
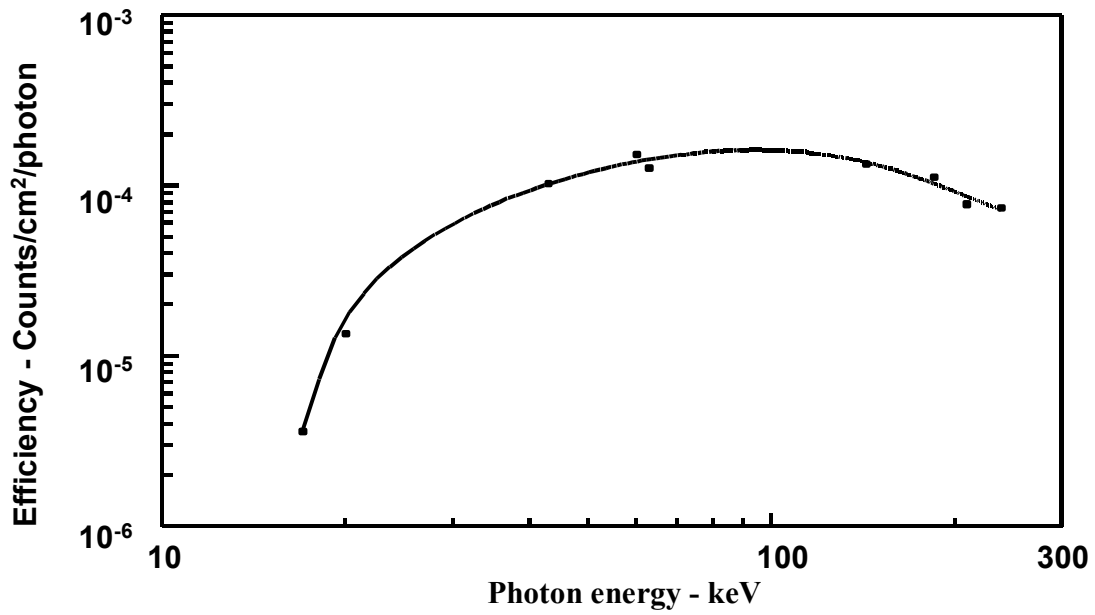
FIG. 16. *Average efficiency of germanium based detection systems for JAERI phantom core.*
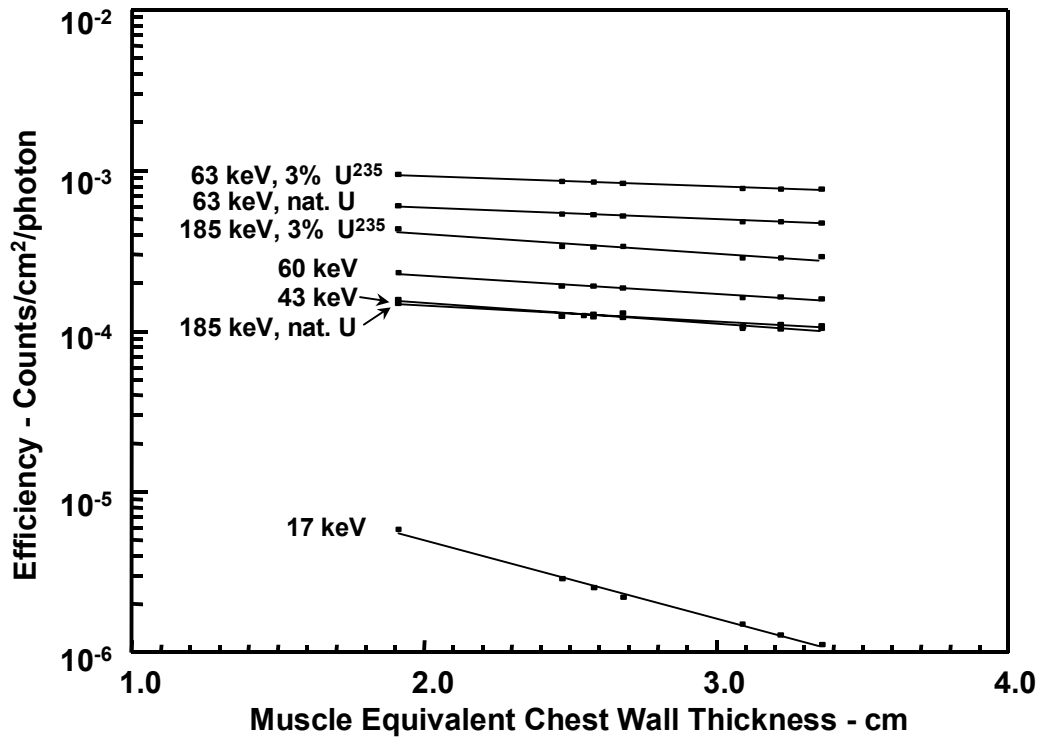
FIG. 17. Average detection efficiencies for participating phoswich detector systems.
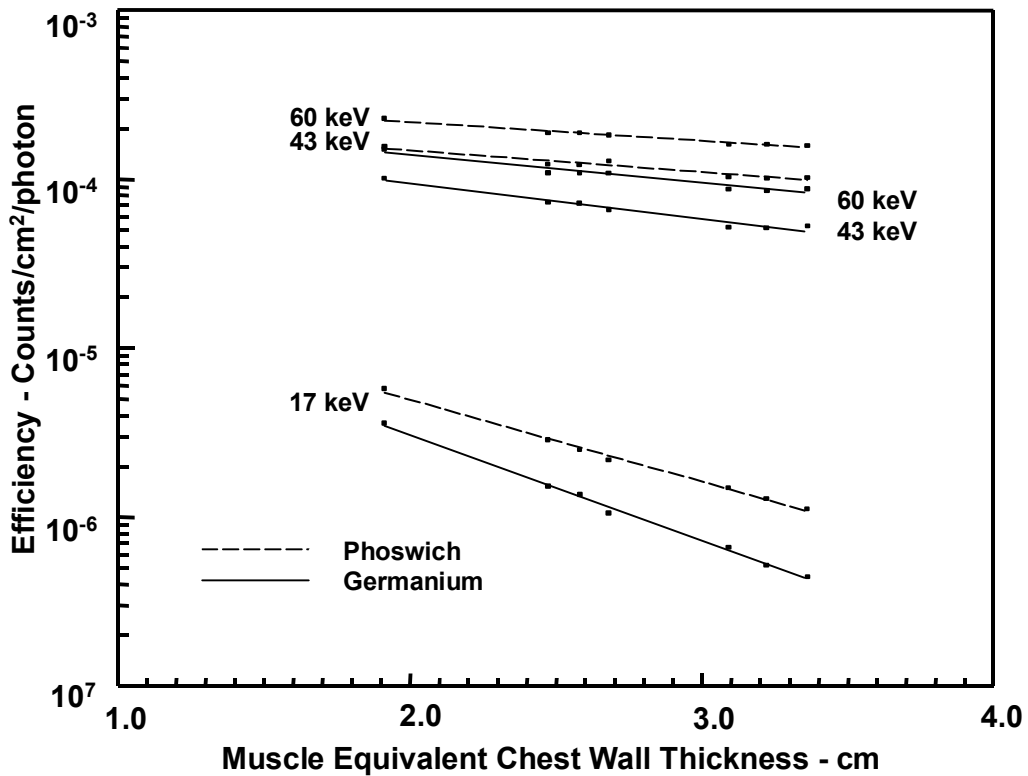
FIG. 18. Comparison of low energy counting efficiencies with phoswich and germanium based counting systems.
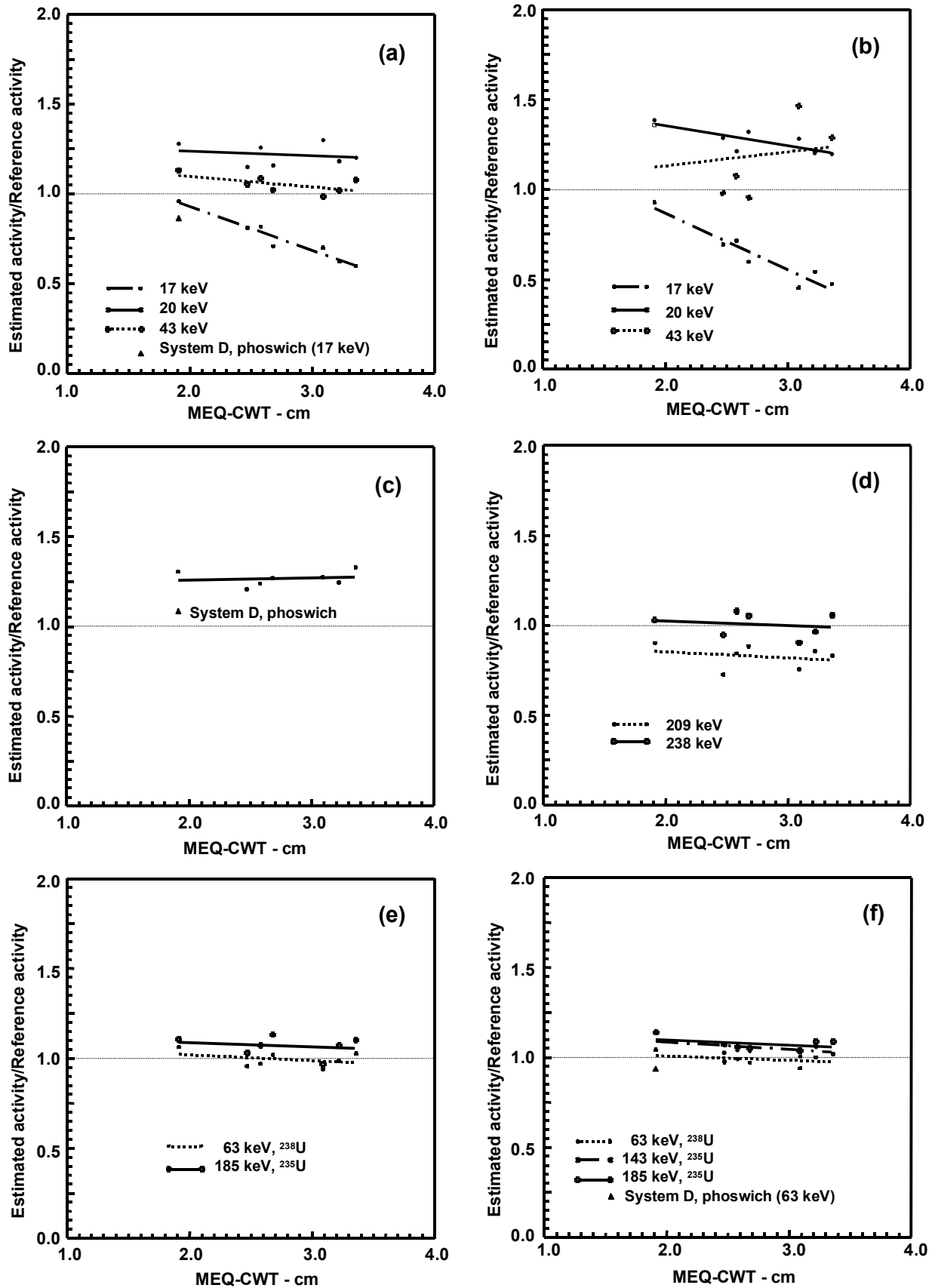
FIG. 19. Ratio of participant estimated activities to reference activities for a) ^{238}Pu (high level), b) ^{238}Pu (low level), c) ^{241}Am, d) natural thorium, e) natural uranium, and f) uranium with 3% ^{235}U enrichment.

6. SUMMARY AND CONCLUSIONS

6.1. General

The intercalibration provided the participants access to unique calibration resources for direct measurement of low energy photon emitting radionuclides in the body. It gave them a valuable opportunity to exchange information and obtain data necessary to improve the performance of their systems. The experience of the CRP was especially useful to Member States with limited previous experience and resources, and provided useful information to improve radiation protection operations. As a result of the CRP, one participant was able to demonstrate to his management that the whole body counting facility was inadequate for the tasks that might be required by the regulatory authority and that it needed to be upgraded.

6.2. Efficiency measurements

- The participants using germanium detector systems achieved reasonable agreement for normalized counting efficiency (counts cm^{-2} $photon^{-1}$).
- The participants using phoswich detectors reports differences of as much as a factor of 4 in normalized efficiency. This may be due to differences in detector placement, and analysis of the poorly resolved phoswich spectra.
- The average normalized efficiencies for the phoswich systems were greater than those for germanium detector arrays.
- Differences in the adipose tissue content of the chest wall overlaying the lungs can be reasonably well compensated by the use of the concept of muscle equivalent chest wall thickness – MEQ-CWT. Although MEQ-CWT is dependent on the energy of the photons in question, MEQ-CWT at 17 keV can be used with a maximum thickness error of about 15% at higher energies. Since the chest wall attenuation at these energies is much less important, this error can be considered acceptable, except in very special situations where very high accuracy may be required.
- The efficiency – MEQ-CWT relationship can be characterized by the exponential, $Efficiency = Be^{-A \bullet MEQ-CWT}$. Typical values of A at 17 keV are greater than one, decreasing to 0.3 or less at energies above 100 keV. When both photon energies are used, the scattered 63 keV photons contribute about 4 to 8 percent to the lower energy 43 keV photon tallies.

6.3. Activity estimates

- Most of the participants using germanium-based systems provided estimates of activity. The reported activity estimates were generally in reasonable agreement with the reference values for each of the lung sets.
- The agreement between estimated activity and the reference values improved for higher energy photon emitters natural uranium, enriched uranium and thorium.
- There was a consistent over estimate of the ^{241}Am loaded lung activities of about 25%. This may indicate either an error in the reference activity assigned to these lungs, or a significant non-uniformity in the distribution of material in the lungs.
- The only participant who reported estimated activity using a phoswich detector also achieved reasonable accuracy, indicating that satisfactory performance can be achieved with these detector systems.
- In general, at 17 keV the agreement between estimated and reference activities got poorer for chest overlays with higher MEQ-CWT, with an increasing tendency toward underestimation.

6.4. Comparison of JAERI and LLNL phantom calibrations

- Those participants who had been involved in the previous CRP with the Livermore phantom reported that there was not a great deal of difference in the calibrations they obtained from the two different phantoms.

- For facilities using large dual-crystal, or "phoswich" detectors, there was very little difference, while for facilities using small high-purity germanium detectors, differences ranged up to 25–40%, depending on the photon energy. This is probably due to differences in the spacing of the ribs in the two phantoms, and therefore in the amount of lung surface viewed by the smaller detectors. Even so, the observed differences in calibration between the two phantoms were less than might have been anticipated considering the differences in the overall size of the phantoms.

- Each of the phantoms has structural deficiencies that must be taken into account in their use. The LLNL phantom has a large heart that blocks a significant fraction of the left lung. This results in a higher ratio of right to left lung counts than would be expected – a factor of two or more. On the other hand, there is a gap between the top edge of the JAERI phantom chest cover and the torso. This can allow streaming of low energy photons (^{238,239}Pu X ray) that would cause errors if detectors are place over or close to the edge of the chest cover. Finally, the JAERI phantom has a recess to accommodate the chest overlays. This is unrealistic, and may cast some doubt on the validity of making measurements without use of one of the overlays.

6.5. MRIPP

- This was the first time the Monte Carlo based computer code, MRIPP has been used an intercalibration programme. In principle, it can be very useful for computational calibration of counting systems. However, the programme proved a bit cumbersome to use, because of very detailed requirements for defining the geometrical relationships among the activity in the lungs and the external detectors, as well as the chest wall thickness and the exact dimensions of the detector materials. However, as participants gain experience with the programme, it may prove to be a valuable adjunct for calibration of detector systems.

- For various reasons, only limited comparison between MRIPP predictions and participant results could be reported. In general, the agreement between the calculations and measurements was very poor, with consistent under estimate by MRIPP.

- The relative results between MRIPP calculations were, however, more satisfactory. For example limited results for right to left lung counting ratios agreed reasonably well with measurements. The same can be said for the change in efficiency with change in adipose content of the overlay.

- One of the most useful applications for MRIPP may be comparative calculations for optimization of detector positioning or similar sensitivity analysis studies.

7. RECOMMENDATIONS

- Future programmes should include calibrations for additional distributions of activity in vivo, such as:
  - material translocated to the axillary lymph nodes from contaminated wounds of the hand
  - activity translocated to the skeleton, which is the primary organ of deposition and retention for transuranic radionuclides that have become systemic.

- Additional emphasis should be placed on intercalibration for uranium and thorium, because many more Member States have operations involving these radionuclides than plutonium and americium.

- Consideration should be given to future calibration/intercomparison activities with specialized phantoms: e.g. bone, liver, lung, LN, GI, etc. or with other phantoms with activity in different organs or the whole body such as the St. Petersburg block phantom used recently by the E.U.

- Steps should be taken to resolve the apparent discrepancy in the reference value of the activity in the ^{241}Am loaded lung set used in this intercalibration. First, the relative activities in lung sets AM1 and AM2 need to be accurately determined. Then one of the lung sets should be destructively assayed using ashing and direct sample counting techniques.

- The reference activities in the other lung sets should also be verified by comparative methods.

REFERENCES

[1]   NEWTON, D., et al. Interlaboratory comparison of techniques for measuring lung burdens of low-energy photon-emitters, Health Phys. **35** (1978) 751–772.

[2]   GRIFFITH, R.V., DEAN, P.N., ANDERSON, A.L., FISHER, J.C., "A tissue-equivalent torso phantom", Advances in Radiation Protection Monitoring (Proc. Conf. Vienna, 1979), IAEA, Vienna (1979) 493–504.

[3]   NEWTON, D., et al. "The Livermore Phantom as a Calibration Standard in the Assessment of Plutonium in Lungs", Assessment of Radioactive Contamination in Man (Proc. Conf. Vienna, 1985), IAEA, Vienna (1985) 183–199.

[4]   TOOHEY, R.E., NEWTON, D., MOISEEV A., BIANCO, A., Personal communication (1991).

[5]   SHIROTANI, T., Realistic torso phantom for calibration of in vivo transuranic nuclide counting facilities, J. Nucl. Sci. Tech. **25** (1988) 875–883.

[6]   BROWNE, E., FIRESTONE, R.B., SHIRLEY, V.S., Table of Radioactive Isotopes, Wiley, New York (1986).

[7]   INTERNATIONAL COMMISSION ON RADIATION UNITS AND MEASUREMENTS, Tissue Substitutes in Radiation Dosimetry and Measurement, Rep. 44, ICRU, Bethesda, MD (1989).

[8]   McMASTER, W.H., KERR DEL GRANDE, N., MALLETT, J.H., HUBBELL, J.H., Compilation of X-ray Cross Sections, Lawrence Radiation Laboratory Rep. UCRL 50174, University of California (1969).

[9]   INTERNATIONAL COMMISSION ON RADIOLOGICAL PROTECTION, Report on Reference Man: Anatomical, Physiological and Metabolic Characteristics, ICRP Publication 23, Pergamon Press, New York (1975).

[10] KRAMER, G.H., HAUCK, B.M., Chest wall thickness measurements of the LLNL and JAERI torso phantoms for germanium counting, Health Phys. **73** (1997) 1–7.

[11] SPITZ, H., et al., Measurement of the Attenuation coefficient for Livermore thoracic phantom lungs fabricated using contemporary materials, Health Phys **67** 1 (1994) 39–46.

[12] GLOVER, S., A Guide to the Fabrication and Evaluation of Lawrence Livermore National Laboratory Phantom Lungs, MS Thesis, College of Engineering, University of Cincinnati, Cincinnati, Ohio (1992).

[13] INTERNATIONAL COMMISSION ON RADIATION UNITS AND MEASUREMENTS, Phantoms and Computational Models in Therapy, Diagnosis and Protection, Rep. 48, ICRU, Bethesda, MD (1992).

[14] AMERICAN NATIONAL STANDARDS INSTITUTE, American National Standard for Performance Criteria for Radiobioassay, ANSI/N13.30 standard, ANSI, New York (1996).

Annex I

DETECTION SYSTEM EFFICIENCY MEASUREMENTS

Tables I-1 to I-6 present the detection efficiency normalized to photon emission in counts per photon. Tables I-7 to I-12 present the normalized sensitivity in terms of counts per photon per cm^2 of detector area. These results are illustrated in Figures I-1 through I-12, which present the participants' detection efficiencies as a function of the muscle equivalent chest wall thickness (MEQ-CWT). The results have been fitted by the equation:

$$Efficiency = Be^{-A\bullet MEQ-CWT}$$

TABLE I-1. DETECTION SENSITIVITY NORMALIZED TO PHOTON EMISSION, Pu-238 (HIGH ACTIVITY)

17 keV			Counts/Photon						
Overlay			None	CZ30826	CZ20853	CZ10879	CZ31541	CZ21559	CZ11577
MEQ-CWT (cm)			1.91	2.47	2.58	2.68	3.09	3.22	3.36
Participant System	Detector Type	Detector Area cm^2							
A	LEGe	154.	3.79E-04	1.75E-04	1.46E-04	1.21E-04	6.07E-05	5.14E-05	4.31E-05
C	LEGe	156.	5.83E-04	2.72E-04	2.38E-04	1.89E-04	1.27E-04	1.09E-04	8.85E-05
F	Phoswich	324.	1.50E-03	7.72E-04	6.65E-04	5.84E-04	4.06E-04	3.48E-04	3.10E-04
G	Phoswich	324.	1.19E-03	6.15E-04	5.34E-04	5.02E-04	3.20E-04	2.72E-04	2.55E-04
J	HPGe	81.7	4.89E-05	-	-	-	-	-	-
M	Phoswich	253.	2.30E-03	1.11E-03	9.74E-04	8.23E-04	5.75E-04	4.96E-04	4.09E-04
N	LEGe	80.	3.38E-04	1.34E-04	1.13E-04	1.00E-04	5.78E-05	4.36E-05	4.19E-05
O	LEGe	120.	4.71E-04	1.89E-04	1.88E-04	1.19E-04	8.93E-05	6.22E-05	5.01E-05
20 keV			Counts/Photon						
Overlay			None	CZ30826	CZ20853	CZ10879	CZ31541	CZ21559	CZ11577
MEQ-CWT (cm)			1.91	2.47	2.58	2.68	3.09	3.22	3.36
Participant System	Detector Type	Detector Area cm^2							
A	LEGe	154.	1.53E-03	8.76E-04	7.98E-04	7.28E-04	4.23E-04	3.80E-04	3.15E-04
C	LEGe	156.	1.87E-03	1.05E-03	9.78E-04	9.38E-04	6.23E-04	6.28E-04	5.14E-04
J	HPGe	81.7	3.65E-04	-	-	-	-	-	-
N	LEGe	80.	1.24E-03	6.36E-04	5.59E-04	5.05E-04	3.41E-04	3.09E-04	2.77E-04
O	LEGe	120.	1.96E-03	9.00E-04	1.02E-03	7.66E-04	6.79E-04	4.62E-04	4.72E-04
43 keV			Counts/Photon						
Overlay			None	CZ30826	CZ20853	CZ10879	CZ31541	CZ21559	CZ11577
MEQ-CWT (cm)			1.91	2.47	2.58	2.68	3.09	3.22	3.36
Participant System	Detector Type	Detector Area cm^2							
A	LEGe	154.	1.18E-02	8.26E-03	8.47E-03	7.73E-03	6.14E-03	6.60E-03	6.11E-03
C	LEGe	156.	1.54E-02	1.19E-02	1.13E-02	1.10E-02	8.99E-03	8.41E-03	8.73E-03
D	Phoswich	253.	4.08E-02	3.28E-02	3.27E-02	3.48E-02	2.68E-02	2.72E-02	2.77E-02
J	HPGe	81.7	5.12E-03	-	-	-	-	-	-
M	Phoswich	253.	3.81E-02	2.98E-02	2.93E-02	3.07E-02	2.56E-02	2.45E-02	2.47E-02
N	LEGe	80.	8.63E-03	6.60E-03	5.97E-03	5.46E-03	4.25E-03	4.42E-03	4.12E-03
O	LEGe	120.	1.50E-02	9.72E-03	1.05E-02	9.17E-03	6.93E-03	6.56E-03	7.71E-03

TABLE I-2. DETECTION SENSITIVITY NORMALIZED TO PHOTON EMISSION, Pu-238 (LOW ACTIVITY)

17 keV			Counts/Photon						
Overlay			None	CZ30826	CZ20853	CZ10879	CZ31541	CZ21559	CZ11577
MEQ-CWT (cm)			1.91	2.47	2.58	2.68	3.09	3.22	3.36
Participant System	Detector Type	Detector Area cm^2							
A	LEGe	154.	3.98E-04	1.52E-04	1.45E-04	1.18E-04		6.22E-05	
C	LEGe	156.	6.02E-04	2.01E-04	1.70E-04	1.48E-04	1.08E-04	9.48E-05	6.49E-05
F	Phoswich	324.	1.68E-03	9.38E-04	7.79E-04	7.69E-04	6.11E-04	5.64E-04	5.18E-04
M	Phoswich	253.	2.02E-03	1.16E-03	8.69E-04	7.42E-04	5.11E-04	5.04E-04	3.62E-04
N	LEGe	80.	2.96E-04	1.19E-04	1.11E-04	6.33E-05	3.35E-05	4.08E-05	5.38E-05
O	LEGe	120.	4.24E-04	1.49E-04	1.16E-04	1.09E-04	8.46E-05	3.66E-05	4.17E-05
20 keV			Counts/Photon						
Overlay			None	CZ30826	CZ20853	CZ10879	CZ31541	CZ21559	CZ11577
MEQ-CWT (cm)			1.91	2.47	2.58	2.68	3.09	3.22	3.36
Participant System	Detector Type	Detector Area cm^2							
A	LEGe	154.	1.69E-03	6.96E-04	6.96E-04	6.46E-04	3.78E-04	3.74E-04	2.85E-04
C	LEGe	156.	2.45E-03	1.22E-03	1.05E-03	8.99E-04	6.95E-04	6.90E-04	5.50E-04
N	LEGe	80.	1.14E-03	5.38E-04	4.98E-04	4.50E-04	3.01E-04	2.58E-04	1.83E-04
O	LEGe	120.	2.23E-03	1.31E-03	9.52E-04	1.10E-03	3.13E-04	5.39E-04	5.39E-04
43 keV			Counts/Photon						
Overlay			None	CZ30826	CZ20853	CZ10879	CZ31541	CZ21559	CZ11577
MEQ-CWT (cm)			1.91	2.47	2.58	2.68	3.09	3.22	3.36
Participant System	Detector Type	Detector Area cm^2							
A	LEGe	154.	1.69E-02	8.52E-03	1.18E-02	1.08E-02	1.12E-02	1.10E-02	8.46E-03
C	LEGe	156.	1.50E-02	3.68E-03	7.66E-03	4.38E-03	6.80E-03	8.64E-03	7.42E-03
D	Phoswich	253.	1.18E-01	1.04E-01	1.13E-01	1.08E-01	1.08E-01	9.01E-02	1.05E-01
N	LEGe	80.	1.10E-02	5.89E-03	5.89E-03	4.66E-03	7.27E-03	6.20E-03	6.21E-03
O	LEGe	120.	1.59E-02	1.18E-02	1.04E-02	8.14E-03	9.24E-03	5.36E-03	7.58E-03

TABLE I-3. DETECTION SENSITIVITY NORMALIZED TO PHOTON EMISSION, Am-241

60 keV			Counts/Photon						
Overlay			None	CZ30826	CZ20853	CZ10879	CZ21541	CZ31559	CZ11577
MEQ-CWT (cm)			1.91	2.47	2.58	2.68	3.09	3.22	3.36
Participant System	**Detector Type**	**Detector Area cm^2**							
A	LEGe	154.	1.73E-02	1.27E-02	1.26E-02	1.30E-02	1.02E-02	1.00E-02	9.97E-03
B	NaI	127.	1.96E-02	1.07E-02	1.32E-02	8.86E-03	1.51E-02	1.16E-02	7.54E-03
C	LEGe	156.	2.54E-02	1.85E-02	1.83E-02	1.79E-02	1.46E-02	1.44E-02	1.43E-02
D	Phoswich	253.	6.58E-02	5.35E-02	5.28E-02	5.18E-02	4.52E-02	4.48E-02	4.27E-02
F	Phoswich	324.	7.06E-02	5.95E-02	5.91E-02	5.70E-02	5.08E-02	5.11E-02	5.05E-02
G	Phoswich	324.	5.76E-02	4.98E-02	4.84E-02	4.84E-02	4.25E-02	4.22E-02	4.12E-02
H	Phoswich	206.	4.12E-02	3.48E-02	-	-	2.83E-02	-	-
I	Thin NaI	253.	6.16E-02	5.14E-02	-	-	4.43E-02	-	-
J	HPGe	81.7	9.92E-03	-	-	-	-	-	-
M	Phowich	253.	6.65E-02	5.40E-02	5.53E-02	5.35E-02	4.50E-02	4.60E-02	4.60E-02
N	LEGe	80.	1.25E-02	9.01E-03	8.69E-03	8.56E-03	7.13E-03	7.06E-03	7.19E-03
O	LEGe	120.	2.12E-02	1.53E-02	1.57E-02	1.59E-02	1.23E-02	1.18E-02	1.30E-02

TABLE I-4. DETECTION SENSITIVITY NORMALIZED TO PHOTON EMISSION, NATURAL URANIUM

Th-234 — 63 keV			Counts/Photon						
Overlay			None	CZ30826	CZ20853	CZ10879	CZ31541	CZ21559	CZ11577
MEQ-CWT (cm)			1.91	2.47	2.58	2.68	3.09	3.22	3.36
Participant System	Detector Type	Detector Area cm^2							
A	LEGe	154.	1.39E-02	9.73E-03	1.03E-02	-	7.48E-03	7.57E-03	7.61E-03
C	LEGe	156.	1.96E-02	1.50E-02	1.39E-02	1.47E-02	1.18E-02	1.16E-02	1.20E-02
D	Phoswich	253.	5.76E-02	5.04E-02	4.72E-02	4.84E-02	4.25E-02	4.17E-02	4.02E-02
F	Phoswich	324.	2.59E-01	2.30E-01	2.32E-01	2.26E-01	2.08E-01	2.09E-01	2.04E-01
G	Phoswich	324.	2.61E-01	2.31E-01	2.31E-01	2.25E-01	2.07E-01	2.05E-01	2.06E-01
H	Phoswich	206.	1.94E-01	1.68E-01	-	-	1.48E-01	-	-
I	Thin NaI	253.	1.79E-01	1.48E-01	-	-	1.27E-01	-	-
M	Phoswich	253.	1.52E-01	1.32E-01	1.31E-01	1.29E-01	1.19E-01	1.19E-01	1.18E-01
N	LEGe	80.	1.07E-02	7.45E-03	7.62E-03	7.51E-03	5.87E-03	5.87E-03	5.92E-03
O	LEGe	120.	1.91E-02	1.33E-02	1.30E-02	1.30E-02	9.84E-03	1.03E-02	9.97E-03
U-235 — 185 keV			Counts/Photon						
Overlay			None	CZ30826	CZ20853	CZ10879	CZ31541	CZ21559	CZ11577
MEQ-CWT (cm)			1.91	2.47	2.58	2.68	3.09	3.22	3.36
Participant System	Detector Type	Detector Area cm^2							
A	LEGe	154.	1.35E-02	9.18E-03	1.05E-02	1.05E-02	7.11E-03	7.94E-03	7.91E-03
B	NaI	127.	2.30E-02	1.01E-02	7.67E-03	1.14E-02	7.82E-03	1.36E-02	8.43E-03
C	LEGe	156.	1.96E-02	1.49E-02	1.50E-02	1.45E-02	1.22E-02	1.23E-02	1.25E-02
E	NaI	324.	7.37E-02	6.33E-02	6.19E-02	6.04E-02	5.20E-02	5.21E-02	4.71E-02
F	Phoswich	324.	5.72E-02	4.91E-02	4.99E-02	4.66E-02	4.26E-02	4.34E-02	4.31E-02
H	Phoswich	206.	4.00E-02	3.35E-02	-	-	2.79E-02	-	-
I	Thin NaI	253.	4.82E-02	4.04E-02	-	-	3.54E-02	-	-
M	Phoswich	253.	3.10E-02	2.52E-02	2.54E-02	2.50E-02	2.12E-02	2.18E-02	2.09E-02
N	LEGe	80.	8.62E-03	6.98E-03	7.03E-03	6.67E-03	5.61E-03	5.44E-03	5.66E-03
O	LEGe	120.	1.39E-02	1.14E-02	8.72E-03	1.16E-02	8.40E-03	9.21E-03	8.53E-03

TABLE I-5. DETECTION SENSITIVITY NORMALIZED TO PHOTON EMISSION, 3% ENRICHED URANIUM

Th-234 — 63 keV			Counts/Photon						
Overlay			None	CZ30826	CZ20853	CZ10879	CZ31541	CZ21559	CZ11577
MEQ-CWT (cm)			1.91	2.47	2.58	2.68	3.09	3.22	3.36
Participant System	Detector Type	Detector Area cm^2							
A	LEGe	154.	1.40E-02	1.03E-02	9.70E-03	7.55E-03	7.71E-03	8.02E-03	7.67E-03
C	LEGe	156.	2.02E-02	1.55E-02	1.47E-02	1.49E-02	1.18E-02	1.20E-02	1.18E-02
D	Phoswich	253.	5.57E-02	4.99E-02	4.83E-02	4.75E-02	4.62E-02	4.53E-02	4.39E-02
F	Phoswich	324.	4.35E-01	3.96E-01	3.92E-01	3.88E-01	3.58E-01	3.56E-01	3.55E-01
G	Phoswich	324.	4.34E-01	3.96E-01	3.91E-01	3.87E-01	3.55E-01	3.52E-01	3.52E-01
H	Phoswich	206.	3.25E-01	2.87E-01	-	-	2.59E-01	-	-
I	Thin NaI	253.	3.74E-01	3.26E-01	-	-	2.89E-01	-	-
M	Phoswich	253.	2.24E-01	2.00E-01	1.98E-01	1.97E-01	1.85E-01	1.85E-01	1.81E-01
N	LEGe	80.	1.03E-02	7.32E-03	7.78E-03	7.64E-03	5.63E-03	5.67E-03	6.00E-03
O	LEGe	120.	1.80E-02	1.35E-02	1.30E-02	1.29E-02	1.01E-02	1.05E-02	9.71E-03
U-235 — 143 keV			**Counts/Photon**						
Overlay			None	CZ30826	CZ20853	CZ10879	CZ31541	CZ21559	CZ11577
MEQ-CWT (cm)			1.91	2.47	2.58	2.68	3.09	3.22	3.36
Participant System	Detector Type	Detector Area cm^2							
A	LEGe	154.	1.53E-02	1.08E-02	9.69E-03	8.62E-03	8.56E-03	9.17E-03	9.14E-03
C	LeGe	156.	2.18E-02	1.64E-02	1.68E-02	1.68E-02	1.36E-02	1.39E-02	1.34E-02
E	NaI	324.	1.46E-01	1.28E-01	1.34E-01	1.28E-01	1.13E-01	1.17E-01	1.13E-01
N	LEGe	80.	1.09E-02	7.74E-03	7.77E-03	7.94E-03	6.00E-03	6.37E-03	6.09E-03
O	LEGe	120.	1.86E-02	1.33E-02	1.32E-02	1.27E-02	1.09E-02	1.01E-02	1.07E-02
U-235 — 185 keV			**Counts/Photon**						
Overlay			None	CZ30826	CZ20853	CZ10879	CZ31541	CZ21559	CZ11577
MEQ-CWT (cm)			1.91	2.47	2.58	2.68	3.09	3.22	3.36
Participant System	Detector Type	Detector Area cm^2							
A	LEGe	154.	1.40E-02	9.93E-03	8.27E-03	7.75E-03	8.52E-03	8.42E-03	8.18E-03
B	NaI	127.	1.10E-02	1.02E-02	1.08E-02	9.24E-03	8.58E-03	1.02E-02	9.69E-03
C	LEGe	156.	1.89E-02	1.51E-02	1.50E-02	1.50E-02	1.24E-02	1.25E-02	1.25E-02
E	NaI	324.	5.45E-02	4.53E-02	4.56E-02	4.56E-02	3.85E-02	3.91E-02	3.88E-02
F	Phoswich	324.	4.56E-02	3.83E-02	3.90E-02	3.86E-02	3.29E-02	3.27E-02	3.28E-02
H	Phoswich	206.	3.40E-02	2.84E-02	-	-	2.44E-02	-	-
I	Thin NaI	253.	4.56E-02	3.60E-02	-	-	3.09E-02	-	-
M	Phoswich	253.	1.84E-01	1.40E-01	1.39E-01	1.39E-01	1.18E-01	1.19E-01	1.21E-01
N	LEGe	80.	8.77E-03	6.95E-03	6.51E-03	6.52E-03	5.14E-03	5.26E-03	5.36E-03
O	LEGe	120.	1.51E-02	1.11E-02	1.12E-02	1.06E-02	8.66E-03	8.96E-03	8.31E-03

TABLE I-6. DETECTION SENSITIVITY NORMALIZED TO PHOTON EMISSION, NATURAL THORIUM

Ac-228 — 209 keV			Counts/Photon						
Overlay			None	CZ30826	CZ20853	CZ10879	CZ31541	CZ21559	CZ11577
MEQ-CWT (cm)			1.91	2.47	2.58	2.68	3.09	3.22	3.36
Participant System	**Detector Type**	**Detector Area cm²**							
A	LEGe	154.	1.02E-02	6.48E-03	7.27E-03	5.35E-03	4.25E-03	6.66E-03	4.23E-03
C	LEGe	156.	1.36E-02	9.39E-03	9.87E-03	1.14E-02	9.49E-03	8.41E-03	9.83E-03
N	LEGe	80.	6.12E-03	4.25E-03	4.36E-03	5.22E-03	3.64E-03	4.54E-03	3.60E-03
O	LEGe	120.	9.65E-03	6.14E-03	7.96E-03	7.90E-03	5.47E-03	5.60E-03	6.21E-03
Pb-212 — 238 keV			**Counts/Photon**						
Overlay			None	CZ30826	CZ20853	CZ10879	CZ31541	CZ21559	CZ11577
MEQ-CWT (cm)			1.91	2.47	2.58	2.68	3.09	3.22	3.36
Participant System	**Detector Type**	**Detector Area cm²**							
A	LEGe	154.	9.21E-03	6.08E-03	7.32E-03	6.13E-03	4.13E-03	6.08E-03	4.63E-03
B	NaI	127.	7.47E-03	4.79E-03	5.54E-03	5.38E-03	4.02E-03	3.86E-03	4.26E-03
C	LEGe	156.	1.38E-02	1.08E-02	1.10E-02	1.09E-02	9.06E-03	9.37E-03	9.07E-03
E	NaI	324.	7.08E-02	6.55E-02	6.06E-02	6.27E-02	5.64E-02	5.71E-02	5.58E-02
K	NaI	324.	6.56E-02	5.86E-02	5.95E-02	6.12E-02	5.76E-02	5.62E-02	5.69E-02
L	NaI	649.	1.22E-01	-	-	-	-	-	-
M	Phoswich	253.	8.18E-03	8.01E-03	6.71E-03	6.69E-03	5.40E-03	6.36E-03	5.65E-03
N	LEGe	80.	5.55E-03	4.68E-03	4.32E-03	4.38E-03	3.57E-03	3.53E-03	3.68E-03
O	LEGe	120.	9.20E-03	6.56E-03	6.96E-03	6.93E-03	5.70E-03	5.50E-03	5.87E-03
Ac-288 — 911 keV			**Counts/Photon**						
Overlay			None	CZ30826	CZ20853	CZ10879	CZ31541	CZ21559	CZ11577
MEQ-CWT (cm)			1.91	2.47	2.58	2.68	3.09	3.22	3.36
Participant System	**Detector Type**	**Detector Area cm²**							
B	NaI	127.	1.89E-02	8.31E-03	6.30E-03	9.39E-03	6.42E-03	1.12E-02	6.92E-03
E	NaI	324.	5.30E-02	4.85E-02	4.66E-02	4.62E-02	4.26E-02	4.38E-02	4.33E-02
K	NaI	324.	2.20E-02	1.95E-02	1.99E-02	2.04E-02	1.99E-02	1.85E-02	1.88E-02
L	NaI	649.	3.99E-02	-	-	-	-	-	-
O	LEGe	120.	6.98E-04	-	-	-	-	-	-
Tl-208 — 2614 keV			**Counts/Photon**						
Overlay			None	CZ30826	CZ20853	CZ10879	CZ31541	CZ21559	CZ11577
MEQ-CWT (cm)			1.91	2.47	2.58	2.68	3.09	3.22	3.36
Partipant System	**Detector Type**	**Detector Area cm²**							
E	NaI	324.3	4.84E-03	4.48E-03	4.51E-03	4.43E-03	3.97E-03	4.22E-03	4.01E-03
K	NaI	324.3	9.52E-03	8.52E-03	8.79E-03	8.82E-03	8.82E-03	7.96E-03	8.02E-03
L	NaI	648.6	1.70E-02	-	-	-	-	-	-

TABLE I-7. DETECTION SENSITIVITY NORMALIZED TO PHOTON EMISSION, Pu-238 (HIGH ACTIVITY)

17 keV		Counts/Photon/cm^2						
Overlay		None	CZ30826	CZ20853	CZ10879	CZ31541	CZ21559	CZ11577
MEQ-CWT (cm)		1.91	2.47	2.58	2.68	3.09	3.22	3.36
Participant System	**Detector Type**							
A	LEGe	2.46E-06	1.14E-06	9.46E-07	7.88E-07	3.94E-07	3.34E-07	2.80E-07
C	LEGe	3.74E-06	1.74E-06	1.52E-06	1.21E-06	8.17E-07	6.99E-07	5.67E-07
F	Phoswich	4.62E-06	2.38E-06	2.05E-06	1.80E-06	1.25E-06	1.07E-06	9.56E-07
G	Phoswich	3.67E-06	1.90E-06	1.65E-06	1.55E-06	9.87E-07	8.40E-07	7.86E-07
J	HPGe	5.99E-07	-	-	-	-	-	-
M	Phoswich	9.10E-06	4.37E-06	3.85E-06	3.25E-06	2.27E-06	1.96E-06	1.61E-06
N	LEGe	4.23E-06	1.67E-06	1.41E-06	1.25E-06	7.22E-07	5.45E-07	5.24E-07
O	LEGe	3.92E-06	1.57E-06	1.57E-06	9.93E-07	7.44E-07	5.19E-07	4.17E-07
20 keV		Counts/Photon/cm^2						
Overlay		None	CZ30826	CZ20853	CZ10879	CZ31541	CZ21559	CZ11577
MEQ-CWT (cm)		1.91	2.47	2.58	2.68	3.09	3.22	3.36
Participant System	**Detector Type**							
A	LEGe	9.91E-06	5.69E-06	5.19E-06	4.73E-06	2.75E-06	2.47E-06	2.05E-06
C	LEGe	1.20E-05	6.72E-06	6.27E-06	6.01E-06	4.00E-06	4.02E-06	3.30E-06
J	HPGe	4.47E-06	-	-	-	-	-	-
N	LEGe	1.55E-05	7.96E-06	6.98E-06	6.31E-06	4.26E-06	3.86E-06	3.46E-06
O	LEGe	1.63E-05	7.50E-06	8.52E-06	6.38E-06	5.66E-06	3.85E-06	3.94E-06
43 keV		Counts/Photon/cm^2						
Overlay		None	CZ30826	CZ20853	CZ10879	CZ31541	CZ21559	CZ11577
MEQ-CWT (cm)		1.91	2.47	2.58	2.68	3.09	3.22	3.36
Participant System	**Detector Type**							
A	LEGe	7.69E-05	5.36E-05	5.50E-05	5.02E-05	3.99E-05	4.29E-05	3.97E-05
C	LEGe	9.88E-05	7.64E-05	7.23E-05	7.06E-05	5.76E-05	5.39E-05	5.60E-05
D	Phoswich	1.61E-04	1.30E-04	1.29E-04	1.38E-04	1.06E-04	1.08E-04	1.09E-04
J	HPGe	6.27E-05	-	-	-	-	-	-
M	Phoswich	1.51E-04	1.18E-04	1.16E-04	1.21E-04	1.01E-04	9.69E-05	9.75E-05
N	LEGe	1.08E-04	8.26E-05	7.46E-05	6.83E-05	5.32E-05	5.52E-05	5.15E-05
O	LEGe	1.25E-04	8.10E-05	8.71E-05	7.64E-05	5.78E-05	5.46E-05	6.42E-05

TABLE I-8. DETECTION SENSITIVITY NORMALIZED TO PHOTON EMISSION, Pu-238 (LOW ACTIVITY)

17 keV		Counts/Photon/cm^2						
Overlay		None	CZ30826	CZ20853	CZ10879	CZ31541	CZ21559	CZ11577
MEQ-CWT (cm)		1.91	2.47	2.58	2.68	3.09	3.22	3.36
Participant System	Detector Type							
A	LEGe	2.58E-06	9.86E-07	9.39E-07	7.64E-07	0.00E+00	4.04E-07	0.00E+00
C	LEGe	3.86E-06	1.29E-06	1.09E-06	9.45E-07	6.92E-07	6.08E-07	4.16E-07
F	Phoswich	5.19E-06	2.90E-06	2.40E-06	2.37E-06	1.89E-06	1.74E-06	1.60E-06
M	Phoswich	8.00E-06	4.59E-06	3.43E-06	2.93E-06	2.02E-06	1.99E-06	1.43E-06
N	LEGe	3.70E-06	1.49E-06	1.39E-06	7.91E-07	4.19E-07	5.10E-07	6.72E-07
O	LEGe	3.54E-06	1.24E-06	9.67E-07	9.05E-07	7.05E-07	3.05E-07	3.47E-07
20 keV		**Counts/Photon/cm^2**						
Overlay		None	CZ30826	CZ20853	CZ10879	CZ31541	CZ21559	CZ11577
MEQ-CWT (cm)		1.91	2.47	2.58	2.68	3.09	3.22	3.36
Participant System	Detector Type							
A	LEGe	1.10E-05	4.52E-06	4.52E-06	4.20E-06	2.46E-06	2.43E-06	1.85E-06
C	LEGe	1.57E-05	7.80E-06	6.72E-06	5.76E-06	4.46E-06	4.42E-06	3.52E-06
N	LEGe	1.43E-05	6.73E-06	6.22E-06	5.63E-06	3.76E-06	3.23E-06	2.28E-06
O	LEGe	1.86E-05	1.09E-05	7.94E-06	9.14E-06	2.61E-06	4.49E-06	4.49E-06
43 keV		**Counts/Photon/cm^2**						
Overlay		None	CZ30826	CZ20853	CZ10879	CZ31541	CZ21559	CZ11577
MEQ-CWT (cm)		1.91	2.47	2.58	2.68	3.09	3.22	3.36
Participant System	Detector Type							
A	LEGe	1.10E-04	5.54E-05	7.65E-05	7.03E-05	7.28E-05	7.14E-05	5.50E-05
C	LEGe	9.63E-05	2.36E-05	4.91E-05	2.81E-05	4.36E-05	5.54E-05	4.76E-05
D	Phoswich	4.66E-04	4.11E-04	4.47E-04	4.27E-04	4.27E-04	3.56E-04	4.15E-04
N	LEGe	1.38E-04	7.37E-05	7.36E-05	5.82E-05	9.09E-05	7.75E-05	7.76E-05
O	LEGe	1.33E-04	9.85E-05	8.62E-05	6.78E-05	7.70E-05	4.46E-05	6.32E-05

TABLE I-9. DETECTION SENSITIVITY NORMALIZED TO PHOTON EMISSION, Am-241

60 keV		Counts/Photon/cm^2						
Overlay		None	CZ30826	CZ20853	CZ10879	CZ31541	CZ21559	CZ11577
MEQ-CWT (cm)		1.91	2.47	2.58	2.68	3.09	3.22	3.36
Participant System	**Detector Type**							
A	LEGe	1.12E-04	8.25E-05	8.19E-05	8.42E-05	6.62E-05	6.53E-05	6.48E-05
B	NaI	1.54E-04	8.42E-05	1.04E-04	6.97E-05	1.19E-04	9.10E-05	5.93E-05
C	LEGe	1.63E-04	1.19E-04	1.18E-04	1.15E-04	9.33E-05	9.23E-05	9.16E-05
D	Phoswich	2.60E-04	2.11E-04	2.09E-04	2.05E-04	1.79E-04	1.77E-04	1.69E-04
F	Phoswich	2.18E-04	1.83E-04	1.82E-04	1.76E-04	1.57E-04	1.58E-04	1.56E-04
G	Phoswich	1.78E-04	1.54E-04	1.49E-04	1.49E-04	1.31E-04	1.30E-04	1.27E-04
H	Phoswich	2.00E-04	1.68E-04	-	-	1.37E-04	-	-
I	Thin NaI	2.43E-04	2.03E-04	-	-	1.75E-04	-	-
J	HPGe	1.21E-04	-	-	-	-	-	-
M	Phoswich	2.63E-04	2.13E-04	2.19E-04	2.11E-04	1.78E-04	1.82E-04	1.82E-04
N	LEGe	1.56E-04	1.13E-04	1.09E-04	1.07E-04	8.91E-05	8.83E-05	8.99E-05
O	LEGe	1.76E-04	1.27E-04	1.31E-04	1.33E-04	1.02E-04	9.80E-05	1.08E-04

TABLE I-10. DETECTION SENSITIVITY NORMALIZED TO PHOTON EMISSION, NATURAL URANIUM

Th-234 — 63 keV		Counts/Photon/cm^2						
Overlay		None	CZ30826	CZ20853	CZ10879	CZ31541	CZ21559	CZ11577
MEQ-CWT (cm)		1.91	2.47	2.58	2.68	3.09	3.22	3.36
Participant System	Detector Type							
A	LEGe	9.05E-05	6.32E-05	6.71E-05	6.72E-05	4.86E-05	4.92E-05	4.94E-05
C	LEGe	1.25E-04	9.61E-05	8.94E-05	9.39E-05	7.54E-05	7.41E-05	7.67E-05
D	Phoswich	2.27E-04	1.99E-04	1.86E-04	1.91E-04	1.68E-04	1.65E-04	1.59E-04
F	Phoswich	7.97E-04	7.08E-04	7.15E-04	6.97E-04	6.41E-04	6.44E-04	6.29E-04
G	Phoswich	8.05E-04	7.11E-04	7.13E-04	6.94E-04	6.38E-04	6.33E-04	6.35E-04
H	Phoswich	9.37E-04	8.16E-04	-	-	7.15E-04	-	-
I	Thin NaI	7.08E-04	5.84E-04	-	-	5.01E-04	-	-
M	Phoswich	5.99E-04	5.20E-04	5.19E-04	5.11E-04	4.72E-04	4.68E-04	4.67E-04
N	LEGe	1.34E-04	9.32E-05	9.53E-05	9.39E-05	7.33E-05	7.33E-05	7.40E-05
O	LEGe	1.59E-04	1.11E-04	1.08E-04	1.08E-04	8.20E-05	8.55E-05	8.31E-05
U-235 — 185 keV		Counts/Photon/cm^2						
Overlay		None	CZ30826	CZ20853	CZ10879	CZ31541	CZ21559	CZ11577
MEQ-CWT (cm)		1.91	2.47	2.58	2.68	3.09	3.22	3.36
Participant System	Detector Type							
A	LEGe	8.74E-05	5.96E-05	6.80E-05	6.84E-05	4.62E-05	5.16E-05	5.14E-05
B	NaI	1.81E-04	7.96E-05	6.04E-05	9.00E-05	6.16E-05	1.07E-04	6.63E-05
C	LEGe	1.26E-04	9.58E-05	9.62E-05	9.32E-05	7.80E-05	7.90E-05	8.02E-05
E	NaI	2.27E-04	1.95E-04	1.91E-04	1.86E-04	1.60E-04	1.61E-04	1.45E-04
F	Phoswich	1.76E-04	1.51E-04	1.54E-04	1.44E-04	1.31E-04	1.34E-04	1.33E-04
H	Phoswich	1.93E-04	1.62E-04	-	-	1.35E-04	-	-
I	Thin NaI	1.90E-04	1.59E-04	-	-	1.40E-04	-	-
M	Phoswich	1.23E-04	9.94E-05	1.00E-04	9.88E-05	8.38E-05	8.60E-05	8.26E-05
N	LEGe	1.08E-04	8.73E-05	8.78E-05	8.34E-05	7.02E-05	6.80E-05	7.07E-05
O	LEGe	1.16E-04	9.53E-05	7.27E-05	9.63E-05	7.00E-05	7.67E-05	7.11E-05

TABLE I-11. DETECTION SENSITIVITY NORMALIZED TO PHOTON EMISSION, 3% ENRICHED URANIUM

Th-234 — 63 keV		Counts/Photon/cm^2						
Overlay		None	CZ30826	CZ20853	CZ10879	CZ31541	CZ21559	CZ11577
MEQ-CWT (cm)		1.91	2.47	2.58	2.68	3.09	3.22	3.36
Participant System	**Detector Type**							
A	LEGe	9.08E-05	6.67E-05	6.30E-05	4.90E-05	5.01E-05	5.21E-05	4.98E-05
C	LEGe	1.30E-04	9.91E-05	9.45E-05	9.53E-05	7.53E-05	7.67E-05	7.57E-05
D	Phoswich	2.20E-04	1.97E-04	1.91E-04	1.87E-04	1.82E-04	1.79E-04	1.73E-04
F	Phoswich	1.34E-03	1.22E-03	1.21E-03	1.19E-03	1.10E-03	1.10E-03	1.09E-03
G	Phoswich	1.34E-03	1.22E-03	1.20E-03	1.19E-03	1.10E-03	1.08E-03	1.09E-03
H	Phoswich	1.57E-03	1.39E-03	-	-	1.25E-03	-	-
I	Thin NaI	1.48E-03	1.29E-03	-	-	1.14E-03	-	-
M	Phoswich	8.86E-04	7.92E-04	7.82E-04	7.77E-04	7.30E-04	7.33E-04	7.16E-04
N	LEGe	1.29E-04	9.14E-05	9.73E-05	9.55E-05	7.03E-05	7.09E-05	7.50E-05
O	LEGe	1.50E-04	1.12E-04	1.08E-04	1.08E-04	8.45E-05	8.71E-05	8.09E-05
U-235 — 143 keV		**Counts/Photon/cm^2**						
Overlay		None	CZ30826	CZ20853	CZ10879	CZ31541	CZ21559	CZ11577
MEQ-CWT (cm)		1.91	2.47	2.58	2.68	3.09	3.22	3.36
Participant System	**Detector Type**							
A	LEGe	9.91E-05	7.02E-05	6.30E-05	5.60E-05	5.56E-05	5.95E-05	5.94E-05
C	LEGe	1.40E-04	1.05E-04	1.08E-04	1.08E-04	8.71E-05	8.91E-05	8.59E-05
E	NaI	4.49E-04	3.95E-04	4.13E-04	3.93E-04	3.50E-04	3.62E-04	3.49E-04
N	LEGe	1.36E-04	9.68E-05	9.71E-05	9.93E-05	7.50E-05	7.96E-05	7.62E-05
O	LEGe	1.55E-04	1.11E-04	1.10E-04	1.06E-04	9.08E-05	8.38E-05	8.91E-05
U-235 — 185 keV		**Counts/Photon/cm^2**						
Overlay		None	CZ30826	CZ20853	CZ10879	CZ31541	CZ21559	CZ11577
MEQ-CWT (cm)		1.91	2.47	2.58	2.68	3.09	3.22	3.36
Participant System	**Detector Type**							
A	LEGe	9.11E-05	6.45E-05	5.37E-05	5.03E-05	5.53E-05	5.47E-05	5.32E-05
B	NaI	8.62E-05	8.04E-05	8.47E-05	7.28E-05	6.75E-05	8.00E-05	7.63E-05
C	LEGe	1.21E-04	9.69E-05	9.62E-05	9.63E-05	7.93E-05	8.04E-05	8.01E-05
E	NaI	1.68E-04	1.40E-04	1.41E-04	1.41E-04	1.19E-04	1.20E-04	1.20E-04
F	Phoswich	1.41E-04	1.18E-04	1.20E-04	1.19E-04	1.02E-04	1.01E-04	1.01E-04
H	Phoswich	1.64E-04	1.37E-04	-	-	1.18E-04	-	-
I	Thin NaI	1.80E-04	1.42E-04	-	-	1.22E-04	-	-
M	Phoswich	7.26E-04	5.53E-04	5.49E-04	5.50E-04	4.68E-04	4.70E-04	4.80E-04
N	LEGe	1.10E-04	8.68E-05	8.13E-05	8.16E-05	6.42E-05	6.57E-05	6.70E-05
O	LEGe	1.26E-04	9.22E-05	9.31E-05	8.81E-05	7.22E-05	7.47E-05	6.93E-05

TABLE I-12. DETECTION SENSITIVITY NORMALIZED TO PHOTON EMISSION, NATURAL THORIUM

Ac-228 — 209 keV		Counts/Photon/cm^2						
Overlay		None	CZ30826	CZ20853	CZ10879	CZ31541	CZ21559	CZ11577
MEQ-CWT (cm)		1.91	2.47	2.58	2.68	3.09	3.22	3.36
Participant System	Detector Type							
A	LEGe	6.62E-05	4.21E-05	4.72E-05	3.47E-05	2.76E-05	4.33E-05	2.75E-05
C	LEGe	8.72E-05	6.02E-05	6.32E-05	7.29E-05	6.08E-05	5.39E-05	6.30E-05
N	LEGe	7.65E-05	5.31E-05	5.46E-05	6.52E-05	4.56E-05	5.68E-05	4.50E-05
O	LEGe	8.04E-05	5.12E-05	6.64E-05	6.58E-05	4.56E-05	4.67E-05	5.17E-05
Pb-212 — 238 keV		Counts/Photon/cm^2						
Overlay		None	CZ30826	CZ20853	CZ10879	CZ31541	CZ21559	CZ11577
MEQ-CWT (cm)		1.91	2.47	2.58	2.68	3.09	3.22	3.36
Participant System	Detector Type							
A	LEGe	5.98E-05	3.95E-05	4.76E-05	3.98E-05	2.68E-05	3.95E-05	3.01E-05
B	NaI	5.88E-05	3.77E-05	4.36E-05	4.24E-05	3.17E-05	3.04E-05	3.35E-05
C	LEGe	8.83E-05	6.90E-05	7.06E-05	6.97E-05	5.81E-05	6.01E-05	5.81E-05
E	NaI	2.18E-04	2.02E-04	1.87E-04	1.93E-04	1.74E-04	1.76E-04	1.72E-04
K	NaI	2.02E-04	1.81E-04	1.84E-04	1.89E-04	1.78E-04	1.73E-04	1.76E-04
L	NaI	1.88E-04	-	-	-	-	-	-
M	Phoswich	3.23E-05	3.17E-05	2.65E-05	2.64E-05	2.13E-05	2.51E-05	2.23E-05
N	LEGe	6.94E-05	5.85E-05	5.39E-05	5.47E-05	4.46E-05	4.41E-05	4.60E-05
O	LEGe	7.67E-05	5.46E-05	5.80E-05	5.77E-05	4.75E-05	4.58E-05	4.89E-05
Ac-228 — 911 keV		Counts/Photon/cm^2						
Overlay		None	CZ30826	CZ20853	CZ10879	CZ31541	CZ21559	CZ11577
MEQ-CWT (cm)		1.91	2.47	2.58	2.68	3.09	3.22	3.36
Participant System	Detector Type							
E	NaI	1.64E-04	1.49E-04	1.44E-04	1.42E-04	1.31E-04	1.35E-04	1.33E-04
K	NaI	6.79E-05	6.02E-05	6.14E-05	6.30E-05	6.14E-05	5.71E-05	5.80E-05
L	NaI	6.15E-05	-	-	-	-	-	-
O	LEGe	2.74E-06	-	-	-	-	-	-
Tl-208 — 2614 keV		Counts/Photon/cm^2						
Overlay		None	CZ30826	CZ20853	CZ10879	CZ31541	CZ21559	CZ11577
MEQ-CWT (cm)		1.91	2.47	2.58	2.68	3.09	3.22	3.36
Participant System	Detector Type							
E	NaI	1.49E-05	1.38E-05	1.39E-05	1.37E-05	1.23E-05	1.30E-05	1.24E-05
K	NaI	2.94E-05	2.63E-05	2.71E-05	2.72E-05	2.57E-05	2.46E-05	2.48E-05
L	NaI	2.62E-05	-	-	-	-	-	-
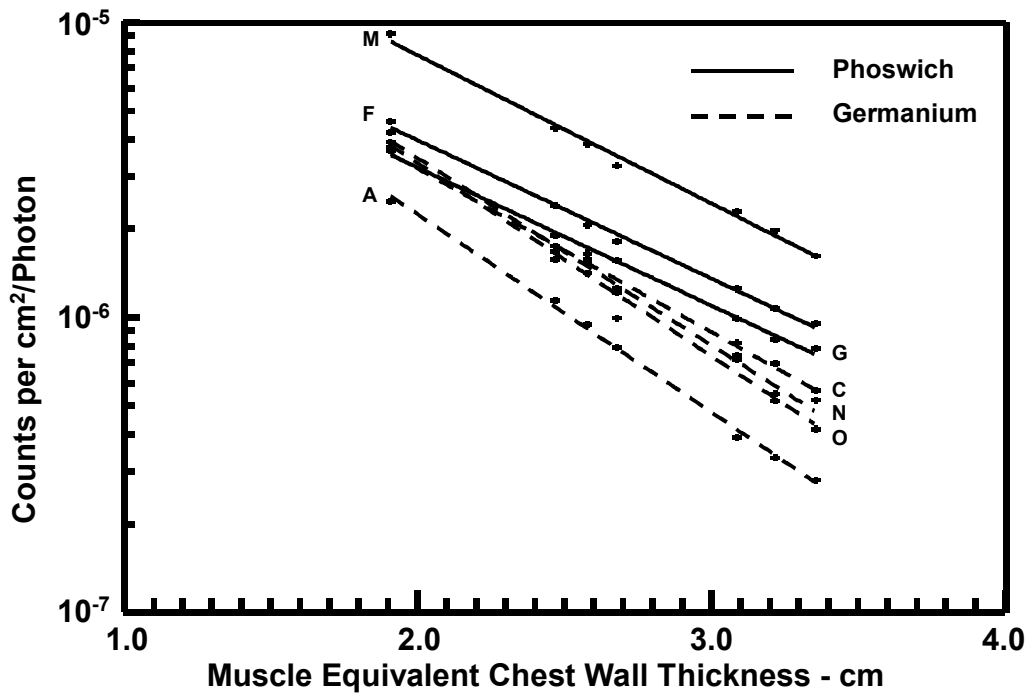
FIG. I-1. Detection efficiency for ^{238}Pu - 17 keV.
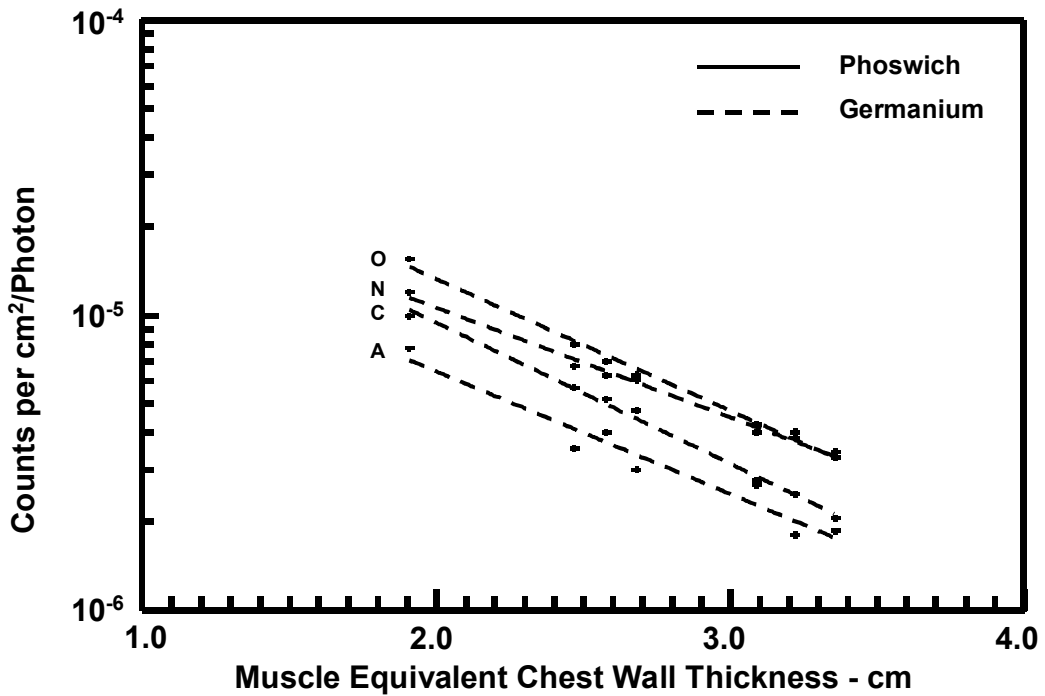
FIG. I-2. Detection efficiency for ^{238}Pu - 20 keV.
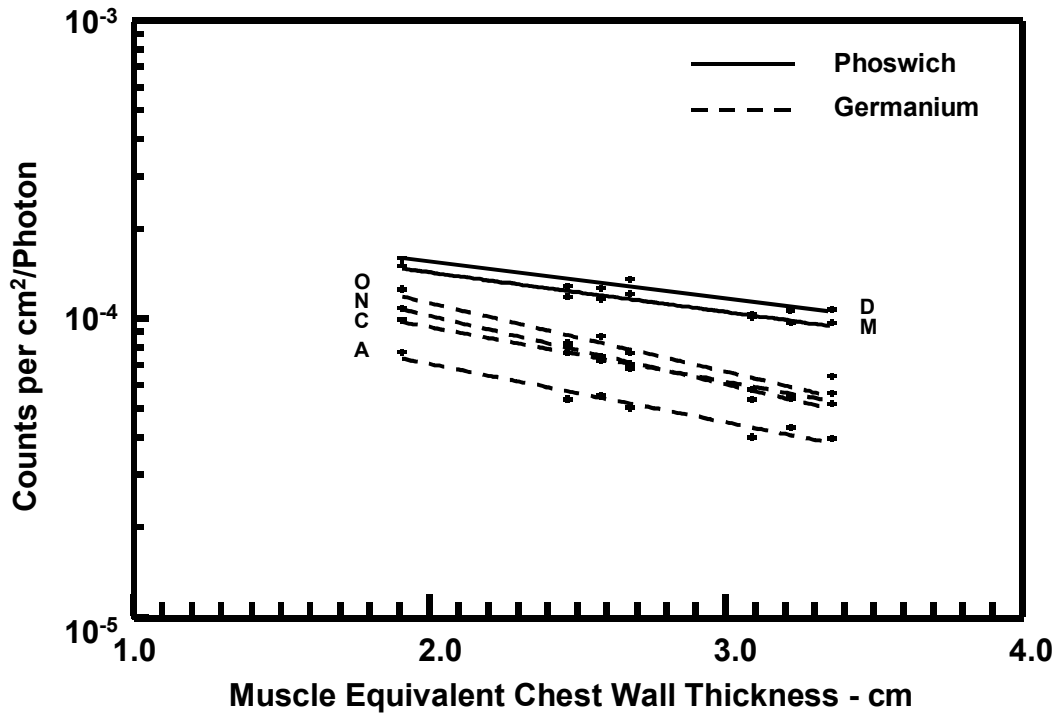
FIG. I-3. Detection efficiency for ^{238}Pu - 43 keV.
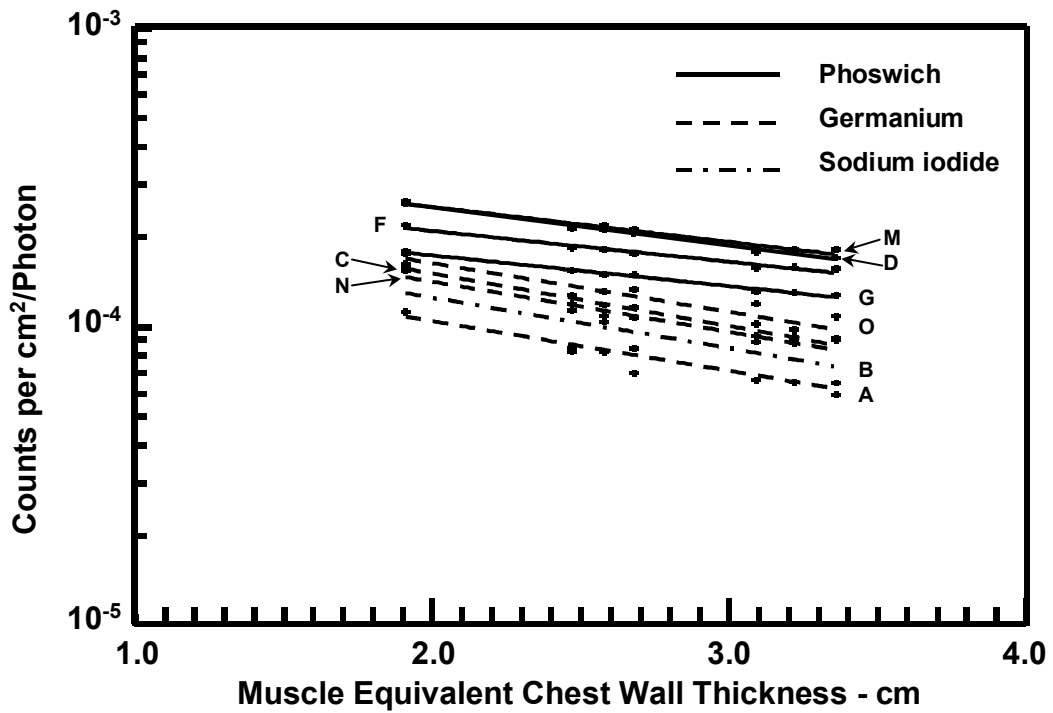
FIG. I-4. Detection efficiency for ^{241}Am - 60 keV.
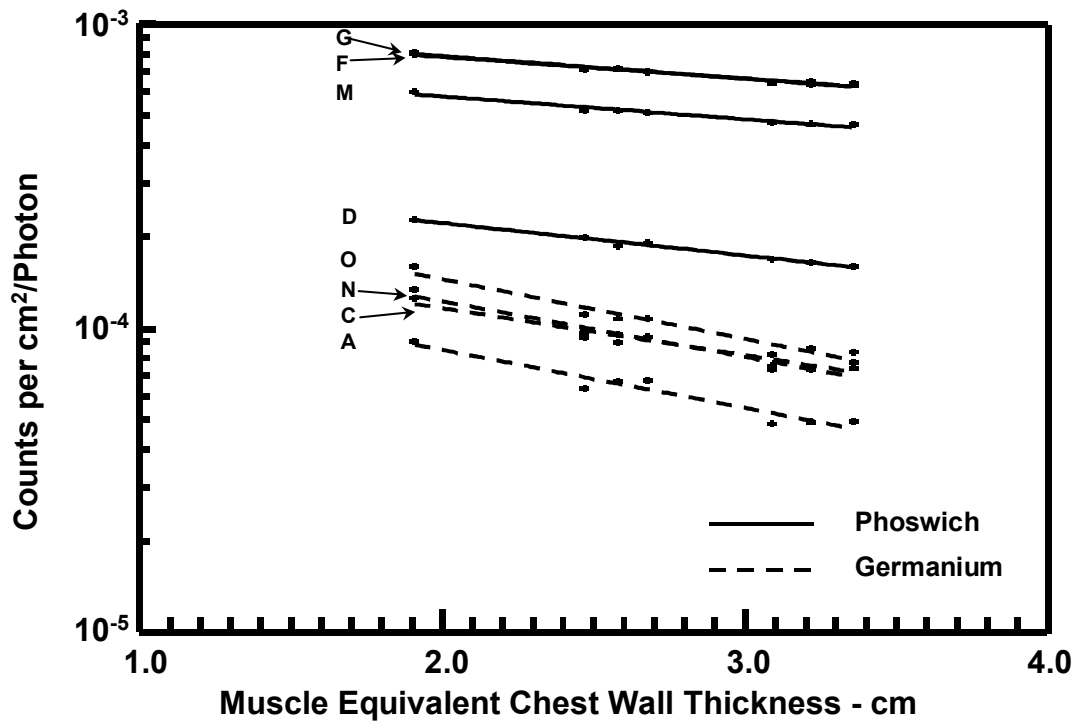
FIG. I-5. Detection efficiency for ^{234}Th - 63 keV (Natural uranium lungs).
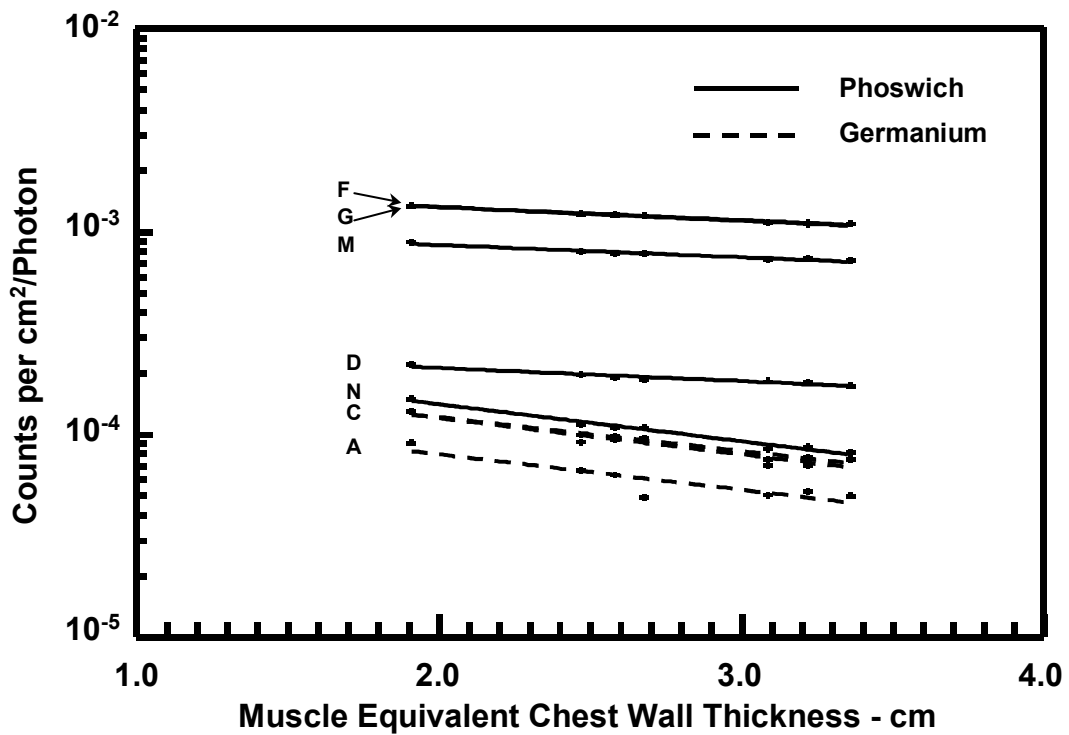
FIG. I-6. Detection efficiency for ^{234}Th - 63 keV (3% enriched ^{235}U lungs).

58
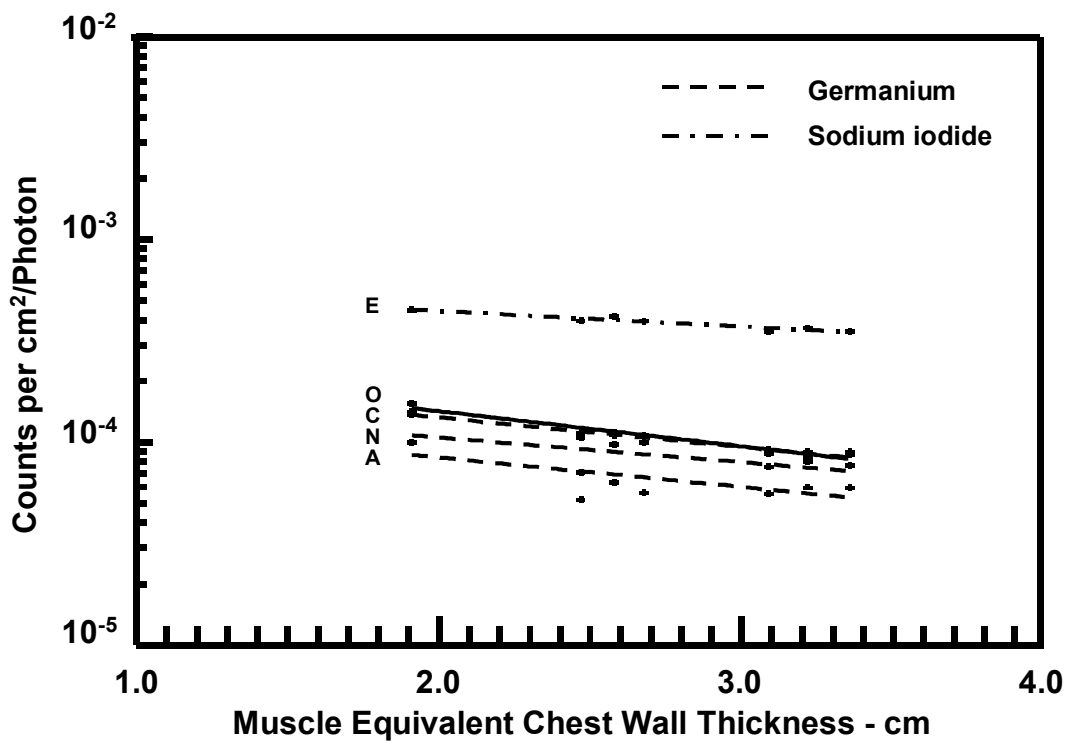
FIG. I-7. Detection efficiency for ^{235}U - 143 keV (3% enriched ^{235}U lungs).
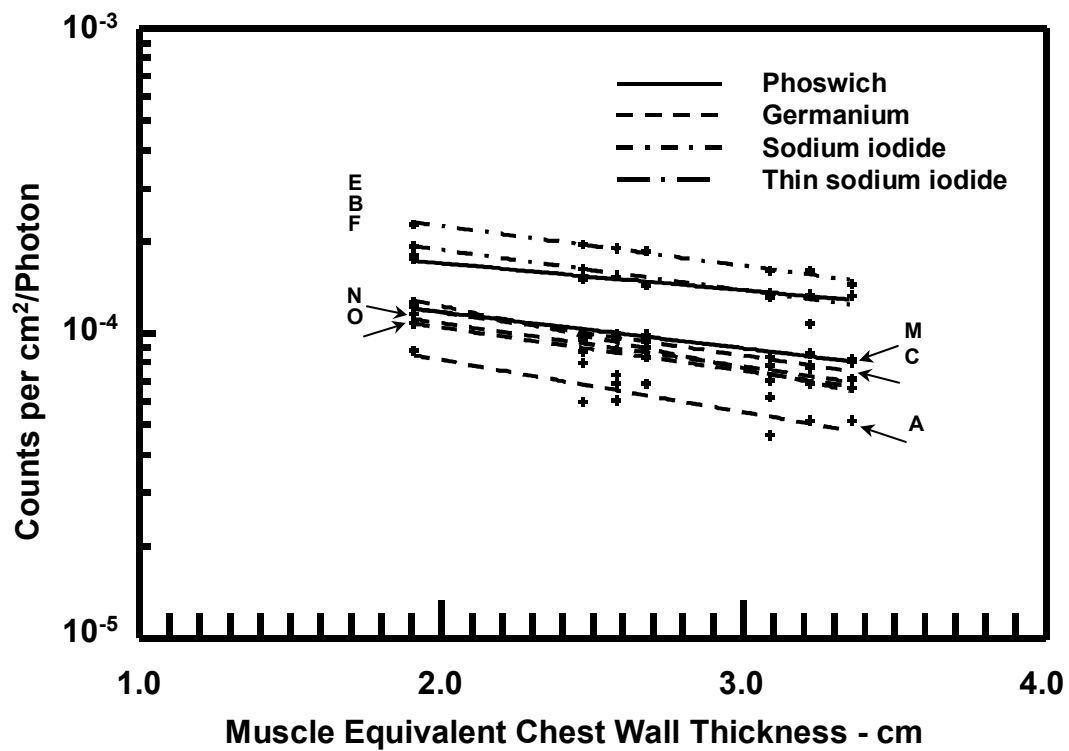
FIG. I-8. Detection efficiency for ^{235}U - 185 keV (Natural uranium lungs).
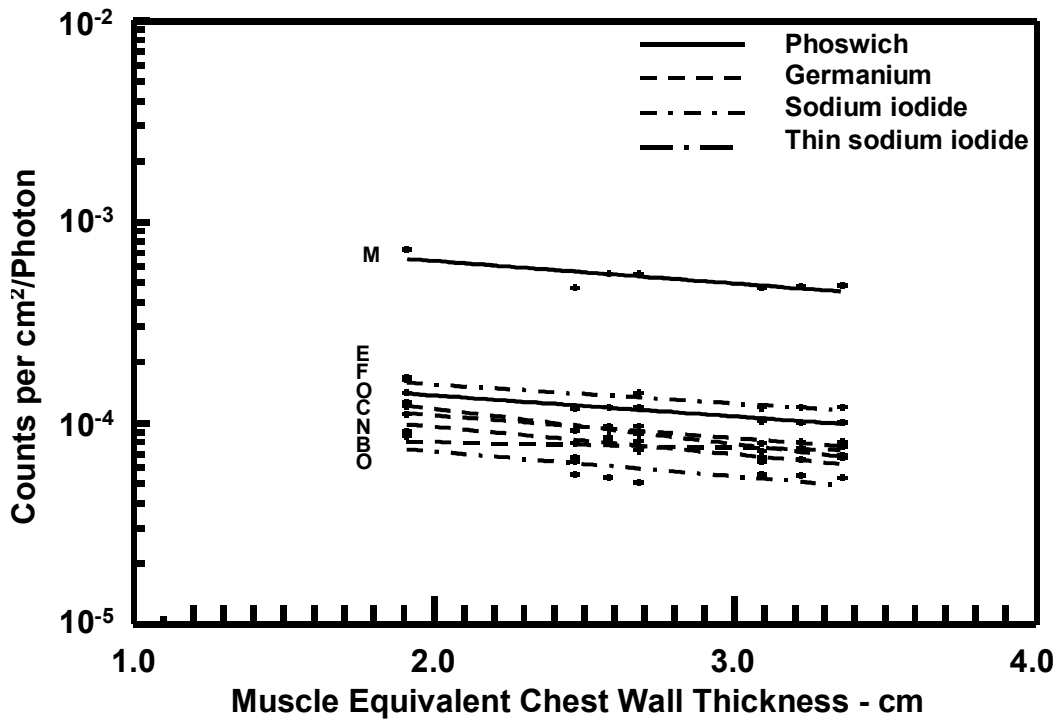
FIG. I-9. Detection efficiency for ^{235}U - 185 keV (3% enriched ^{235}U lungs).
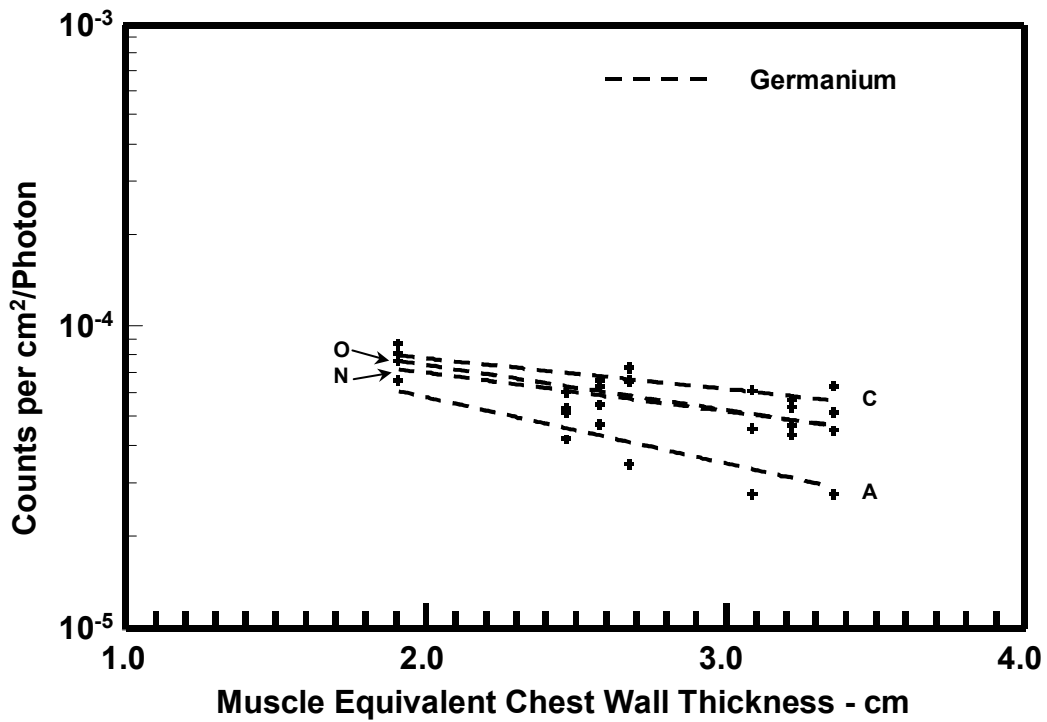
FIG. I-10. Detection efficiency for ^{228}Ac - 209 keV.
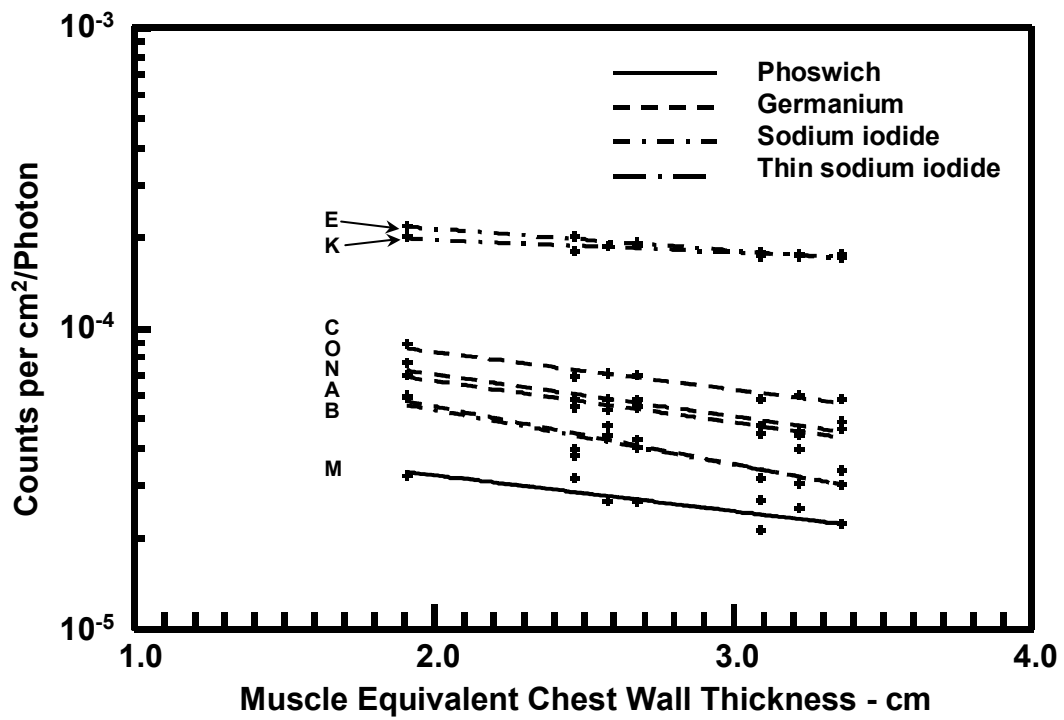
FIG. I-11. Detection efficiency for ^{212}Pb - 238 keV.
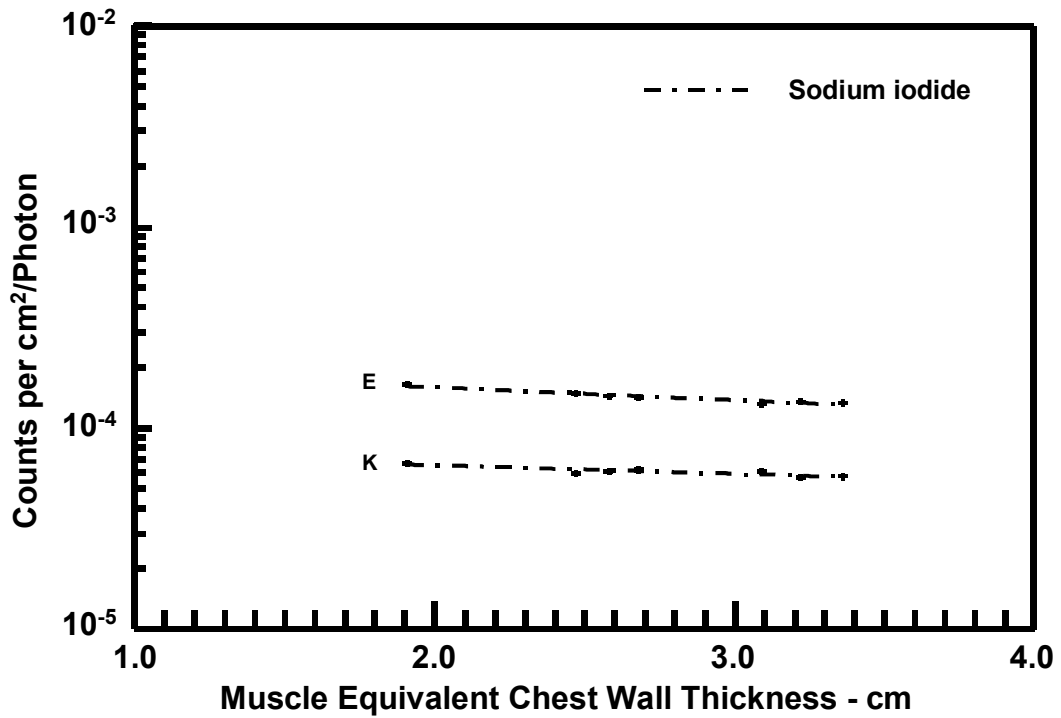
FIG. I-12. Detection efficiency for ^{228}Ac - 911 keV.

Annex II

PARTICIPANTS' ESTIMATES OF ACTIVITIES

As an optional aspect of the intercalibration, the participants were asked to provide estimates of the activities in each of the lung sets. Only four participants using commercial LEGe systems provided these estimates for most lungs and geometries. In addition, estimates determined using one phoswich system were provided for the phantom core only and selected lung sets. Estimates were reported as being on the based of the indicated photons. The tables summarizing these results follow.

TABLE II-1. RATIO OF PARTICIPANT ACTIVITY ESTIMATES TO REFERENCE ACTIVITY VALUES FOR ^{238}Pu (HIGH LEVEL LUNG SET)

Chest Overlays		Participating detection system					Average	Minimum	Maximum
I.D.	MEQ-CWT cm	A	C	D	N	O			
17 keV		Reference Activity = 4.08E+4 Bq							
None	1.91	0.98	0.32	0.86	1.40	1.14	0.94	0.32	1.40
CZ30826	2.47	0.87	0.31	-	1.15	0.91	0.81	0.31	1.15
CZ20853	2.58	0.82	0.35	-	1.07	1.03	0.82	0.35	1.07
CZ10879	2.68	0.77	0.28	-	1.04	0.74	0.71	0.28	1.04
CZ31541	3.09	0.62	0.30	-	0.99	0.89	0.70	0.30	0.99
CZ21559	3.22	0.61	0.28	-	0.88	0.71	0.62	0.28	0.88
CZ11577	3.36	0.61	0.18	-	0.94	0.66	0.60	0.18	0.94
20 keV		Reference Activity = 4.08e+4 Bq							
None	1.91	1.08	0.59	-	1.46	1.98	1.28	0.59	1.98
CZ30826	2.47	0.99	0.63	-	1.31	1.68	1.15	0.63	1.68
CZ20853	2.58	0.99	0.67	-	1.25	2.12	1.26	0.67	2.12
CZ10879	2.68	0.98	0.66	-	1.21	1.79	1.16	0.66	1.79
CZ31541	3.09	0.80	0.68	-	1.19	2.52	1.30	0.68	2.52
CZ21559	3.22	0.80	0.73	-	1.20	1.98	1.18	0.73	1.98
CZ11577	3.36	0.75	0.51	-	1.20	2.35	1.20	0.51	2.35
43 keV		Reference Activity = 4.08e+4 Bq							
None	1.91	0.89	0.96	-	1.17	1.50	1.13	0.89	1.50
CZ30826	2.47	0.77	1.07	-	1.14	1.23	1.05	0.77	1.23
CZ20853	2.58	0.82	1.06	-	1.08	1.38	1.09	0.82	1.38
CZ10879	2.68	0.78	1.02	-	1.02	1.27	1.02	0.78	1.27
CZ31541	3.09	0.73	1.13	-	0.94	1.14	0.98	0.73	1.14
CZ21559	3.22	0.82	1.08	-	1.03	1.14	1.02	0.82	1.14
CZ11577	3.36	0.80	1.08	-	1.01	1.42	1.08	0.80	1.42

TABLE II-2. RATIO OF PARTICIPANT ACTIVITY ESTIMATES TO REFERENCE ACTIVITY VALUES FOR ^{238}Pu (LOW LEVEL LUNG SET)

Chest Overlays		Participating Detection System				Average	Minimum	Maximum
I.D.	MEQ-CWT cm	A	C	N	O			
17 keV		Reference Activity = 4.63E+3 Bq ^{238}Pu						
None	1.91	1.03	0.34	1.21	1.14	0.93	0.34	1.21
CZ30826	2.47	0.75	0.28	0.96	0.79	0.69	0.28	0.96
CZ20853	2.58	0.82	0.32	1.02	0.70	0.71	0.32	1.02
CZ10879	2.68	0.75	0.26	0.64	0.74	0.60	0.26	0.75
CZ31541	3.09	0.00	0.31	0.56	0.93	0.45	0.00	0.93
CZ21559	3.22	0.74	0.25	0.72	0.46	0.54	0.25	0.74
CZ11577	3.36	0.00	0.18	1.10	0.62	0.47	0.00	1.10
20 keV		Reference Activity = 4.63E+3 Bq ^{238}Pu						
None	1.91	1.20	0.76	1.33	2.25	1.39	0.76	2.25
CZ30826	2.47	0.79	0.85	1.07	2.44	1.29	0.79	2.44
CZ20853	2.58	0.86	0.92	1.10	1.98	1.21	0.86	1.98
CZ10879	2.68	0.87	0.80	1.05	2.57	1.32	0.80	2.57
CZ31541	3.09	0.72	0.93	1.03	2.46	1.28	0.72	2.46
CZ21559	3.22	0.79	0.76	0.95	2.31	1.20	0.76	2.31
CZ11577	3.36	0.68	0.68	0.75	2.69	1.20	0.68	2.69
43 keV		Reference Activity = 4.63E+3 Bq ^{238}Pu						
None	1.91	1.19	1.15	1.49	1.59	1.36	1.15	1.59
CZ30826	2.47	0.79	0.59	1.01	1.51	0.98	0.59	1.51
CZ20853	2.58	1.14	0.74	1.06	1.36	1.08	0.74	1.36
CZ10879	2.68	1.09	0.72	0.87	1.13	0.95	0.72	1.13
CZ31541	3.09	1.33	1.41	1.61	1.51	1.46	1.33	1.61
CZ21559	3.22	1.37	1.11	1.44	0.94	1.21	0.94	1.44
CZ11577	3.36	1.11	1.13	1.52	1.39	1.29	1.11	1.52

TABLE II-3. RATIO OF PARTICIPANT ACTIVITY ESTIMATES TO REFERENCE ACTIVITY VALUES FOR ^{241}Am

Chest Overlays		Participating detection system					Average	Minimum	Maximum
I.D.	MEQ-CWT cm	A	C	D	N	O			
60 keV		Reference Activity = 4.88E+2 Bq ^{241}Am							
None	1.91	1.09	1.24	1.08	1.49	1.39	1.26	1.08	1.49
CZ30826	2.47	0.99	1.25		1.34	1.24	1.21	0.99	1.34
CZ20853	2.58	1.02	1.25		1.35	1.33	1.24	1.02	1.35
CZ10879	2.68	1.09	1.21		1.38	1.41	1.27	1.09	1.41
CZ31541	3.09	0.99	1.29		1.34	1.48	1.27	0.99	1.48
CZ21559	3.22	1.03	1.30		1.39	1.27	1.25	1.03	1.39
CZ11577	3.36	1.07	1.28		1.49	1.48	1.33	1.07	1.49

TABLE II-4. RATIO OF PARTICIPANT ACTIVITY ESTIMATES TO REFERENCE ACTIVITY VALUES FOR NATURAL THORIUM

Chest Overlays		Participating detection system				Average	Minimum	Maximum
I.D.	MEQ-CWT cm	A	C	N	O			
209 keV		Reference Activity = 1.20E+2 Bq ^{232}Th						
None	1.91	0.79	0.83	1.02	0.98	0.90	0.79	1.02
CZ30826	2.47	0.59	0.76	0.83	0.72	0.73	0.59	0.83
CZ20853	2.58	0.68	0.86	0.89	0.97	0.85	0.68	0.97
CZ10879	2.68	0.51	0.93	1.09	1.01	0.88	0.51	1.09
CZ31541	3.09	0.45	0.94	0.86	0.77	0.76	0.45	0.94
CZ21559	3.22	0.74	0.76	1.12	0.82	0.86	0.74	1.12
CZ11577	3.36	0.49	0.97	0.92	0.95	0.83	0.49	0.97
238 keV		Reference Activity = 1.20E+2 Bq ^{232}Th						
None	1.91	0.80	1.22	1.07	1.03	1.03	0.80	1.22
CZ30826	2.47	0.61	1.24	1.06	0.87	0.95	0.61	1.24
CZ20853	2.58	0.76	1.58	1.01	0.97	1.08	0.76	1.58
CZ10879	2.68	0.65	1.54	1.05	0.96	1.05	0.65	1.54
CZ31541	3.09	0.49	1.26	0.97	0.90	0.91	0.49	1.26
CZ21559	3.22	0.75	1.22	0.99	0.90	0.96	0.75	1.22
CZ11577	3.36	0.59	1.57	1.08	1.00	1.06	0.59	1.57

TABLE II-5. RATIO OF PARTICIPANT ACTIVITY ESTIMATES TO REFERENCE ACTIVITY VALUES FOR NATURAL URANIUM

Chest Overlays		Participating detection system				Average	Minimum	Maximum
I.D.	MEQ-CWT cm	A	C	N	O			
63 keV		**Reference Activity = 1.16E+3 Bq ^{238}U**						
None	1.91	0.87	0.93	1.28	1.17	1.06	0.87	1.28
CZ30826	2.47	0.75	0.97	1.10	1.01	0.96	0.75	1.10
CZ20853	2.58	0.83	0.92	1.17		0.97	0.83	1.17
CZ10879	2.68	0.86	0.96	1.20	1.06	1.02	0.86	1.20
CZ31541	3.09	0.72	1.00	1.09	0.94	0.94	0.72	1.09
CZ21559	3.22	0.77	1.01	1.14	1.03	0.99	0.77	1.14
CZ11577	3.36	0.81	1.03	1.21	1.05	1.03	0.81	1.21
185 keV		**Reference Activity = 5.33E+1 Bq ^{235}U**						
None	1.91	0.94	0.99	1.23	1.25	1.10	0.94	1.25
CZ30826	2.47	0.75	0.98	1.18	1.21	1.03	0.75	1.21
CZ20853	2.58	0.88	1.11	1.23		1.07	0.88	1.23
CZ10879	2.68	0.91	1.10	1.21	1.31	1.13	0.91	1.31
CZ31541	3.09	0.69	0.97	1.15	1.07	0.97	0.69	1.15
CZ21559	3.22	0.80	1.12	1.15	1.22	1.07	0.80	1.22
CZ11577	3.36	0.82	1.16	1.25	1.17	1.10	0.82	1.25

TABLE II-6. RATIO OF PARTICIPANT ACTIVITY ESTIMATES TO REFERENCE ACTIVITY VALUES FOR NATURAL URANIUM WITH 3% ^{235}U ENRICHMENT

Chest Overlays		Participating detection system					Average	Minimum	Maximum
I.D.	MEQ-CWT cm	A	C	D	N	O			
63 keV		Reference Activity = 1.53E+3 Bq ^{238}U							
None	1.91	0.88	0.96	0.93	1.23	1.10	1.02	0.88	1.23
CZ30826	2.47	0.79	1.00	-	1.08	1.02	0.97	0.79	1.08
CZ20853	2.58	0.78	0.97	-	1.19	1.02	0.99	0.78	1.19
CZ10879	2.68	0.63	0.97	-	1.22	1.06	0.97	0.63	1.22
CZ31541	3.09	0.74	1.00	-	1.05	0.97	0.94	0.74	1.05
CZ21559	3.22	0.81	1.04	-	1.10	1.05	1.00	0.81	1.10
CZ11577	3.36	0.82	1.01	-	1.22	1.03	1.02	0.82	1.22
143 keV		Reference Activity = 3.10E+2 Bq ^{235}U							
None	1.91	0.95	1.11	-	1.30	1.21	1.14	0.95	1.30
CZ30826	2.47	0.79	1.11	-	1.10	1.10	1.03	0.79	1.11
CZ20853	2.58	0.73	1.15	-	1.15	1.13	1.04	0.73	1.15
CZ10879	2.68	0.67	1.14	-	1.21	1.12	1.04	0.67	1.21
CZ31541	3.09	0.75	1.14	-	1.04	1.09	1.01	0.75	1.14
CZ21559	3.22	0.84	1.19	-	1.15	1.05	1.06	0.84	1.19
CZ11577	3.36	0.87	1.13	-	1.15	1.16	1.08	0.87	1.16
185 keV		Reference Activity = 3.10E+2 Bq ^{235}U							
None	1.91	0.98	1.11	-	1.26	1.21	1.14	0.98	1.26
CZ30826	2.47	0.81	1.12	-	1.18	1.17	1.07	0.81	1.18
CZ20853	2.58	0.69	1.17	-	1.14	1.22	1.06	0.69	1.22
CZ10879	2.68	0.67	1.16	-	1.18	1.19	1.05	0.67	1.19
CZ31541	3.09	0.82	1.17	-	1.05	1.10	1.04	0.82	1.17
CZ21559	3.22	0.84	1.21	-	1.12	1.19	1.09	0.84	1.21
CZ11577	3.36	0.85	1.16	-	1.19	1.14	1.09	0.85	1.19

COUNTRY REPORTS: DESCRIPTION OF PARTICIPANTS' FACILITIES

AUSTRALIA

P. Burns
Australian Radiation Protection and Nuclear Safety Agency
Melbourne, Australia

Introduction

The Australian Radiation Protection and Nuclear Safety Agency is an agency of the Australian Government with the responsibility of undertaking research and providing advice in relation to radiation protection and nuclear safety. In addition the agency has the responsibility of regulating those radiation practices undertaken by Australian Government organizations.

The activities of ARPANSA include monitoring the doses to workers in Australia. Internal dose assessment from the inhalation of insoluble dusts is a significant problem in industries associated with the mining and milling of radioactive ores and in the rehabilitation of sites contaminated by activities associated with the development of nuclear weapons. In order to assess doses to these workers ARPANSA has refurbished its whole body monitor as a lung monitor.

The internal dimensions of the shielded room are 2.1 m long × 1.7 m wide × 1.8 m high. The shielding comprises 18 cm of laminated steel sheets, 2 cm of laminated lead sheets and 3 mm of copper. A hydraulically powered sliding door occupies half of one wall to allow access. Air to the room is filtered to remove radon and radon daughters.

Subjects are measured using a bed geometry with the detectors arranged above them. There are four large area low energy germanium detectors (Canberra LEGe) each 70 mm diameter (active area 3800 mm^2) and 25 mm thick (Figures 1 and 2). The detector window is made from 0.6 mm carbon composite material. There are two 7 liter Canberra ACT II dewars each with a cryostat that holds two detectors. The dewars are mounted on a frame that allows adjustment for height and position and the angle of the detectors is also adjustable both laterally and longitudinally.

The lung monitoring facility is used routinely to monitor workers involved in the clean up of plutonium contaminated sites by assessing the 59.5 keV gamma ray from ^{241}Am which is present in the plutonium. Mineral sands workers have also been assessed by monitoring the 238 keV gamma ray from the decay of ^{212}Pb which is a daughter product of ^{232}Th.

Calibrations

All calibration measurements were performed with a Lawrence Livermore 'Realistic' Phantom. The phantom has no head, neck, arms or lower torso. Calibration was performed with 5 chest plates: 16, 22.5, 27.7, 33 and 39 mm. thicknesses. Efficiency calibration was conducted for 6 energies: 13, 26, 60, 122, 245 and 344 keV. The ^{241}Am and ^{152}Eu sources are traceable to NBS (NIST), with an uncertainty 3.5%. The sources were prepared on paper/Mylar sheets inserted into a specially modified sliced pair of lungs for use with the Lawrence Livermore Phantom. Two additional lung sets were used, one containing natural uranium and the other ^{235}U both mixed uniformly in the lungs, to verify the calibration carried out with ^{241}Am and ^{152}Eu.

Intercomparison Measurements

The original LLNL phantom was based on a male 1.77 meters tall weighing 76 kg. The Japan Atomic Energy Research Institute phantom is based on an average size Japanese male 1.68 m tall and weighing 63.5 kg. Shapes of the lungs in the two phantoms are different. The LLNL phantom has short deep lungs and JAERI phantom's lungs longer and not as deep. The heart of LLNL phantom is much larger and obscures a larger portion of the left lung compared to JAERI phantom. The JAERI phantom is supplied with torso plate, containing a skeleton and 6 chest plates of two thicknesses ($\approx$25 mm and 33 mm) and three different adipose to muscle ratios 10:90 20:80 and 30:70.

Table 1 below shows the results for the JAERI Phantom. Measured results were determined using the Canberra calibration. Six sets of lungs containing uniformly mixed nuclides were measured in the IAEA Phantom. The nuclides were ^{238}Pu (low and high activity), ^{241}Am, ^{232}Th, natural uranium and uranium with a 3% ^{235}U enrichment.

Table 1. ACTIVITY MEASUREMENTS RESULTS FOR JAERI PHANTOM COMPARED WITH REFERENCE VALUES

Nuclide	Photon Energy KeV	Measured Activity(M)	Stated Activity(S)	Ratio(M/S)
^{238}Pu	17	30800	40840	0.7542
	20	37270	40840	0.9126
	43	32710	40840	0.8009
^{238}Pu	17	3780	4626	0.8171
	20	3902	4626	0.8435
	43	5305	4626	1.1468
^{241}Am	60	507	488	1.0389
^{232}Th	209	72.7	120	0.6058
	238	83.4	120	0,6950
^{235}U 3%	63	1210	1550	0.7806
	143	248	310	0.8000
	185	251	310	0.8097
U-Nat	63	927.4	1158	0.8009
	185	44	53.3	0.8255
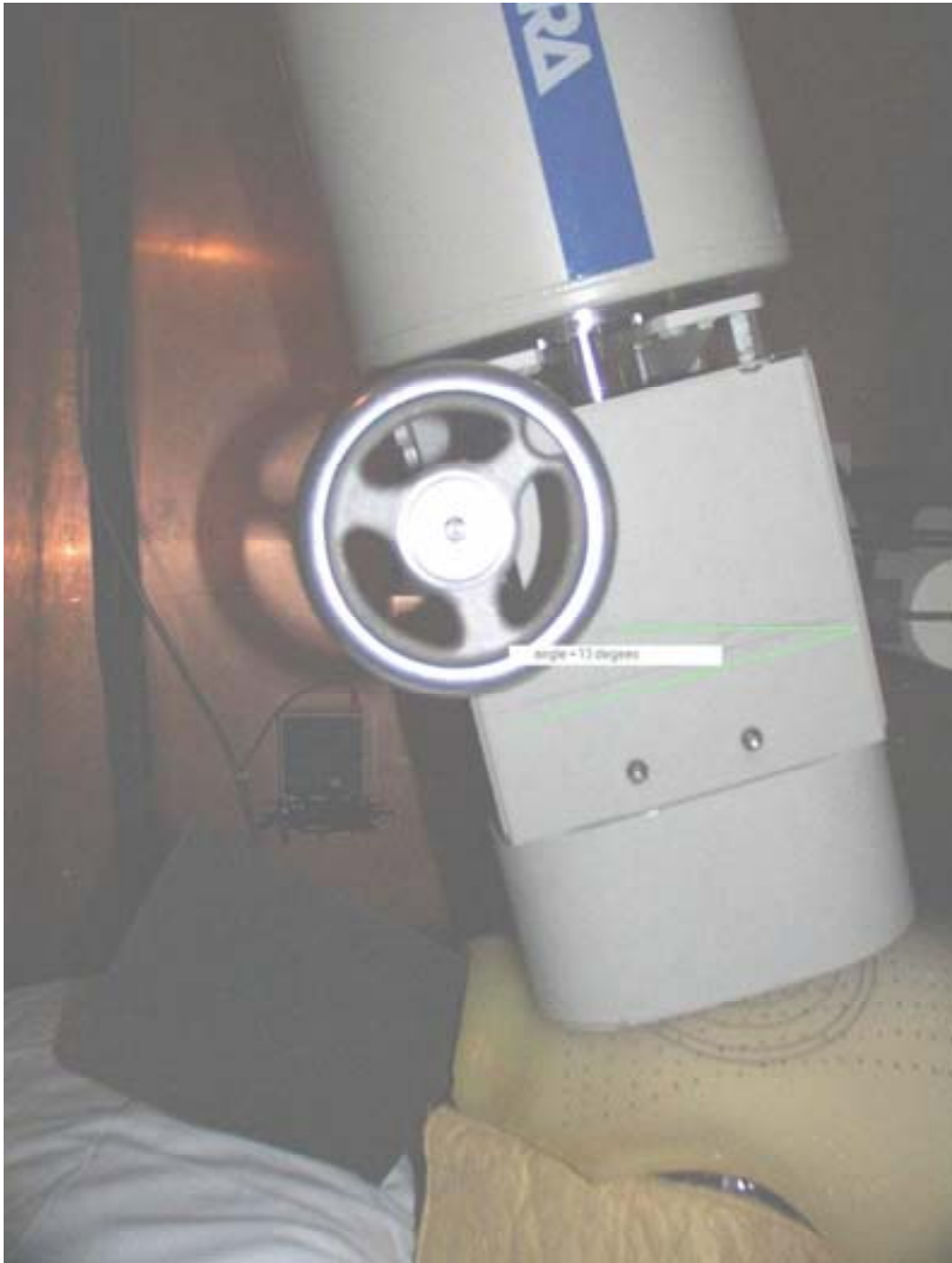
Fig. 1. LEGe detector array in place over phantom chest overlay.

.75 cm

21.3 cm

8.2 cm

12.4 cm

Note: Detectors 1&2 and Detectors 3&4 are two fixed assemblies
with independent positioning of each assembly.

Teflon
Copper
Vacuum
Stainless Steel Type 304
Ge
Pb
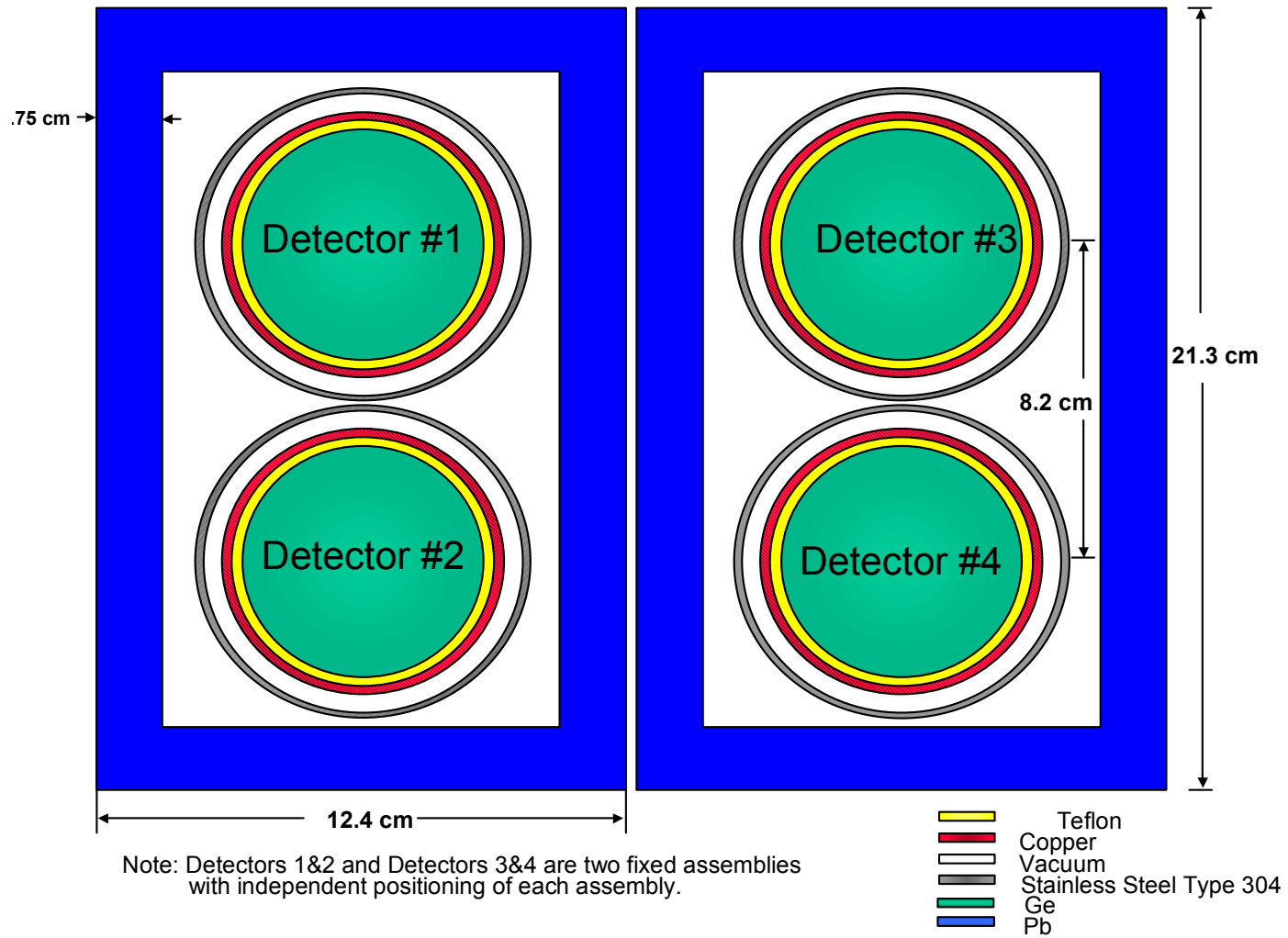
Figure 2a. ARPNSA ACTII LEGe array.
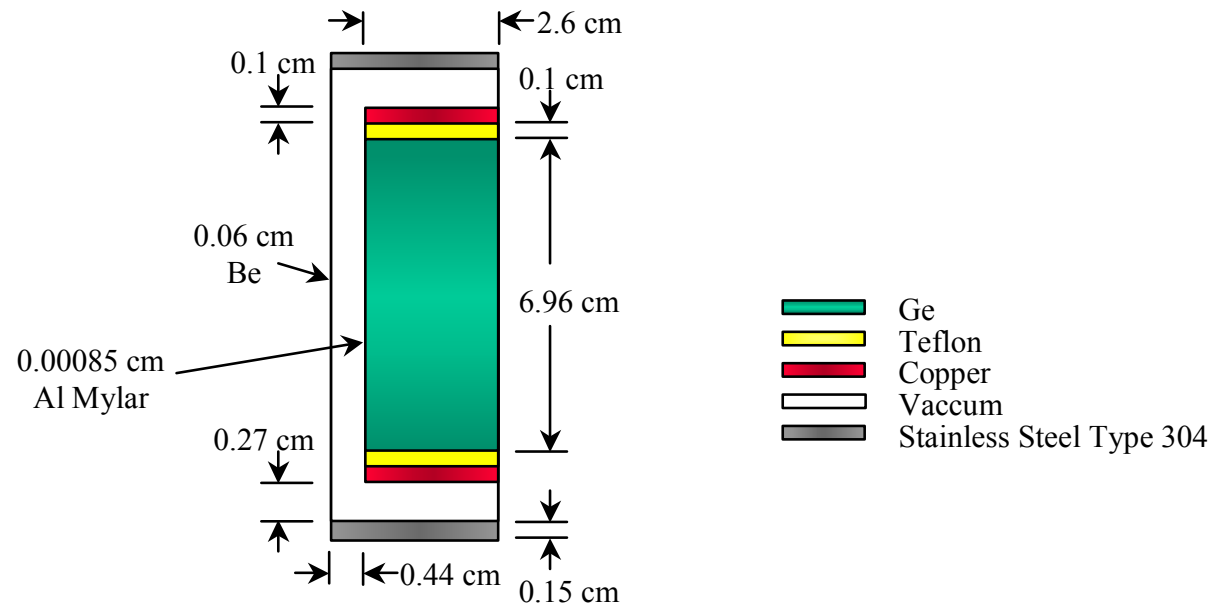
Figure 2b. ARPNSA ACTII LEGe detector side (side view). All detectors are the same.

BANGLADESH

A.S. Mollah
Institute of Nuclear Science and Technology
Atomic Energy Research Establishment (AERE)
Dhaka, Bangladesh

Introduction

Radionuclides are being widely used in medicine, agriculture, industry and research and development nowadays, and are likely to be incorporated to hazardous levels in the course of work. In order to ensure that the radiation doses received by the occupational workers, due to internal exposures, do not exceed the prescribed safe limits, proper internal contamination monitoring programmes are required. Internal doses due to incorporated radioactivity can conveniently be assessed directly through the in vivo measurement of body radioactivity externally by using a whole body counter (WBC) comprising of an appropriate detector assembly. Body monitoring provides direct information on the amount of radioactivity present inside the body in the case of most radionuclides and is an important part of the radiation protection programme.

Body monitoring can be placed into two categories by energy: 1) low energy (<100 keV) photon emitting radionuclides and 2) high energy (> 100 keV) photon emitting radionuclides. The former category includes only a few radionuclides and requires much more sensitive detector/shield systems compared to the latter category that covers the majority of the radionuclides.

AERE Whole Body Counting Facility

In order to assess body radioactivity, a self-shielded chair geometry WBC has been designed and installed at the Atomic Energy Research Establishment, Savar. The external background contribution has been reduced using shielding materials made of high Z materials such as Pb and Fe. A shielding thickness of 3.5 cm Pb + 2.5 cm Fe was used around the detector. The detector is a 5" × 5" NaI(Tl) crystal (Fig. 1). A 90% average background reduction in the energy range 0.1 to 3 MeV was achieved using this shielding configuration.

For low energy photon (LEP) detection, the low energy background needs to be reduced, so the shielding configuration has been modified. The interior of the Pb + Fe shield is provided with 0.937 mm of Cu lining which serves to reduce background below 100 keV. The use of 0.937 mm Cu shield achieves the lowest possible low-energy ambient background up to 10 keV (Fig. 2). An overall 94% background reduction was achieved. With this shielding configuration, several spectra were recorded with Canberra 35 + MCA. The recorded spectra of ^{241}Am, ^{210}Pb and ^{137}Cs are shown in Figures 3–5. From the figures, it is apparent that the low energy photon emitters could be detected with this system. Further work on calibration of the system with low energy radionuclides is progress.

Front View
(Cross- Section)

Side View
(Cross- Section)

0.508cm

14.7cm

13.46cm

20.7cm

25.3cm

0.508 cm

12.7cm

NaI(Tl)   Al   Cu   Pb   Fe
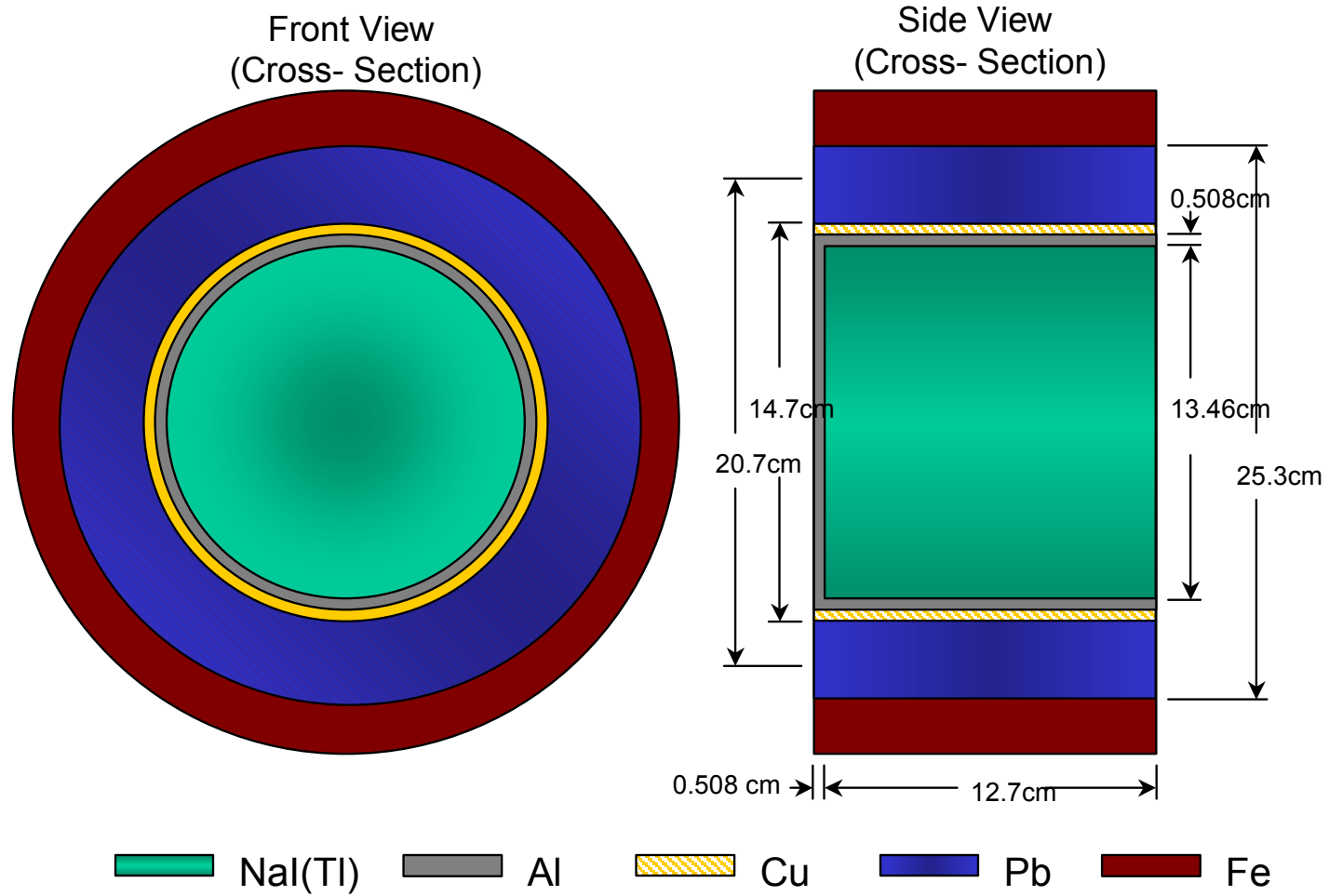
Figure 1 - AERE sodium iodide detector
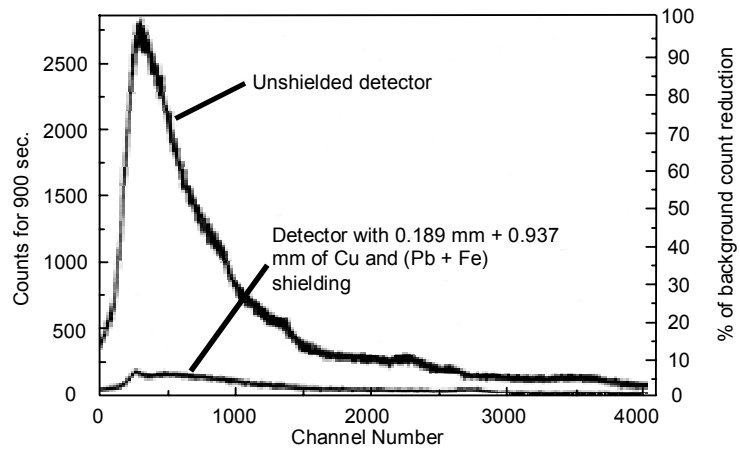
Figure 2 - Background spectra for NaI(Tl) Detector
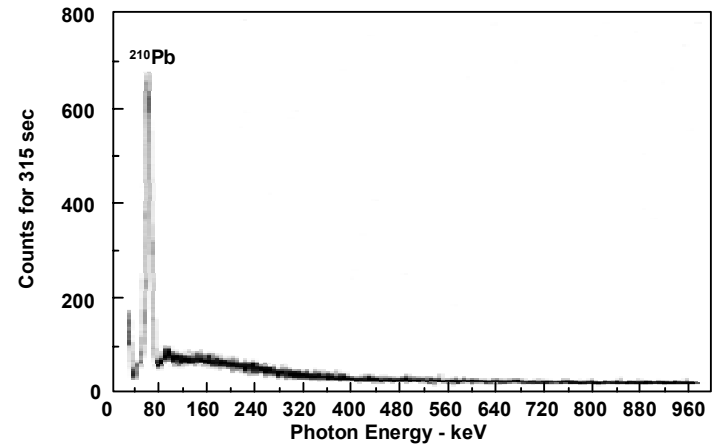
Figure 4 - Photon spectrum for ^{210}Po
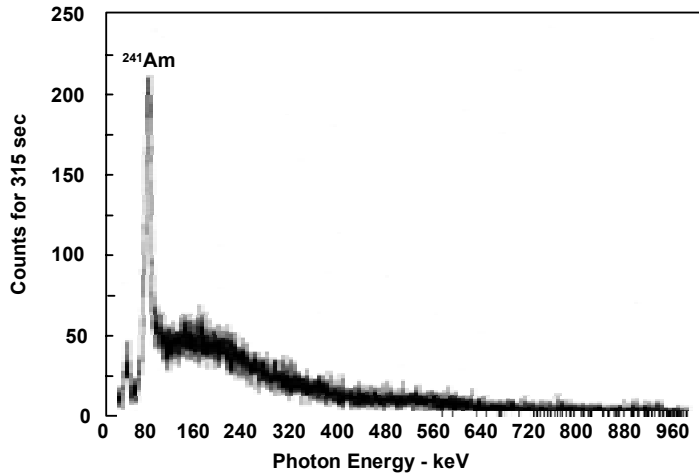
Figure 3 - Photon spectrum for ^{241}Am
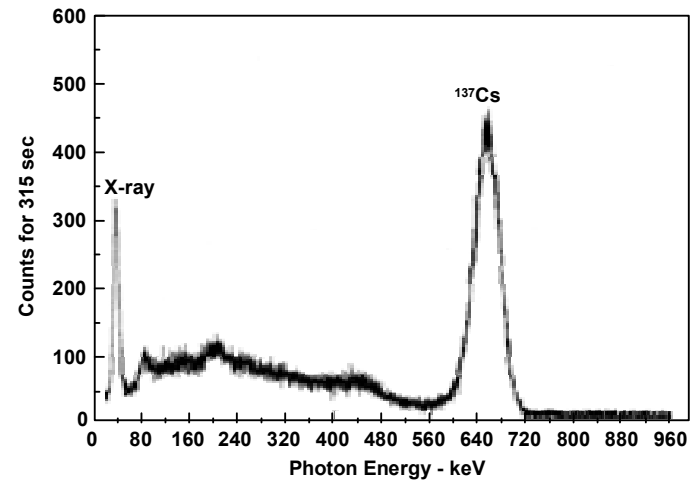
Figure 5 - Photon spectrum for ^{137}Cs

76

CANADA

G.H. Kramer
Human Monitoring Laboratory
Radiation Protection Bureau
Ottawa, Ontario, Canada

INTRODUCTION

The Human Monitoring Laboratory (HML) operates the Canadian National Calibration Reference Centre (NCRC) for *In Vivo* Monitoring [1]. The main function of the HML is to provide quality assurance to the regulator, the Atomic Energy Control Board (AECB), the licensee who operates an *In Vivo* facility [2], and the worker that is monitored in said facility. The purpose of the quality assurance is to ensure that the equipment is working satisfactory and meets the AECB's performance criteria. The HML also provides *In Vivo* capability to persons who are otherwise unable to obtain this service or in the case of accidents or emergencyies. The HML is also a national resource for internal dosimetry and its staff has the necessary expertise to evaluate doses resulting from an internal contamination.

The measurement of internal dose can only be made after the activity of the radionuclide(s) that has been incorporated into the body has been estimated. The quantification can be performed either by direct measurement, indirect measurement or in certain cases by area monitoring. Direct measurement includes whole body counting, lung counting and thyroid monitoring. Indirect measurement includes urinalysis, faecal analysis, and breath analysis. Area monitoring, for the purpose of estimating internal dose, is called personal air sampling (PAS) and is only performed for radionuclides that are difficult or impossible to measure by direct or indirect methods (e.g. type S ^{233}U). This report summarizes the internal dosimetry programmes in the HML that incorporate direct measurement techniques. Indirect methods and PAS are outside the scope of the CRP will not be discussed.

The regulator in Canada for facilities handling radioactive materials is the AECB. This is a federal body. Other aspects of radiation (i.e. X rays) are regulated by provincial governments, or Health Canada (radiation emitting devices). Some aspects are not regulated at all; for example, naturally occurring radioactive materials. The AECB is given its powers by the Nuclear Regulatory Act. The AECB will soon become the Canadian Nuclear Safety Commission (CNCS) with a complete new range of powers. The AECB is in the process of publishing new regulations which will take Canada from its present level of ICRP 2 [3] directly to ICRP 60 [4]. Most facilities in Canada that have radiation protection programmes are using ICRP 30 [5] philosophy and recommendations to control exposures to their employees.

The ICRP 60 philosophy will be adopted almost in total, the only difference being in the treatment of pregnant workers. The dose limit for workers not classified as Radiation Workers will be 1 mSv but the AECB will only require facilities to perform bioassay if they cannot demonstrate that effective doses to their personnel can be kept below 5 mSv. If doses are projected to exceed this level bioassay (including *In Vivo* monitoring) will be mandatory.

The NCRC tests *In Vivo* monitoring facilities on a yearly basis to ensure that their equipment is working satisfactorily. The results of the tests are reported to the participating facilities, the AECB, and the public. The performance criteria are under development by the AEC13 and have been heavily influenced by the N13.30 criteria recently published [6]. Table 1 shows the development of the performance criteria over the last five years. As can be seen the performance criteria have been disconnected from the minimum detectable activity (MDA).

TABLE 1. CANADIAN PERFORMANCE CRITERIA FOR IN VIVO MONITORING FACILITIES

Past criteria	Bias	Precision	Activity range
	−20% < measured bias < 20%	< 20%	>10 MDA
	−50% < measured bias < 50%	< 40%	1 –1 10 MDA
Present criteria			
	−25% < measured bias < 50%	not measured	>5 MDA

Dose estimation

Once an internal contamination has been detected it must be converted to dose. Facilities vary greatly in the qualifications of their staff. The facilities mentioned in the whole body and lung counting sections above have well trained health physicists who are capable of obtaining a dose. Commercially available software typically used in these facilities include: CINDY, GENMOD, REMEDY, INDOS, MIRDOSE, and LUDEP.

Staff at the facilities who perform thyroid monitoring range in qualification from health physicist to radiation safety officer to untrained. These persons will rely on help from either Health Canada, the AECB or a health physicist from another nearby organization.

Activity determination by direct methods

Whole body counting

There are 13 whole body counters in Canada as shown in Table 2. CRL and WRL are Atomic Energy of Canada Limited (AECL) sites. TGH, MAC, UOW are hospitals. HQ, NBP and all OH sites are nuclear power generating stations.

The needs of the three types of facilities are, of course, quite different. The AECL sites are involved in diverse research using many different types of radionuclides as well as radionuclide production for subsequent worldwide sale. Combined, these sites perform between 2,000 to 3,000 counts per year. Staff will be scheduled based on the type of material they are handling. The most common whole body counting frequency is annual and is increased to semi-annual or quarterly for certain higher risk groups.

The hospitals have very different needs for their counters. TGH uses their whole body counter for the measurement of neutron-activated calcium for patients. It is kept on standby for occupational monitoring in case a nearby reactor has an accident on the OH counters cannot be used. The remaining two hospital's counters are used for a variety of radionuclides. The most common being [131]I. MAC does have a university reactor nearby and its whole body counter is used to annually monitor the few reactor personnel. The most common internal contaminant is [110m]Ag.

The HML's whole body counter, which is mounted in a steel lead lined counting chamber, is mainly used for other Federal Government employees. The most common subject has been employees of the Foreign Affairs Department either going to the Former Soviet Union (FSU) or returning from the FSU. It is also used for ^{131}I monitoring. Typically, the HML will measure 200–400 persons per year. The HML also has a portable whole body counter that is designed to be flown (or driven) into remote regions of Canada. It has been used to assess the internal burdens of native peoples in the northern parts of Canada and also the internal burdens of immigrants to Israel from the Chernobyl region of the FSU [7].

TABLE 2. SUMMARY OF CANADIAN WHOLE BODY COUNTING FACILITIES

Facility	Type of WBC	Detector	Number (cm)	Diameter (cm)	Thickness
CRL	Scanning shadow shield	NaI (Ge)	1 (1)	30 (25%)	10 (25%)
WRL	Tilt chair	NaI	1	40	15
TGH	Static bed	NaI	8	-	$10 \times 10 \times 41$
MAC	Scanning shadow shield	NaI	1	30	10
U0W	Scanning shadow shield	NaI	1	30	10
HQ	Scanning shadow shield	Ge	1	20%	-
NBP	Canberra FastScan	NaI	2	-	$8 \times 13 \times 41$
OH-W	Scanning shadow shield	NaI	1	30	10
OH-P	Canberra FastScan	NaI	2	-	$8 \times 13 \times 41$
OH-D	Canberra FastScan	NaI	2	-	$8 \times 13 \times 41$
OH-13A	Canberra FastScan	NaI	2	-	$8 \times 13 \times 41$
OH-1313	Canberra FastScan	NaI	2	-	$8 \times 13 \times 41$
HML	Scanning detector	NaI	6	13	10
HML	Portable	NaI	2	13 & 8	10 & 8

The remaining sites are all nuclear power generating stations. Employees are usually measured annually and the most common internal contaminants are ^{137}Cs (often from venison and not occupational exposure) and ^{60}Co.

With the exception of the shadow shield and FastScan whole body counters, the remaining whole body counters are mounted is low background steel counting chambers. All chambers have some degree of graded shielding. Internal contaminations in the above facilities are infrequent and often result in negligible dose.

Lung counting

There are only three lung counters in Canada (Table 3). The HML's lung counter has been refurbished from a phoswich system to a Ge system. The detectors are shown in Figure 1. It is mainly used for other Federal Government employees and research into lung counting. The most common subject has been employees of the Foreign Affairs Department either going to the Former Soviet Union (FSU) or returning from the FSU. It is also used for ^{125}I monitoring where two of the detectors will be positioned above the subject's thyroid with the neck in an extended position. Typically, the HML will measure 100 persons per year. The last use of the lung counter for an accident evaluation was to estimate the dose following a ^{14}C release at a local company [8].

The Phoswich counting system at CRL is optimised for plutonium. However, it is also used to measure uranium and other transuranics. Typically, CRL will monitor 200–500 persons per year. The most common frequency is semi-annually.

CAM is a uranium mining and refining company. Its lung counter has been optimised for uranium counting only. No other radionuclides are measured in this system. The lung counter is a unique design in Canada as it has two Phoswich detectors mounted above a supine subject and two detectors mounted underneath. Until the HML acquired the Asian phantom it was unable to verify calibrations for this system, as the North American Torso phantom is not anthropometric for rear mounted detectors. The number of personnel being counted has been reduced over the last few years due to company downsizing. Currently the

facility is measuring about 800 persons per year. The counter is also kept on standby to measure ^{14}C in the lung for a nearby nuclear power generating station.

All the lung counters are mounted in low background steel counting chambers with some form of graded shielding. The CRL is the most elaborate, with layers of lead, iron, cadmium and copper.

TABLE 3. CANADIAN LUNG MONITORING FACILITIES

Facility	Type	Detector	Number	Diameter (cm)	Thickness (cm)
HML	Chair/bed	Ge	4	7	3
CRL	Bed	Phoswich	2	13	0. 1 (Nal)
CAM	Bed	Phoswich	4	13	0.4 (Nal)

Thyroid counting

The facilities previously mentioned use their whole body counters for ^{131}I. Some of the facilities also measure ^{125}I and they have a separate detector system for that purpose. However the bulk of thyroid counting in Canada is performed by a variety of other institutions. The most numerous are nuclear medicine departments which handle large quantities of both radioiodines. The thyroid gland is treated with ^{131}I for diagnostic and therapeutic reasons. Immunoassay is performed with ^{125}I. Some nuclear medicine departments use ^{123}I but the regulator does not require facilities to monitor for this radionuclide (except for external dose).

Other facilities that handle radioiodines include universities, radiopharmaceutical companies, oil companies, federal and provincial laboratories, and private companies. Not all of these facilities monitor their employees but if the amount handled is deemed potentially hazardous by the regulator, monitoring becomes mandatory. There are about 200 such facilities in Canada.

The most common type of detector is NaI. Sizes and thickness vary widely and does the data acquisition systems attached to the detectors. The former ranges from 2.5 cm diameter to 30 cm diameter and thicknesses vary in a similar manner. The data acquisition systems range from hand held scalers with no window capability to sophisticated multi channel analysers.

Thyroid counters vary widely in their situation. The range is from heavily shielded (i.e. in a low background counting chamber) to collimated to a gamma camera that is used for patient examination. Frequency of monitoring, as might be expected, also varies greatly. Monitoring frequency will range from monthly to a before and after handling material.

The AECB has mandated that thyroid counters in nuclear medicine departments must have an MDA of better than 1 kBq. Today the range of operational MDA's varies from a few Becquerels to just under that limit. Despite the apparent chaos that appears to reign in the field of thyroid monitoring, working conditions are safe and overexposures are very rare. The last reportable case being in about 1990. The dose was negligible.

CALIBRATION OF IN VIVO FACILITIES

The accuracy of an activity estimate is only as good as the calibration. Radiation detectors can only measure the number of photons that interact in their sensitive volume. This value, in itself, gives no information about the amount of radioactivity in the source unless a calibration factor is applied to the result.

The source used for calibrating an *In Vivo* counter should be similar, if not exactly the same, as the subject being monitored. This is especially true as the photon energy decreases. The NCRC holds a large variety of different phantoms for the calibration and testing of whole body counters, lung counters and thyroid monitors.

Whole body counters

Canadian whole body counters are calibrated by means of the Bottle Manikin Absorber (BOMAB) phantom. The HML has a wide variety of sizes [9] available to Canadian facilities. These are summarised in Table 4. The phantoms P4, P10, PF, and PM were all designed from ICRP Reference Man data [10]. The PM5 and PM95 were designed from Canadian anthropomorphic data. The P4 and PM series also have a set of overlay plates for the chest, gut and thigh sections of the phantom so that overlaying tissue can be simulated in a whole body counter.

TABLE 4. HML BOMAB PHANTOM SERIES

Phantom series	Size
P4	4 year old
P10	10 year old
PF	Female
PM	Male
PM5	5th percentile male
PM95	95th percentile male

Lung counters

The HML has two torso phantoms for calibrating lung counters: The LLNL torso phantom and the Asian, phantom. There are a variety of lung phantoms available for these phantoms in the HML. The LLNL phantom has ^{241}Am, ^{238}Pu, enriched uranium natural uranium, natural thorium ^{241}Am/^{152}Eu, and a ^{241}Am/^{152}Eu set that is sectioned into sixteen pieces (eight per lung) to study the effect of heterogeneous deposition of the activity determination. The Asian phantom has ^{241}Am/^{152}Eu, natural uranium and ^{241}Am currently available. The HML and Battelle Pacific Northwest National Laboratory (PNNL) are constructing more lung sets for this phantom. PNNL now has access to a set of lung moulds that were developed as part of a joint HML-PNNL research project and has the expertise to make tissue equivalent Asian phantom lung sets with the activity homogeneously distributed throughout the tissue equivalent material.

The Canadian lung counters at CAM and the HML were calibrated with these phantoms. The lung counter at CRL was originally calibrated with a torso phantom from Radiology Support Devices (previously Humanoid Systems Inc.) that is a different design from the LLNL phantom.

There are an increasing number of females in the workforce in Canada. The Asian phantom was purchased by the HML to provide a base for calibrating this population group. Overlaying breast tissue remains a problem, it is currently simulated with two flexible containers of a liquid tissue substitute which are temporarily fixed to the phantom for the duration of the count.

The LLNL phantom has been accepted as the de facto standard phantom in North America [11] and has been evaluated elsewhere [12, 13]. The Asian phantom has also been

evaluated for its anthropomorphic characteristics and the chest wall thickness (CWT) has been determined for Ge counting.

The two phantoms have some significant physical differences that are shown in Table 5. The lung shapes between the two phantoms are quite different. However, results [14,15] from a joint research projects (HML–KAERI, HML–Cameco) indicate that this and the other anthropomorphic differences shown in Table 5 are insignificant when using a lung counter consisting of Ge or Phoswich detectors. Both phantoms appear to give very similar calibration factors over the energy range 17–340 keV.

TABLE 5. TORSO PHANTOM DEFICIENCIES

LLNL	Asian
Overlarge heart	Limited chest wall thickness (CWT) range
Truncated lungs	Limited adipose content
Barrel-chested shape	Lung tissue equivalent material (TEM) density
No scapula	Short sternum
No GI tract	
Spine not anthropomorphic	
Inconsistent OVP (Adipose Mass Fraction changes with CWT)	
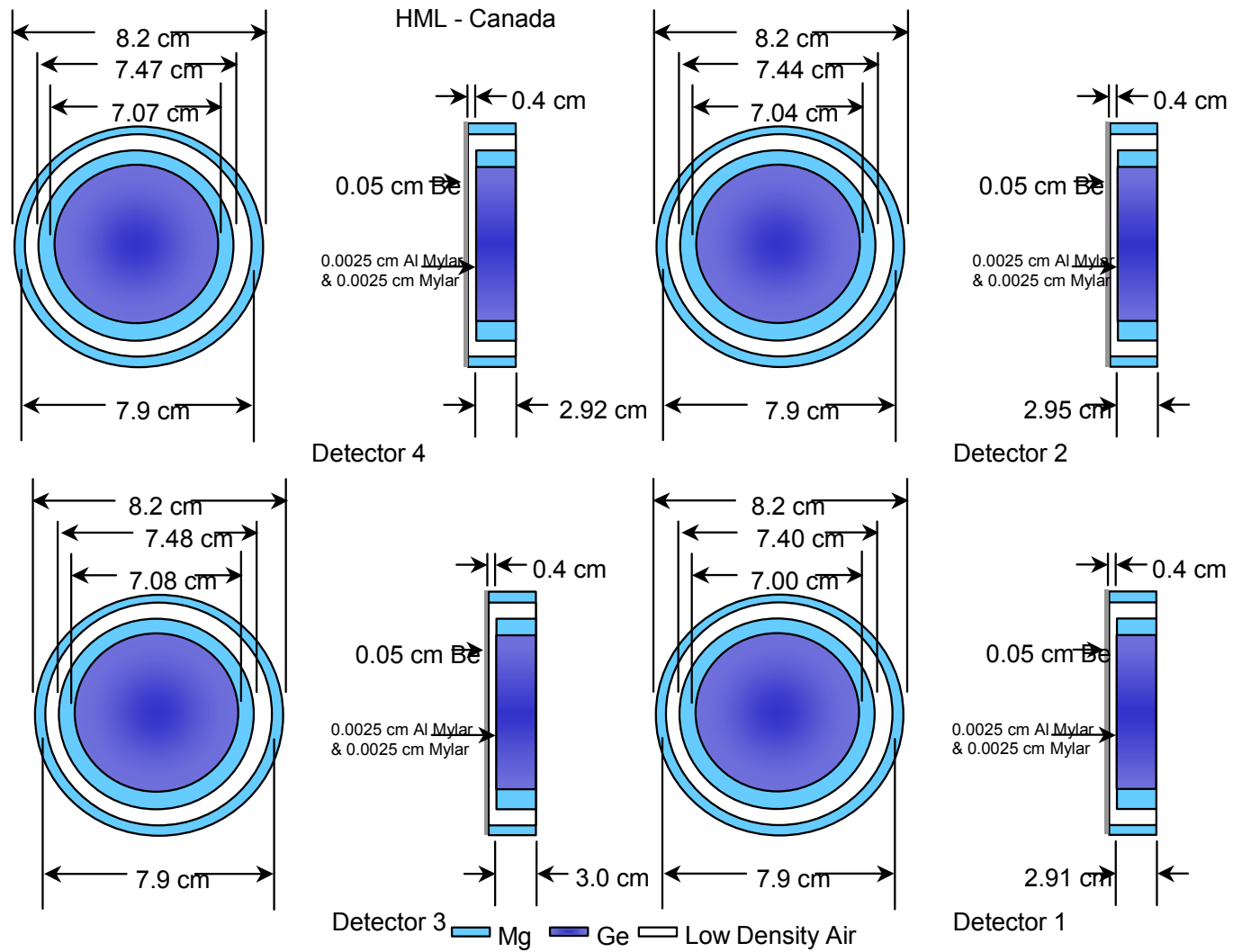
Figure 1 - HML LEGe detector array.

REFERENCES

[1] Kramer G.H. and Limson Zamora M., The Canadian National Calibration Reference Centre for Bioassay and In-Vivo Monitoring, A Program Summary, Health Physics 67(2), 192–196, (1994).

[2] Kramer G.H., The Canadian Whole Body Counting Intercomparison Programme; A Summary Report for 1989–1993. Health Physics 69(4), 560–565, (1995).

[3] International Commission on Radiological Protection. Report of committee II on permissible dose for internal radiation. ICRP Publication 2, (1959).

[4] International Commission on Radiological Protection. 1990 Recommendations of the International Commission on Radiological Protection, November 1990. ICRP Publication 60 (1991).

[5] International Commission on Radiological Protection. Limits for intakes of inhaled radionuclides. Annals of the ICRP 2(3/4). ICRP Publication 30 Parts 1–4 (19).

[6] American National Standards Institute, An American National Standard. Performance Criteria for Radiobioassay. Health Physics Society: McLean VA. American National Standard HPS N 13.30; 1996.

[7] Quastel M.R., Kramer G.H., Goldsmith J.R, Po1jak S., Kordysh E., Cohen R., Noel L., Gorodisher R. Radiocesium Body Burdens in Immigrants to Israel from Areas of the Ukraine. Byelorus and Russia near Chernobyl. Health Physics 69(l.):102–1 10; 1995.

[8] Kramer G.H., Badreddine A., Tran T., Meyerhof D.P. Dosimetry of an Incident Involving ^{14}C. Health Physics 70(3): 418–424; 1996.

[9] Kramer G.H., Noel L. and Burns L.C. The BRMD BOMAB Family. Health Physics, 61(6) 895902, 1991.

[10] International Commission on Radiological Protection. Report on Reference Man: Anatomical, physiological and metabolic characteristics. New York: Pergammon Press; ICRP Publication 23; 1975.

[11] Kramer G.H. and Inn K.G.W. A Summary of the Proceedings of the Workshop on Standard Phantoms for In-Vivo Radioactivity Measurement. Health Physics 61(6) 893–894, 1991.

[12] Kramer G.H. and Webber C.E. Evaluation of The Lawrence Livermore National Laboratory (LLNL) Torso Phantom by Bone Densitometry and X ray. Appl. Radiat. Isot. 43(6) 795–800, 1992.

[13] Kramer G.H. and Webber C.E. Measurement of the Natural Uranium Content of Fabricated, Tissue Substitute Lung Sets by Dual Photon Absorptiometry. Appl. Radiat. Isot. 45(7) 749–752, 1994.

[14] Kramer G.H.; Lee T.Y.,;Kim J.S. A joint HML-KAERI project, comparison of the LLNL and JAERI torso phantoms using four 50 mm Ge detectors. Health Phys. 74(5):613–618; 1998.

[15] Kramer G.H.; Hauck, B.M.; Allen, S.A. Comparison of the LLNL and JAERI torso phantoms using Ge detectors and phoswich detectors. Health Phys. 74(5), 594–601, 1998.

CHINA

HU Zunsu, FAN Yaoguo, JIN Yueru, HAN Yueqin
China Institute for Radiation Protection
Taiyuan, Shanxi, China

Introduction

In vivo measurement of radionuclides is performed at a number of facilities in China, as summarized in the following list.

- China Institute for Radiation Protection, Personal Dose Management and Service, Center, CNNC — This facility provides support to the nuclear industry.
- China Institute of Atomic Energy — Provides personal dose control in the Institute.
- Institute of Radiation Medicine, Beijing — The facility if primarily devoted to medical diagnosis and treatment.
- Beijing Industrial Hygiene Laboratory, Ministry of Public Health — Offers services for other applications of radioisotopes and radiation.
- Suzhou Medical College — Devoted to teaching and local services).
- Other Nuclear Facilities and Institutions including the Daya Bay Nuclear Power Plant.

The China Institute for Radiation Protection (CIRP) is located in Taiyuan, Shanxi Province. It was founded in 1962. CIRP is affiliated with the China National Nuclear Corporation (CNNC) which is also named China Atomic Energy Authority (CAEA) The CIRP has a total staff of 1083 people, with eight Research and Development, components:

- Department of Health Physics and Nuclear Safety
- Department of Life Science
- Department of Environment Science
- Department of Waste Management
- Department of Irradiation Technology
- Department of Biological Technology
- Department of Electronics and Information Technology
- Research Unit of Environmental Medicine (supervised jointly by CNNC and NEPA)

In addition, it has six management and service centers operated on behalf of CNNC:

- Personnel Dose Management and Service Center
- Radiation Protection Instrument Test Center
- Environmental Monitoring and Assessment Center
- Nuclear Emergency Technical Support Center
- Occupational diseases Registration
- Center Radiation Protection Training Center

Table 1 presents a list of the in vivo measurement facilities in China.

TABLE 1 - WHOLE BODY RADIOACTIVITY MONITORS IN CHINA

Institute	Operating since	Technical Information
Lanzhou Nuclear Fuel Plant	1979	Inside size 2.0 × 1.5 × 1.9m. Graded shield from outside to inside: 30cm concrete,15cm iron., 0.3cm Pb, 0.05cm Cu and 0.3 cm plastic. Four thin NaI detectors (two 10 × 0.2 cm and two 10 × 0.1cm) and two 10 × 10 cm NaI
Beijing Industrial Hygiene Laboratory	1975	CANBERRA Model 2270 Body Burden Analysis System

Daya Bay NPP	1993	CANBERRA
		  i) FASTSCAN: two large stationary NaI
		  detectors(4" × 4" × 16" each)
		  ii) ACCUSCAN II: two moveable stand
		  holding HPGe detectors

China Institute for Radiation Protection	1967 1975 1990	Single detector scanning shadow shield whole body counter: one 8" × 4" NaI crystal Single detector chair: (one 8" × 4" NaI) small lead room Underground iron chamber, one or two 8" × 4" NaI detectors, scanning, standard chair and arc chair whole body counter and, low X & γ energy counter low X & Y energy counter(one CsI/NaI detector)
China Institute of Atomic Energy	1979	Multi-detector stretcher technique: four NaI detectors, 100 × 100mm each Monitoring room: ground level, inside size 2.2 × 1.0 × 1.5m. Graded shield from outside to inside: 40 cm arenaceous quartz,10cm iron,0.3cm Pb and 0.4 cm plastic
Institute of Radiation Medicine, Beijing	1981	Single detector scanning and chair: (9" × 4" NaI). Monitoring room: ground level inside size 2.4 × 1.5 × 2.0 m. Graded shield from outside to inside: 70 cm arenaceous quartz, 10 cm iron, 0.3 cm Pb, 0.04 cm Cd, 0.1 cm Cu and 0.5 cm plastic
Suzhou Medical College	1983	Single detector scanning and chair: (9" × 4" NaI). Monitoring room: ground level inside size 2.4 × 1.5 × 2.0 m. Graded shield from outside to inside: 70 cm arenaceous quartz, 10 cm iron, 0.3 cm Pb, 0.04 cm Cd, 0.1 cm Cu and 0.5 cm plastic
Institute of Biophysics, Academia Sinica	1975	Lead shielded shadow shield with single scanning detector: (one 9" × 4" NaI) whole body counter
821 plant	1979	Multi-detector scanning bed with four 10 × 10 cm NaI crystals. Basement monitoring room

CIRP Internal Dosimetry Programme

The objectives of the internal dosimetry programme are to:

- carry out internal dose assessment for workers in nuclear industry
- work on in vivo measurements and their calibration, including the construction of phantoms for a Chinese male
- develop computer codes for internal dose assessment

- collect data for a standard Asian man and
- investigate parameters of dosimetric models

A number of facilities and resources are maintained as part of the in vivo measurement programme:

- Shadow shield whole body counter
- Lead chamber whole body counting system
- A set of phantoms for medium and high energy calibration
- Water filled phantom for low-energy calibration
- Chest phantom made of human skeleton
- An underground counting iron chamber

In recent years, the activities have included:

- Participation in the IAEA intercalibration of in vivo measurement by means of a realistic chest phantom
- Retrospective assessment of Rn exposure by measuring ^{210}Pb in the skull for uranium and tin miners
- Evaluation of worker chest wall thickness with a B-type ultrasonic tomography system
- Study of the correlation between the thickness of chest wall and other anatomic parameters

Intercomparison Measurements

Two detectors were used for the intercomparison:

Detector No. 1:

Detector type: Phoswich (Figure 1)

NaI(Tl), 12.7 cm in dia. by 0.3 cm thick
CsI(Na), 12.7 cm in dia. by 5 cm thick
Entrance Window: Be, 0.02 cm thick
Side shielding: Stainless steel, 0.037 cm thick, consisting of

Fe	Cr	Ni	Mn
70.1%	18.7%	9.2%	2.0%

Detector No. 2:

Detector type: Sodium iodide
20.3 cm in dia. by 10.2 cm thick
Entrance Window: Al
Side shielding: Stainless steel

The counting electronics for low energy photon measurement contains pulse shape discriminator, preamplifier, delay amplifier, amplifier, high voltage supply. Details are shown in Table 2:

TABLE 2. COUNTING SYSTEM SUB-ASSEMBLIES

Item	Type	Manufacturer
Detector	20MSSH3NV5B-X	Harshaw Chemical Co.
Pre-amplifier	NB-25A	Harshaw Chemical Co.
PSD (pulse-shape discriminator)	NC-25A	Harshaw Chemical Co.
Delay amplifier	FH1058A	BNIF, China
MCA	DIDAC80	France

The detector is mounted at the center of an iron chamber in a room 5 meters underground. Three meters of concrete and soil provide shielding from cosmic rays. All low energy photon counting results are based on the summation of two separate counts made with a single phoswich detector placed alternately over each lung using the positions marked on the phantom. This is intended to simulate simultaneous counting with two detectors. The recorded count time is that for a single detector count. The detector geometry for use in MRIPP is presented in Table 3. The coordinates X and Z are in centimeters, and the angles (p and 0 are in degrees. The high energy detector (NaI(Tl), 20.32 cm dia. by 10. 16 cm) is located over the center of the phantom.

TABLE 3. DETECTOR GEOMETRY

Detector	X	Z	φ	θ
low energy detector (CIRP 1) over the left lung (+X)	7.8	6.3	21°	18.5°
low energy detector (CIRP 1) over the right lung (-X)	−7.8	6.3	21°	-16°
high energy detector (CIRP2)	0.0	0.0	0°	0°

Following the CRP Protocol, the energies used for measurement of each radionuclide are listed in Table 4. In Table 4, the plus sign "+" represents the summation of multiple energies in a common peak. This is necessary due to poor detector resolution. Since the photons with different energies are from the radionuclides to be measured, their summation is useful for measurement purposes. However, counting efficiencies for single energies were requested for the purpose of intercomparison, so two versions of the spreadsheets were prepared, one with the combined counts (iaea4p.xlw) and the other with counts stripped off for a single energy from the mixture (iaea4p 1.xlw). The simple source measurements were conducted with the point source on the axis of the detector. The source - detector distances 5 cm for the phoswich detector (CIRP1) and 10 cm for the high energy detector (CIRP2). Attenuation of the overlays is fitted with a quadratic exponential function. The parameters are shown in Table 4.

TABLE 4. PHOTON ENERGIES SELECTED FOR EACH RADIONUCLIDE MEASUREMENT [1]

Radionuclides	Photon Energies
^{238}Pu	13.6+17.1+20.3 keV
	43.5 keV
^{241}Am	59.5 keV
Natural uranium	63.3+84.2+90.0+92.4+92.8+93.4
	143.8 and 185.7 keV
Enriched uranium(3%)	63.3+84.2+90.0+92.4+92.8+93.4
	143.8 and 185.7 keV
Natural thorium	238.6, 911.1+964.6+968.9
	2615 keV

Discussion

As noted above, some peaks in the detector spectra are the mixture of photons with different energies. For example, in the spectrum of ^{238}Pu, the lower peak is the mixture of photons with energies of 13.6, 17.1 and 20.3 keV. Because all these photons are emitted from ^{238}Pu, for the purpose of practical applications, we can treat this mixed peak as a single peak, and do not have to separate the components. On the other hand, for the purpose of intercomparison, data of 17.1 and 20.3 keV peaks should be reported separately. In order to strip a single peak from the mixture, reference peaks of single energy photons emitted from the same matrix are necessary. Unfortunately, relevant reference peaks related to an Asian man are not available. So we can only strip off the peak of 63.3 keV for natural uranium and enriched uranium by using the 59.5 keV peak of ^{241}Am as reference.

The photon emission yields of ^{238}U, ^{235}U and their equilibrium daughters are listed in Table 5. As mentioned above, when photons from natural uranium or enriched uranium (3% ^{235}U) are measured, the counts in the range 40 to 105 keV area include the contribution of the photons emitted from ^{238}U and ^{235}U. However, while the radioactivity compositions of ^{238}U and ^{235}U in natural and enriched (3%) uranium are known, the counting efficiencies (cps.Bq^{-1}) of ^{238}U and ^{235}U can be calculated by means of a set of linear equations. Assuming that the counting efficiencies of ^{238}U and ^{235}U are E_8 and E_5, we have

$$A_{n8} E_8 + A_{n5} E_5 = C_n$$
$$A_{e8} E_8 + A_{e5}.E_5 = C_e$$

Where A_{n8} and A_{n5} are the activities of ^{238}U and ^{235}U in natural uranium, A_{e8} and A_{e5} are the activities of ^{238}U and ^{235}U in 3% enriched uranium; and C_n and C_e are the total count rates of natural and enriched uranium, respectively.

In our case, A_{n8} = 1158 Bq and A_{n5} = 53.26 Bq;
A_{e8} = 1550Bq and A_{e5} = *310*Bq; and
C_n = 10.98 cps and C_e = 23.80 cps,

then we have E_8 =0.0077 cps.Bq^{-1}, and E_5 = 0.039 cps.Bq^{-1}.

By using the values of E_8 and E_5, the counting efficiency for uranium with different enrichments can be calculated.

Measurements were made using various detector positions and angles to optimize the counting geometry. The results are presented in Tables 7 and 8. The measurements show that the response of the detector is not very sensitive to the variation in angle over a limited range, but is more sensitive to the detector position due to the position of ribs and sternum.

A comparison of counting sensitivities between the Asian and the Caucasian phantoms is given in Table 9 for ^{238}Pu and ^{241}Am. It can be seen that, for ^{241}Am the counting sensitivity for the Asian phantom is about 7% higher than that for the Caucasian phantom. For ^{238}Pu, the counting sensitivity for the Asian phantom is considerably lower than that for the Caucasian phantom. This is likely due to the difference of shape and size of the two phantoms, but with a view of practical applications, these differences are not significant.

TABLE 5. PARAMETERS USED TO FIT QUADRATIC FUNCTION $Y(x) = e^{Ax^2 + Bx + C}$

Source	Photon Energy keV	Energy band used for counting keV	A	B	C
^{239}Pu	13.6+17.1+20.3	13–25	0.21025	−2.26710	5.251
^{239}Pu	43.5	33–53	0.03305	-0.46722	0.331
^{241}Am	59.5	45–70	0.04817	-0.55119	3.303
Natural uranium	63.3+84.2+90.0+92.4+92.8+93.4	40-105	0.02049	-0.30202	2.895
3% enriched uranium	63.3+84.2+90.0+92.4+92.8+93.4	40–105	0.03590	-0.35424	3.714
Natural uranium	63.3 (stripped)	37.5–73.5	0.00795	-0.29003	1.457
3% enriched uranium	63.3 (stripped)	37.5–73.5	0.05552	-0.44749	1.844
Natural uranium	185.7	163–209	-0.0488	-0.08714	1.052
3% enriched uranium	185.7	163–209	0.04594	-0.48925	2.956
3% enriched uranium	143.8	128–156	0.00414	-0.2004	1.920
Natural thorium	238.6	215–267	0.02320	-0.29301	1.788
Natural thorium	911.1+964.6+968.9	873–1036	0.05753	-0.45330	1.263
Natural thorium	2615	2515–2710	-0.00035	-0.12981	-0.294

TABLE 6. THE PHOTON EMISSION YIELDS OF ^{238}U, ^{235}U AND THEIR EQUILIBRIUM DAUGHTERS [1]

Radionuclide	Energy (keV)	Yield (%)
^{238}U	63.3	3.81
	92.4	2.73
	92.8	2.69
^{235}U	93.4	5.51
	90.0	3.38
	84.2	6.50

TABLE 7. PHOTOPEAK COUNTS WITH VARIOUS DETECTOR ANGLES

Measuring position	Radionuclide	φ	θ	Counts in photopeak (relative values)
right lung	^{241}Am	17°	18°	7.03 ± 0.26
		18°	15°	7.29 ± 0.27
		21°	12°	6.95 ± 0.26
		24°	16°	7.10 ± 0.27
left lung	^{238}Pu	14°	16°	2.92 ± 0.17
		26°	14°	3.11 ± 0.18
		26°	24°	3.29 ± 0.18
		26°	27°	3.39 ± 0.18
		31°	18°	3.24 ± 0.18

TABLE 8. COUNT RATES OF ^{238}PU IN PHANTOM LUNGS WITH A PHOSWICH DETECTOR AT DIFFERENT POSITIONS

Thickness of overlay	Count-rate C_1 [1] in position 1 [2]	Count-rate C_2 [1] in position 2 [3]	C_2/C_1
1.91	152.	181.0	1.18
2.47	82.6	90.1	1.09
2.58	70.2	79.7	1.14
2.68	55.2	70.9	1.28
3.09	40.6	44.4	1.10
3.22	33.3	38.4	1.15
3.36	29.3	33.0	1.13

[1]   Count rate in energy range of 13–15 keV in cpm.
[2]   Position 1 of the detector: X = –7.0, Z = 6.3 (cm).
[3]   Position 2 of the detector: X = –7.8, Z = 6.3 (cm).

TABLE 9. COMPARISON OF COUNTING SENSITIVITIES BETWEEN THE ASIAN AND THE CAUCASIAN PHANTOMS

Radionuclide and energy range	Chest wall thickness cm	Sensitivity for Asian phantom S_a	Sensitivity for Caucasian phantom S_c	Ratio of sensitivity S_c/S_a
^{238}Pu	1.91	0.165	0.190	1.15
13–25 keV	2.25	0.108	0.128	1.19
	3.36	0.030	0.040	1.33
^{241}Am	1.91	31.71	29.29	0.92
40–80 keV	2.25	28.76	26.75	0.93
	3.36	21.15	19.94	0.94

REFERENCE

[1]   International Commission on Radiological Protection, Radionuclide Transformations: Energy and Intensity of Emissions, Annals of the ICRP 11–13, ICRP Publication 38 (1983).
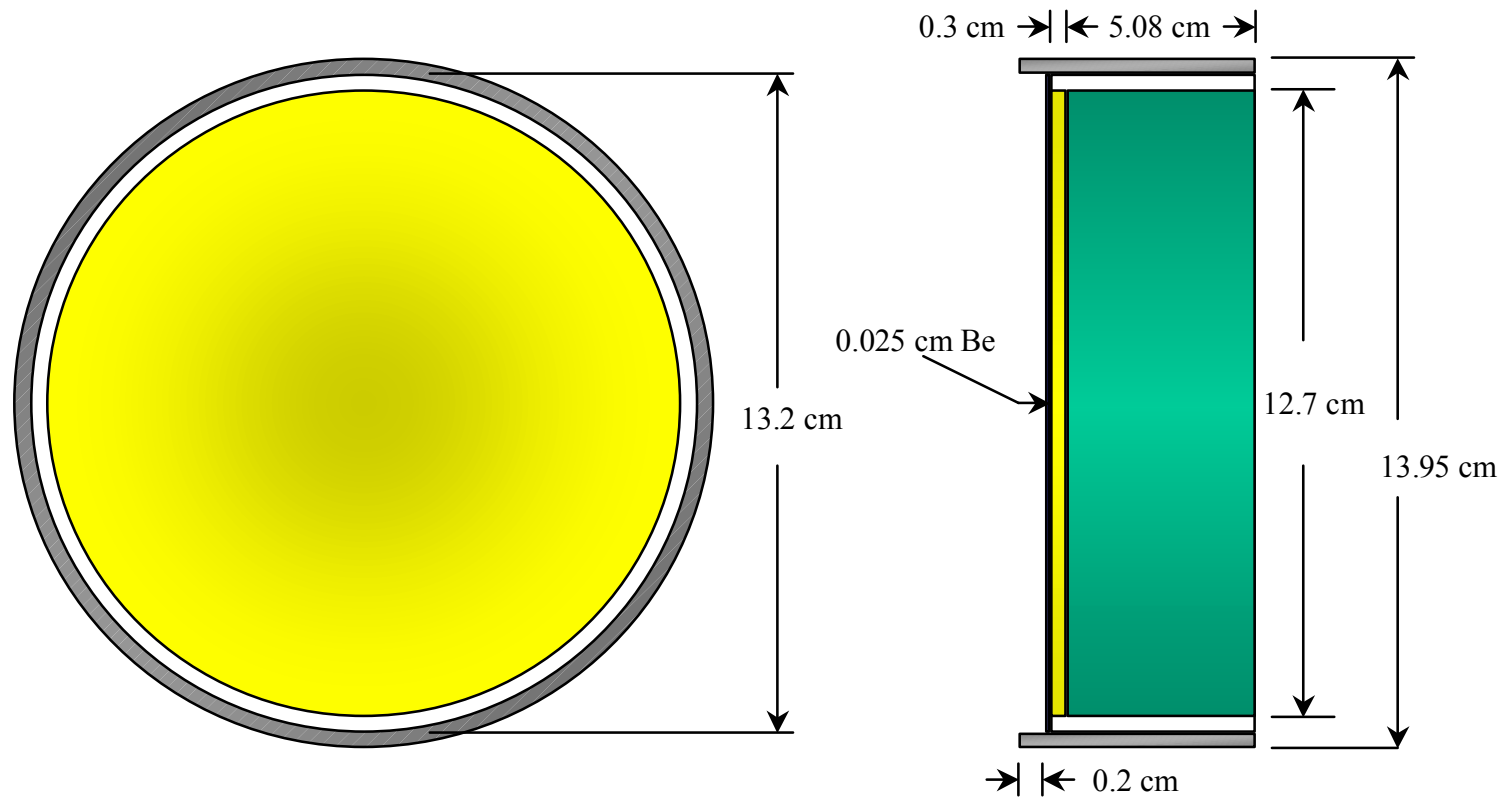
FIG. 1. China Institute for Radiation Protection phoswich detector

INDIA

R.C. Sharma, T. Surendran, T.K. Haridasan, C.B. Ghatikar
Environmental Assessment Division
Bhabha Atomic Research Centre
Trombay, Mumbai, India

Introduction

The facility is located in the Internal Dosimetry Section of the Health Physics Division (Low-level Counting Laboratories) at Bhabha, Atomic Research Center, Deonar, Mumbai. Approximately 300 measurements are performed annually for transuranics, with another 150 measurements for uranium and 25 measurements for thorium. About 5% of the measurements are performed on females.

There are two counting rooms in a common shield; the larger room is used for gamma ray measurements of the whole body, and the smaller, for lung counting. The size of the smaller room is 2.4 m long by 1.9 m wide by 1.8 m high. The outer walls are 200 mm of steel, and a wall of 152 mm of steel separates the two rooms. The smaller room is lined with 3 mm of lead, 2 mm of cadmium, and 0. 5 mm of copper. A flat bed is contained in each room.

Intercomparison Measurements

At BARC , two types of measurements were made: a) with the standard point sources in a chosen standard geometry for each detector used for the phantom measurements and b) with the Reference Asian Phantom and chest overlays including measurements with blank and radioactivity loaded lung sets. A number of detection systems were employed for these measurements in a variety of counting geometries over the phantom.

Three types of phoswich detectors operating with their optimized PSD electronics, were calibrated. Each phoswich detector was used in a suitable counting geometry and measurements were made for all the actinides except natural thorium. The detectors used were:

i)   A 20 cm diameter phoswich that had been in use for many years,
ii)   A new 20 cm diameter phoswich and,
iii)   A square phoswich with an area of 103.2 cm^2.

Two types of NaI(Tl) scintillation detectors were used:

i)   A 20 cm diameter × 10 cm thick detector in two counting geometries — static and dynamic (linear scan) for measurements of ^{232}Th and its daughters and,
ii)   A 12.7 cm diameter × 1.27 cm thick detector in a twin detector geometry with the measurements being made for all actinides except ^{238}Pu and ^{232}Th.

Finally, a single hyper pure (HP) Ge detector, 51 mm diameter and 18.5 mm sensitive depth, (LO-AX) was used in two configurations: a chest mapping configuration and an array consisting of four detectors. These measurements were made only for ^{238}Pu and ^{241}Am lungs.

A brief description of the radiation detectors, their associated electronics, shielding, counting geometries employed, and a summary of data on reference point sources and Reference Asian Phantom are given below.

Detection Systems

For low energy photon emitters, the following detection systems were employed for the measurements of actinides (^{238}Pu, ^{241}Am, Nat. U and 3% enriched U) emitting low energy photons (< 200 keV).

Phoswich Detectors:

- New Phoswich Detector (BARC 1): This detector consists of a primary detector NaI(Tl) — 200 mm diameter × 12.7 mm thick, having an MIB entrance window (Model 203 YBE 12.7 W 51 from Quartz & Silice, France). The back of the NaI(Tl) is optically coupled to one face of a CsI(Na) crystal — 200 mm dia × 50 min thick, coupled to three specially selected low noise photomultiplier tubes (EMI 9765 Bo3), 76 mm diameter each.

- Old Phoswich Detector (BARC 2): The primary detector is NaI(Tl) — 200 mm dia × 3 mm thick, having a 1 mm thick Be entrance window (Figure 1). The rear section of NaI(Tl) is optically coupled to one face of a CsI(Tl) crystal — 200 mm diameter × 50 mm thick, which is coupled through a light guide to a 170 mm diameter single photomultiplier type EMI 9623 B. The detector is Model 203YBE of Quartz and Silice.

- Square Phoswich Detector (BARC 3): This detector has a face area of 103.2 cm^2. Its primary detector is NaI(Tl) — 12.7 mm thick having Al as the entrance window. The rear section of NaI(Tl) is optically coupled to one face of a square CsI(Na) crystal — 50 mm thick – in turn coupled to a 90 mm dia ADIT photomultiplier. The detector is Model No. 4 × 4 × H.5 Q/NaI(Tl)/CsI(Na)/3.5 SSL — X of BICRON, USA

The principal component of phoswich instrumentation is the pulse shape discriminator (PSD). Through pulse shape discrimination, the secondary detector is operated as an anticoincidence device for reducing the low energy background of the primary NaI(Tl) detector. The PSD electronics are based on the ORTEC pulse shape analyzer PSA Model 458. The PSD settings were optimised separately for each phoswich before actual data collection. The schematic diagram for the electronics associated with the phoswich detectors is shown in Figure 2a.

Thin NaI (Tl) Scintillation Detector (BARC 4): The detector is 127 mm in diameter and 12.7 mm thick and has an entrance window of 1 mm Be. It is an integral assembly supplied by BICRON (Model No. 5M.5Q/5 SSAL). The schematic diagram for associated electronics is shown in Figure 2b.

High Purity (HP)Ge Detector (BARC 5): The detector has 51 mm diameter and a crystal length of 18.5 mm. It is provided with a 0.27 mm thick Al entrance window. End cap to crystal distance is 3 mm. The detector is ORTEC model No. LOAX. 51 XXX /20.S CFGSL-LOAX having liquid nitrogen dewar of 30 L. The schematic diagram for associated electronics is shown in Figure 2c.

Thick NaI(Tl) detector (BARC 6): This detector was used for the measurement of high energy photon emitters (> 200 keV), viz. ^{232}Th and its daughters. The detector is 20.3 cm diameter and 10. 2 cm thick with an entrance window of 0.25 mm stainless steel. It is an integral assembly of HARSHAW make (Type No. 32 MBS 16/3B). The schematic diagram for associated electronics is shown in Figure 2d.

Counting Room

All measurements were made in a totally shielded steel room with 20 cm mild steel walls. The room is divided into two compartments separated by a 15 cm thick steel wall. The detectors employed for in vivo assessment of low energy photon emitters are housed inside the specially designed small compartment of the steel room (inner dimensions 2.4 m × 1.8 m × 1.9 m). This compartment has a graded lining (Pb 3 mm + Cd 2 mm + Cu 0.5 mm). The thick NaI(Tl) is used in the larger compartment with a 3 mm Pb lining (inner dimensions 3.8 m × 1.8 m × 1.9 m) and is operated for the measurement of high energy (>200 keV) gamma emitters.

The entire instrumentation except detector preamplifiers (PSD electronics, data acquisition and recording equipment, and other electronic units) is located outside the steel shield (Figure 3). The data acquisition and recording equipment are common to all detector systems and consist of microprocessor based 4 K multichannel pulse height analysers (BARC Model HPD 4 K) linked with a personal computer for on line data transfer, analysis, storage and retrieval. The detectors employed for measuring low energy photon emitters are shown in Figure 4.

Counting Geometries

For each detection system, the reference point sources were positioned in a standard geometry on the central axis of the detector, with no scattering material at the back of the source. The distance between the source and the detector window was kept as 100 mm. The counting geometries adopted for the six detection systems for Reference Asian Phantom measurements are as follows:

- BARC 1 and BARC 2: The single phoswich detectors were positioned centrally over the anterior chest of the phantom with its face horizontal This is termed as the Trombay Standard Geometry (TSG). The longitudinal phantom line divides the detector area in two equal halves. The upper periphery of the detector passes through the bottom of the sternal notch. The separation between the phantom surface and the detector centre is about 1.2 cm. The coordinates of the detector centre with respect to the marked coordinate system were: X=0; Y=0; Z=3.7 cm.

- BARC 3: A twin detector geometry is simulated with a single square phoswich detector. The detector is first placed over right and then over left lung. The right and left lung readings were summed. One of the corners of the horizontal square detector is placed over the phantom reference point or the origin of the phantom co-ordinate system with the entire detector area lying in the (+Z, +X) quadrant over left lung. In this position, the two detector sides are parallel to and touching the +Z and +X axes respectively. The right lung position is a reflection of left lung position in the + Z axis. The co-ordinates of the detector centre for left and right positions were as follows:

  Left Position : X=5.4 cm ; Y = 0; Z=5.4 cm ; Right Position : X=–5.4cm; Y=0; Z=–5.4 cm.

- BARC 4: The twin detector geometry is simulated with a single thin NaI detector. The detector is first placed over right and then over left lung. The right and left lung readings were summed. For positioning the detector in this geometry, first the detector is placed centrally over chest and tilted to follow the chest contour with the detector edge being 3 cm below the bottom of sternal notch. From this central position, the detector is moved

over to right and left lung positions respectively. The longitudinal phantom line divides the left and right lung positions and is tangent to the detector circle. In terms of the phantom coordinate system, the coordinates of the detector centre are:

Over left lung X + 6.6 cm; Y = −1.3 cm; Z = + 6.0 cm; Over right lung X 6.6 cm; Y = − 1.3 cm; Z + 6.0 cm.

- BARC 5: Four detector array geometry is simulated with a single HPGe detector, with two detector positions over right and two over the left lung respectively. The coordinates of the detector centre with respect to the coordinate axes marked on the phantom are :

Position 1: X=7 cm. ; Y=0; Z=12cm
Position 2: X=−7cm; Y=0; Z= 12cm
Position 3: X=−7 cm; Y=0; and Z =5 cm
Position 4: X=7 cm; Y=0; Z=5cm.

A single NaI(Tl) scintillation detector (20.32 cm. diameter × 10. 16 cm thick) (BARC 6)was used in three counting geometries.

- A single detector static geometry: The single detector was positioned centrally over supine phantom chest, with the vertical line tangential to the detector surface passing through the bottom of sternal notch. The phantom was placed on 10 cm thick mattress on a flat bed.

- Twin Detector Static Geometry: The counting geometry is same as for single detector over static chest. The phantom was measured with single detector first over supine chest and then over prone chest in that geometry.

- Twin Detector Linear Scan Geometry: The detector positions with respect to the bed (one above and another below) were similar to those of twin detector static chest geometry. The bed is moved in a linear orbit and the scan length is 180 cm. The phantom is positioned with its supposed head at one end of the bed.

Summary of BARC Measurements

Table 1 lists the reference point sources measured with each of the six detection systems used. The observed reference source counting efficiencies in counts/cm^2/10^6 photons of the 59.6 keV gamma ray of ^{241}Am for various detection systems used for measurements on the JAERI phantom are listed in Table 2. The values for ^{232}Th are listed separately in cps/Bq in Table 3. Table 4 is a summary of BARC measurements carried out using the phantom lung sets. Detection systems and counting geometries used have been given. The measurement results of all the detection systems can be found in Annex I of this report. Analysis of experimental data for one of the systems, namely the new phoswich, yielded the bets fitted equations listed in Table 5. The JAERI and LLNL realistic phantoms were compared for ^{241}Am loaded lungs. The results are presented in Table 6. These pertain to the same detector (20 cm dia old Phoswich) use din the identical counting geometries over the two phantoms.

TABLE 1. THE DETECTION SYSTEMS USED FOR MEASURING
THE REFERENCE POINT SOURCES

.No.	Detection System	Reference point sources measured
1	New Phoswich	^{238}Pu, ^{241}Am, Nat.U and 3% enriched U
2	Old Phoswich	^{238}Pu, ^{241}Am, Nat.U and 3% enriched U
3	Square Phoswich	^{241}Am, Nat.U, 3% enriched U
4	Thin NaI(Tl)	^{241}Am, Nat.U, 3% enriched U
5	HPGe	^{238}Pu, ^{241}Am
6	Thick NaI(Tl)	^{232}Th

TABLE 2. REFERENCE SOURCE COUNTING EFFICIENCIES IN counts/cm^2/10^6 59.6 keV ^{241}Am GAMMA RAYS FOR VARIOUS DETECTION SYSTEMS USED FOR JAERI PHANTOM MEASUREMENTS[a]

No.	Detection System	Counting efficiency (counts/cm^2/10^6 photons)
1	New Phoswich	504
2	Old Phoswich	457[b]
3	Square Phoswich	353
4	Thin NaI (Tl)	319
5	HP Ge	529

a) Reference source positioned on the detector axis with a 10 cm source-detector window distance.
b) This detector was used in the previous IAEA intercomparison. The result presented in that unpublished report was in error. The correct efficiency using the LLNL Realistic phantom was 344 counts/cm^2/10^6 photons.

TABLE 3. REFERENCE SOURCE COUNTING EFFICIENCIES IN cps Bq^{-1} OF ^{232}Th FOR THE THICK NaI(Tl) DETECTOR (20.32 cm dia. × 10.16 cm thick)[a]

No.	Radionuclide	Peak energy – keV	Counting efficiency (cps Bq^{-1})
1	^{212}Pb	238	0.0850
2	^{228}Ac	911	0.0395
3	^{208}Tl	2620	0.0100

a) Reference source positioned on the detector axis with a 10 cm source-detector window distance.

TABLE 4. SUMMARY OF BARC MEASUREMENTS ON THE REFERENCE ASIAN PHANTOM LUNG SETS

Sr. No.	Detection Systems	Counting Geometries	Reference Asian Phantom	
			Lung sets	Energy bands
1.	New Phoswich	Trombay Standard Geometry	^{238}Pu	14–25 keV
			^{241}Am	32–76 keV
			Nat.U	40–120 keV; 160–232 keV
			3% En.U	40 –120 keV; 160–232 keV
2.	Old Phoswich	Trombay Standard Geometry	^{238}Pu High	14–25 keV
			^{241}Am	32–76 keV
			Nat.U	40–120 keV
			3% En.U.	40–120 keV
3.	Square Phoswich	Twin Detector Geometry; one detector over each lung	^{241}Am	43–76 keV
			Nat,U	40–120 keV 165–215 keV
			3% En.U	40–120 keV 165–215 keV
4.	Thin NaI(Tl)	Twin Detector Geometry; one detector over each lung	^{241}Am	43–76 keV
			Nat.U	40–120 keV 165–215 keV
			3% En.U	40–120 keV 165–215 keV
5.	HP Ge	Four Detector Array; two detectors over each lung	^{238}Pu High	16.20–18.19 keV 19.52–21.29 keV 42.62–43.84 keV
			^{241}Am	58.76–60.52 keV
6.	Thick NaI(Tl)	i) Single Detector static chest	^{232}Th	228–311 keV 780–1040 keV 2425–-2825 keV
		ii)Twin Detector Static chest	^{232}Th	228–311 keV 780–1040 keV 2425–2825 keV
		iii)Twin Detector Linear scan	^{232}Th	228–311 keV 780–1040 keV 2425–2825 keV

TABLE 5. BEST FIT EQUATIONS FOR THE COUNTING DATA FROM THE JAERI PHANTOM FOR ^{238}Pu, ^{241}Am AND URANIUM USING THE NEW PHOSWICH DETECTOR

Radionuclide/lung set	Energy band (keV)	Fitted equation Y-cps/Bq; X=CWT(cm)	Half value thickness (cm)
^{238}Pu (low)	14–25	$Y=3.4 \times 10^{-4} \cdot e^{-7742X}$	0.895
^{238}Pu (high)	14–25	$Y=5.80 \times 10^{-4} \cdot e^{-1.079X}$	0.642
^{241}Am	32–76	$Y=3.86 \times 10^{-2} \cdot e^{-0.2357X}$	2.94
Nat. U (^{238}U)	40–120	$Y=1.35 \times 10^{-2} \cdot e^{-0.1661X}$	4.17
Nat. U (^{235}U)	160–232	$Y=4.40 \times 10^{-2} \cdot e^{-0.2029X}$	3.42
3% ^{235}U (^{238}U)	40–120	$Y=2.20 \times 10^{-2} \cdot e^{-0.1487X}$	4.66
3% ^{235}U (^{235}U)	160–232	$Y=3.80 \times 10^{-2} \cdot e^{-0.2414X}$	2.87

TABLE 6. COMPARISON OF ^{241}AM COUNTING EFFICIENCIES FOR 60 keV PHOTONS USING A 20 cm DIAMETER PHOSWICH DETECTOR PLACED OVER THE PHANTOM CHEST USING THE TROMBAY STANDARD GEOMETRY (TSG) FOR THE JAERI AND LLNL REALISTIC PHANTOMS

Chest wall thickness (CWT) cm	Counting efficiency (counts/photon)	
	JAERI Phantom[a]	LLNL Phantom[b] (50% muscle + 50% adipose CWT)
1.91	4.71×10^{-2}	3.92×10^{-2}
2.68	3.90×10^{-2}	3.33×10^{-2}
3.36	3.31×10^{-2}	2.88×10^{-2}
2.58	3.92×10^{-2}	3.39×10^{-2}
3.22	3.39×10^{-2}	2.97×10^{-2}
2.47	4.01×10^{-2}	3.48×10^{-2}
3.09	3.42×10^{-2}	3.05×10^{-2}

a) Measured values. The best fit to the data is: $Y=7.46 \times 10^{-2} \exp(-0.2465)$
b) Measured values. The best fit to the data is: $Y=5.91 \times 10^{-2} \exp(-0.2140)$
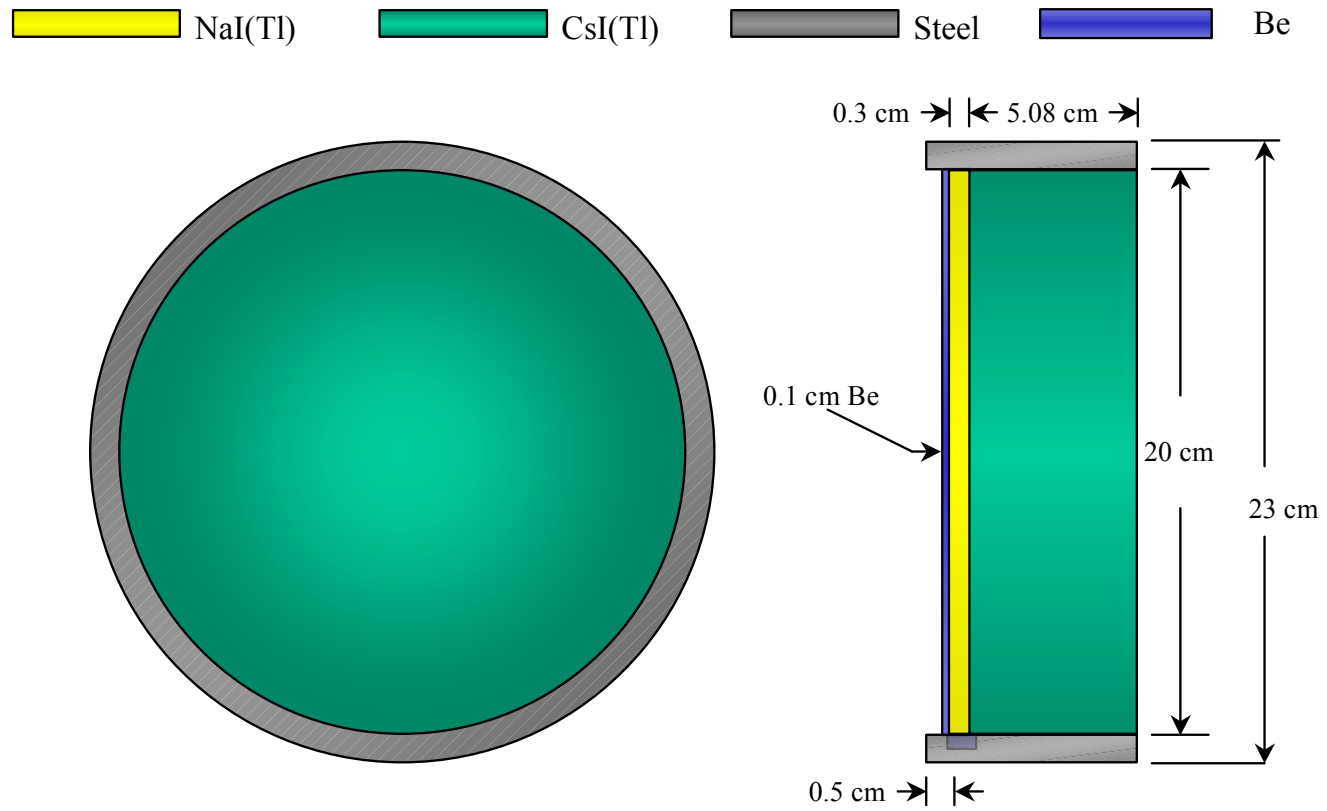
FIG. 1. BARC phoswich detector

FIG. 2. General view of the BARC whole body control room.

FIG. 3. Interior of BARC counting room with detectors used for CRP.

JAPAN

N. Ishigure
Division of Radiotoxicology & Protection
National Institute of Radiological Sciences (NIRS)
Chiba, Japan

Introduction

Extensive animal studies are carried out at the national Institute of Radiological Sciences (NIRS) to investigate biokinetics and biological effects of radionuclides, especially transuranic elements. The Institute has a staff of 90 plus 60 regular contractors who are allowed to work in the research facility. These people are counted twice a year. Another several dozen seasonal workers are counted at the beginning and the end of each contract. NIRS is also responsible for medical preparedness for radiation accident. If a patient seriously contaminated with plutonium is taken to NIRS, the lung monitor is used for the assessment of contamination level.

Intercomparison Measurements

The measurements were conducted in the shielded whole body counter. The counting room is 2.3 m wide, 1.5 m deep and 1.6 m high. The shielding is provided by a graded liner of iron (200 mm), lead (3 mm), copper (1 mm) and plastic (3 mm). The room air is filtered with a high efficiency particulate (HEPA) air supply.

Counting is performed using two sodium iodide, cesium iodide phoswich detectors, 125 mm in diameter (Figure 1). The entrance window is $75 \mu m$ thick aluminum. Resolution in the plutonium L X ray region is 35% (Apparent), and 16% in the gamma-ray region of ^{241}Am. The normal background is 0.10 counts per minute in the L X ray region and 0.13 counts per minute for γ-ray region of ^{241}Am. The minimum detectable activity for ^{241}Am is 30Bq.

Data processing is conducted using a 16bit, 20MHz Personal Computer. Spectrum analysis software is used, and dose calculations are based on the ICRP 30 model [1].

Results

The measured ^{238}Pu (13.6 keV + 17.1 keV + 20.3 keV) counting efficiency for the Asian (JAERI) phantom is shown in Figure 2 together with the measured efficiencies for the Western (Livermore) phantom. The Figure shows close agreement between the Asian and Western phantoms with 100% muscle overlays. The comparison when the 50% adipose and 87% adipose overlays are used illustrates the effect of tissue composition at these low energies. The separate counting efficiencies for the right and left lungs is shown in Figure 3, indicating a significant difference in the relative contribution of the two sides for these phantoms. It is likely that this results in large part from shielding of the left lung in the Western phantom by the heart, which is acknowledged to be enlarged. The counting efficiency for the 43 keV gamma rays from ^{238}Pu is shown in Figure 4.

Figure 5 presents the counting efficiency for the 59.5 keV gamma ray from ^{241}Am for the Asian and Western phantoms. There is a systematic difference of about 25%. Because the Western phantom has been used for some time and may be considered well characterized, this suggests that this difference may be due, in part, to an error in the assay of the ^{241}Am content of this lung set.

102
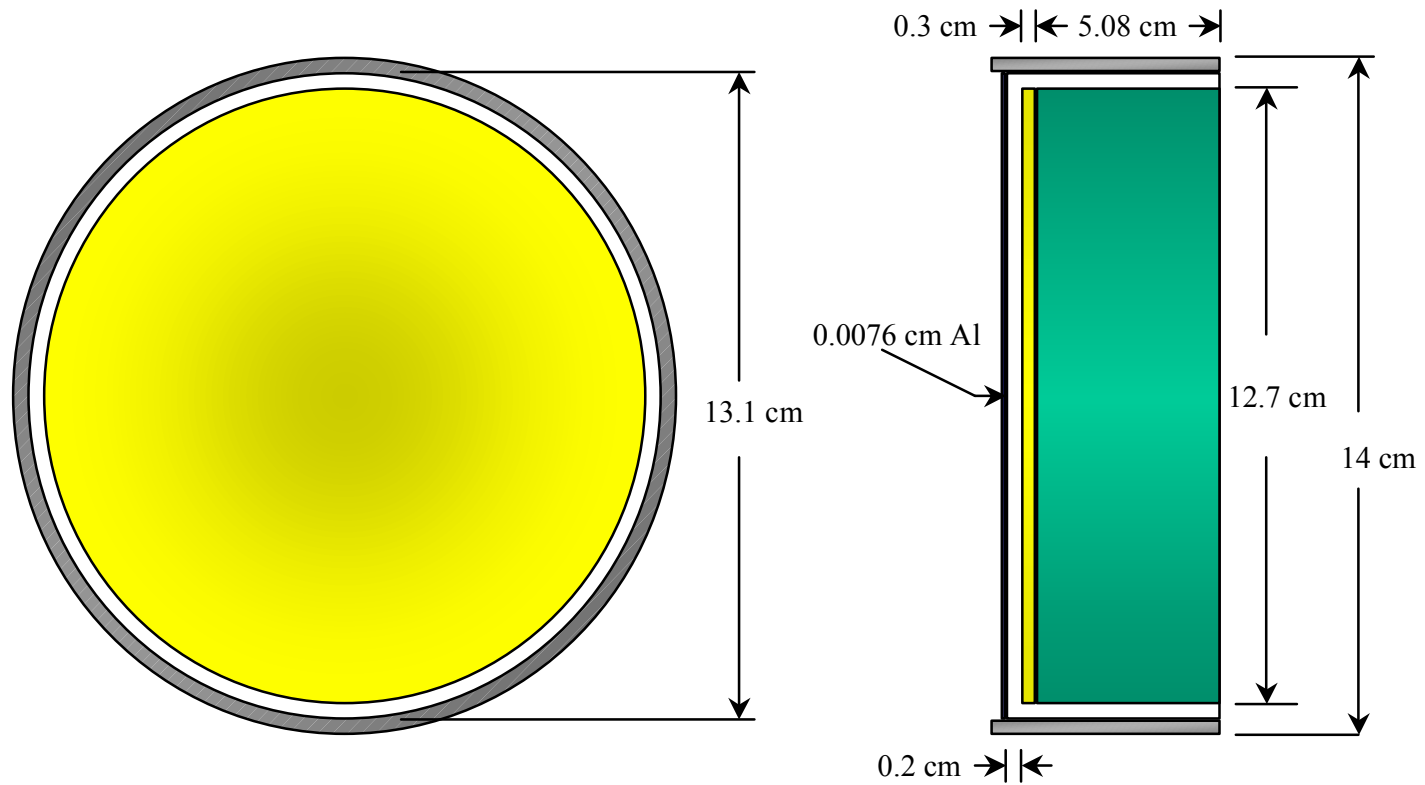
FIG. 1. NIRS phoswich.
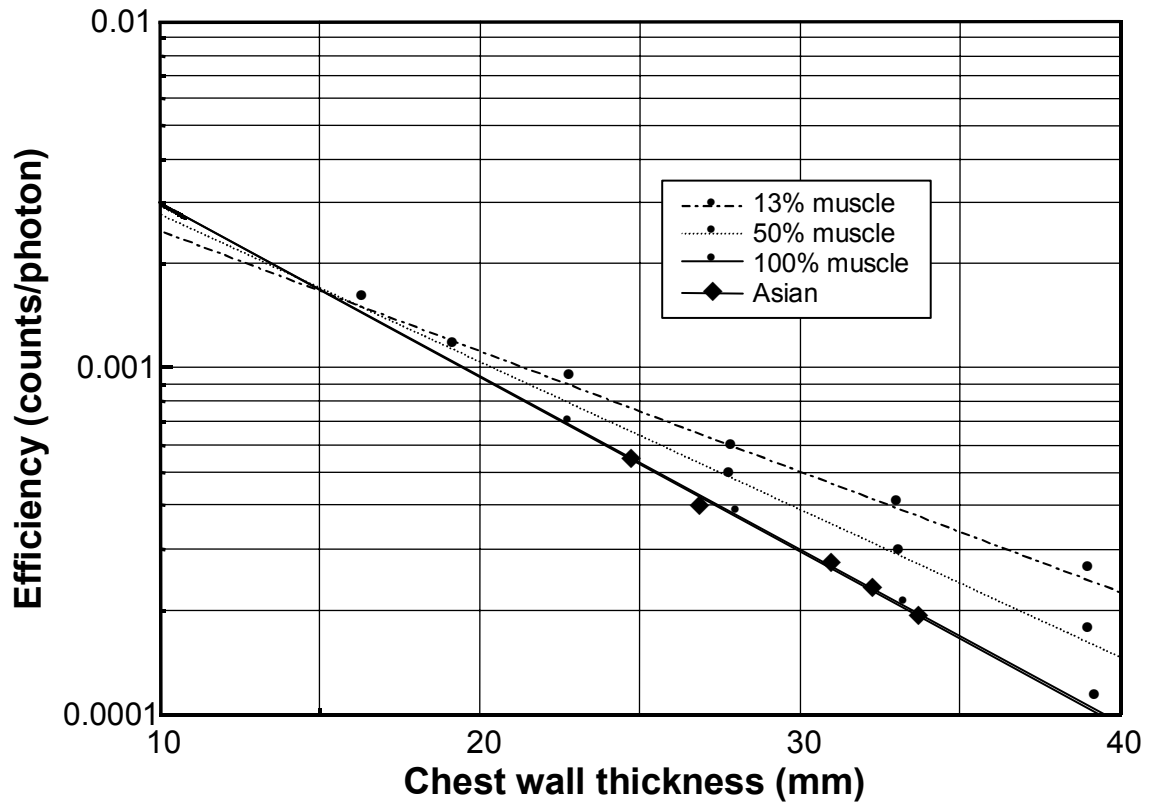
FIG. 2. Counting Efficiency for L X-rays from Pu-238.
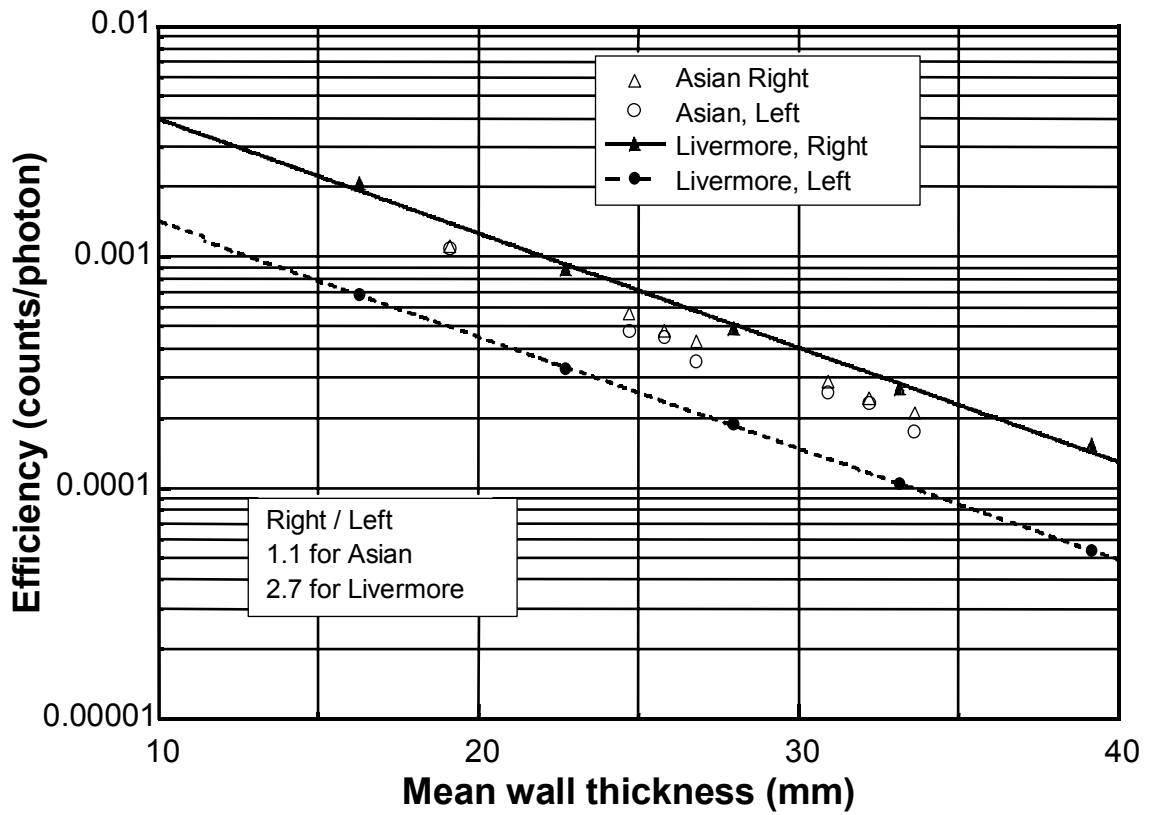
FIG. 3. Difference between Left and Right Detectors.
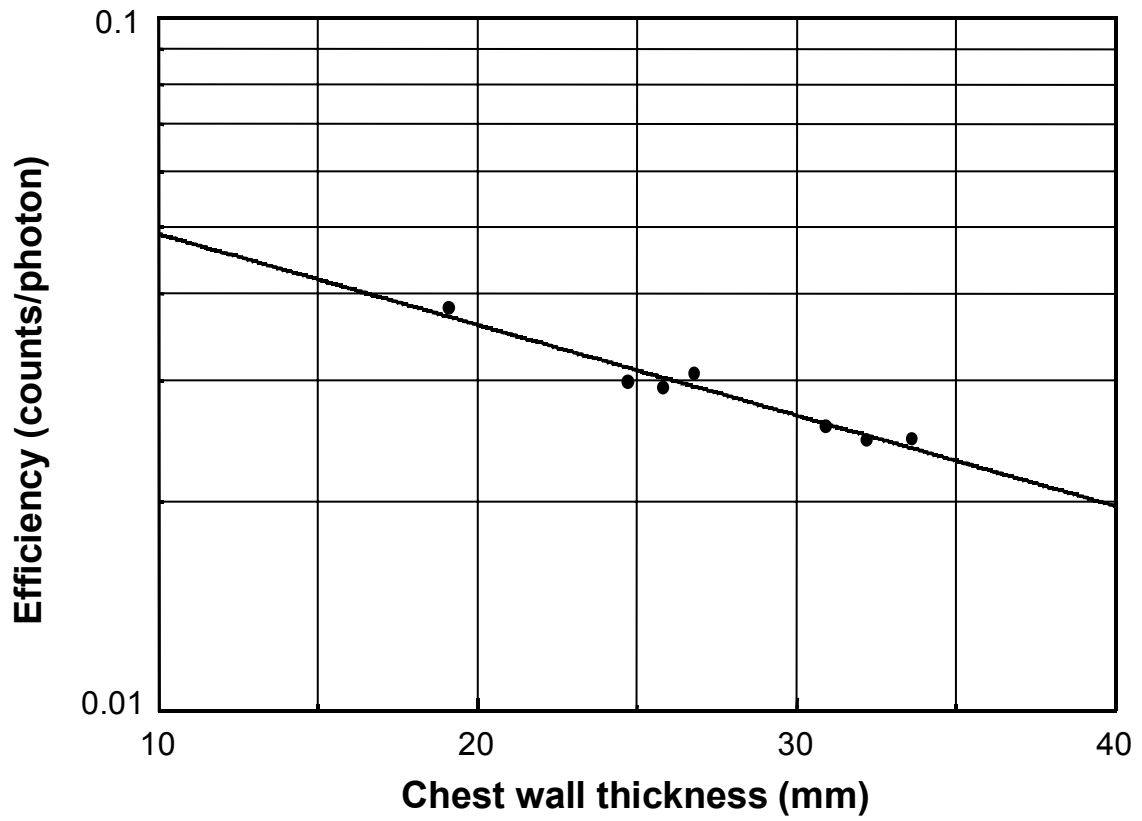
FIG. 4. Counting efficiency for 43 keVγ-rays from Pu-238.
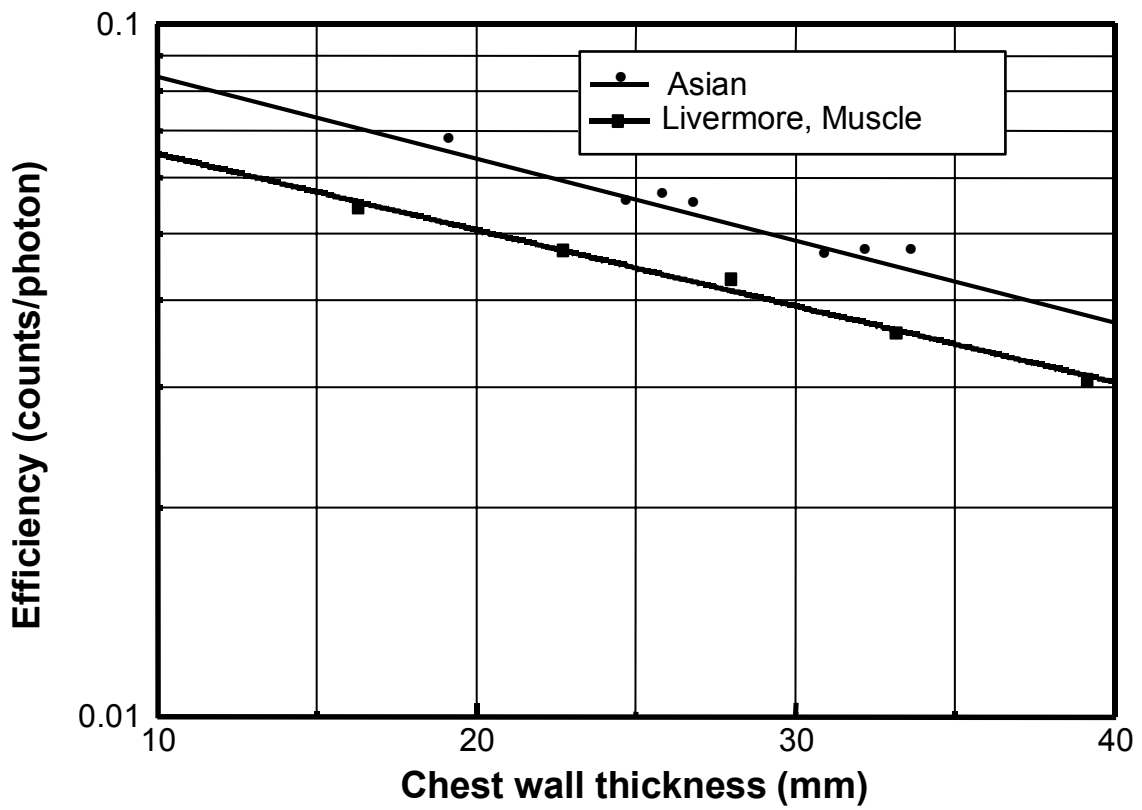
FIG. 5. Counting Efficiency for 59.5 keV γ-rays from Am-241.
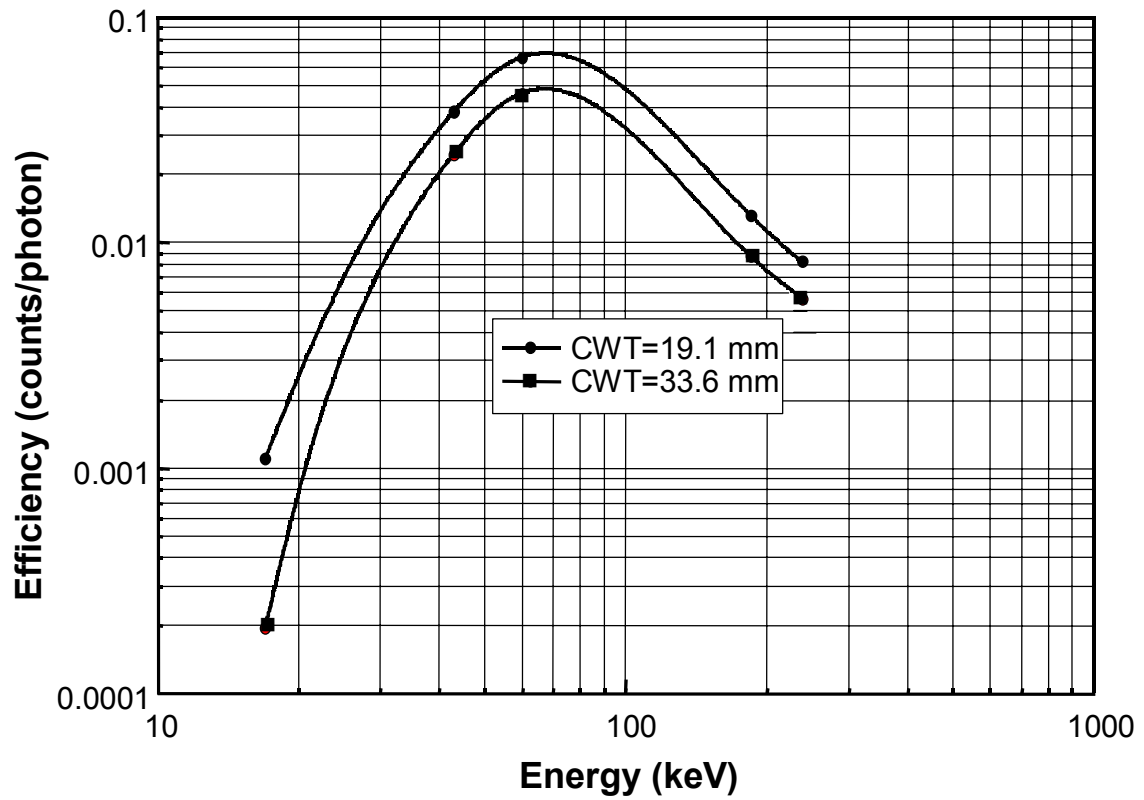
FIG. 6. Energy Dependence of Counting Efficiency.
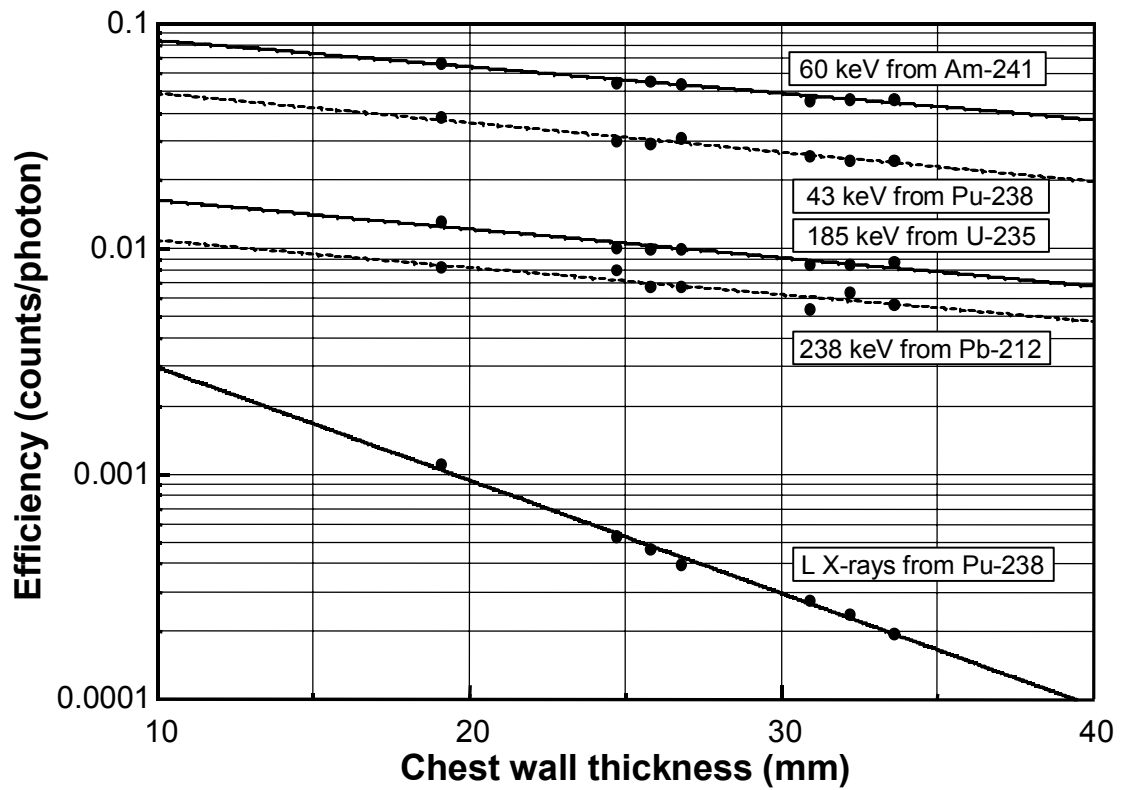
FIG. 7. CWT Dependence of Counting Efficiency.

Figure 6 shows the energy dependence of the counting efficiency for our system for the phantom core with no overlays, and the 15 mm thick overlay set. The counting efficiencies as a function of muscle equivalent chest wall thickness (MEQ-CWT) are shown in Figure 7. The MEQ-CWT values for 43 keV were used for this purpose. Figure 7 illustrates the effect of chest wall attenuation, particularly for the ^{238}PU L X ray. For higher energy photons, the slopes of the efficiency curves are essentially constant.

REFERENCE

[1]   International Commission on Radiological Protection. Limits for intakes of inhaled radionuclides. Annals of the ICRP 2(3/4). ICRP Publication 30 Parts 1–4 (1979).

REPUBLIC OF KOREA

Tae-Young Lee
Health Physics Department
Korea Atomic Energy Research Institute
Taejon, Republic of Korea

Introduction

The Korea Atomic Energy Research Institute (KAERI) has a state-of-the-art In Vivo Radioassay and Research Facility (IVRRF) facility designed expressly for in vivo measurement of radioactive material. Although the IVRRF's primary activity is providing routine in vivo counting services to KAERI radiation workers, the facility also conducts work for clients including a fuel fabrication facilities and nuclear facilities.

Counting System

KAERI in vivo counter combines the characteristics of the U/Pu lung counter and the advantage of a high sensitivity scanning NaI(Tl) whole body counter into one compact system. The low energy lung counter is designed for facilities that need to accurately measure lung depositions of actinides such as uranium, plutonium and americium. The scanning whole body counter is designed to detect and identify the location of higher energy nuclides anywhere in the body.

The detection system of the low energy lung counter consists of two arrays of ACT (Actinide)-II detector system which combines two ACT I LEGe (Low Energy Germanium) detectors and end caps onto a single 7 liter multi-attitude cryostat. These have been designed specially for the detection of internally deposited actinides, particularly uranium, plutonium and americium. Figure shows the detectors in place over the JAERI Phantom. For comparison, Figure 2 shows the same detector placed over the Livermore Realistic Torso Phantom. Each LEGe detector equipped with a 0.5 mm. Be window has active area of 20 cm^2 and thickness of 20 mm (Fig. 3). The resolution of four LEGe detectors averages 400 eV FWHM at 5.9 keV and 700 eV FWHM at 122 keV. One cm Pb and 0.5 mm Cu are attached around sides of ACT-II detectors to reduce the contribution from ^{40}K and scattered background from the subject and surrounding materials. The detector-subject positioning mechanism allows the optimum placement of detectors on the chest of the subject.

The whole body counter utilizes a large 7.6 cm × 12.7 cm × 40.6 cm scanning NaI(Tl) in a linear geometry, which significantly improves the measurement accuracy for internal depositions for subjects of varying sizes. The linear efficiency response and scan length minimize systematic errors due to variations in the location of radioactivity and the subject's height and weight. The positional spectrum acquired by the counter provides a method of locating and quantifying the location of internal depositions and their movement. This information is essential for accurate organ dose calculations. In addition, the positional spectrum is very useful in identifying the presence and location of external contamination.

The Lower Limit of Detection with the counting chamber and LEGe detectors is 4.5 Bq (1.3 nCi) ^{241}Am or ^{235}U for a 30 minute count of a person with a 2.3 cm chest wall thickness at the 95% confidence level. The Lower Limit of Detection with the counting chamber and scanning NaI(Tl) detector is a approximately 188 Bq (5 nCi) ^{60}Co for a five minute count at the 95% confidence level.

- The electronics system for the low energy lung counter consists of HV power supplies, preamplifiers, amplifiers and an analog multiplexer. The multiplexer accepts analog signals from multiple amplifiers and routes them into their respective segments of MCA memory. The MCA is configured to provide 8192 channels of memory, and the ADC parameter of MCA is configured to provide four 2K groups. So data from detector #1 is stored in the first 2048 channel group, data from detector #2 is stored in the second. 2048 channel group, and so on. This results in four individual spectra, each representing the spectrum obtained from individual detectors. The MCA employs a PC based MCA acquisition board that is supported by DOS software. Spectra from NaI(Tl) scanning detector are accumulated into an AccuSpec multichannel analyzer(MCA) and associated electronics.

Low Energy Lung Counter Calibration

Evaluation of internally deposited, photon-emitting radionuclides by in vivo measurements requires calibration of the counter for converting the counts obtained into the amount of activity deposited in the lungs. The counter may be calibrated using realistic phantoms, human volunteer inhalation programmes and theoretical calculation. The approach that has been used at KAERI is based on measurements made with the LLNL torso phantom with accurately known activities.

The calibration source with the LLNL torso phantom used at KAERI is a mixture source of ^{241}Am and ^{152}Eu providing a number of prominent photon emissions with energies between 17 keV and 344 keV. The mixed source is deposited on the planar sheets to simulate a uniform activity matrix throughout the volume of the LLNL torso phantom lung inserts.

The lung inserts are placed in both lungs of the LLNL torso phantom, and the phantom is positioned on the counting bed. Detector positions are adjusted to place the detector faces at the reference lung marking on the phantom chest wall. Detector angles are adjusted to position the face of each detector as close as possible to being tangent at point of contact with the phantom.

A calibration count is performed on phantom with the torso plate cover only. Calibration counts are also performed using chest overlays to increase the wall thickness from 17.8 mm to 40.7 mm. These calibrations are performed with the 50% muscle-50% adipose fraction overlay set.

Whole Body Counter Calibration

Calibration of the scanning NaI(Tl) detector for whole body distributed radionuclides is performed using the BOMAB phantom family uniformly loaded with mixed gamma sources. Calibration measurements are supplemented by Monte Carlo calculations for body sizes differing the standard phantom dimension. The BOMAB phantom family consists of the following phantoms based on ICRP Publication 23 data [1]:

- Reference Male
- Reference Female
- Reference 10 year old
- Reference four year old.

Calibration of the scanning NaI(Tl) detector for thyroid depositions is performed using the American National Standards Institute (ANSI) Neck phantom with mixed gamma sources. These measurements are supplemented by Monte Carlo calculations.

Theoretical Study of Calibration of In Vivo Measurement Systems

Currently, surrogate human structures or phantoms are employed to represent the human body during the calibration process. Radioactivity distributed in the phantom tissue substitutes permits the determination of appropriate calibration factors for the in vivo measurement system. Despite efforts to develop more realistic phantoms with increasing complexity, the fundamental problem with their use remains that the phantom generally represents an average human body. Significant corrections must still be made to phantom based calibration factors in order to obtain absolute calibration efficiencies applicable to a given individual.

The Magnetic Resonance Image Photon Phantom (MRIPP) demonstrates a new way to calibrate systems used for in vivo measurements. It supplements the use of physical phantoms, which are expensive to produce, and only simulate standard man. MRIPP is being used to obtain the theoretical calibration factor of in vivo measurement system.

Quality Assurance

IVRRF operations are governed by an approved quality assurance plan. Measurement data reliability is ensured through periodic calibration of the counting system with anthropomorphic phantoms, daily control measurements, careful data review, and participation in measurement intercomparison programmes.

Determining the presence of radioactive material involves an analysis of the measurement data to reduce the probability of false positive or false negative results. The current in vivo counting programme meets the intent of ANSI N13.30 [2]. The IVRRF's measurement performance meets or exceeds the N13.30 criteria for both accuracy and precision. The IVRRF programme is designed to receive accreditation through DOE Laboratory Accreditation Programme when it is instituted.

Research at the IVRRF

A study on improvement of the thyroid monitoring system using Monte Carlo calculations seeks to establish the optimal detection method by assessing effect of the factors such as:

- detector size
- neck to detector distance
- detector miss-positioning
- neck thickness
- activity distribution in body
- thyroid displacement

The thyroid monitoring system is composed of either ANSI neck phantom or BOMAB phantom, and NaI(Tl) detector. The MCNP code is used for the Monte Carlo simulations.

Intercomparison Results

The JAERI phantom counting efficiencies for the five lung sets in counts per second (cps) per Becquerel (Bq) are shown in figures 4 through 8. The efficiencies for the promanent photons for each radionulcide set are presented as a function of muscle equivalent chest wall thickness (MEQ-CWT). It is obvious that the transmission of the 17.1 keV X ray from ^{238}Pu is most dependent on the chest wall thicknes (Figure 7).
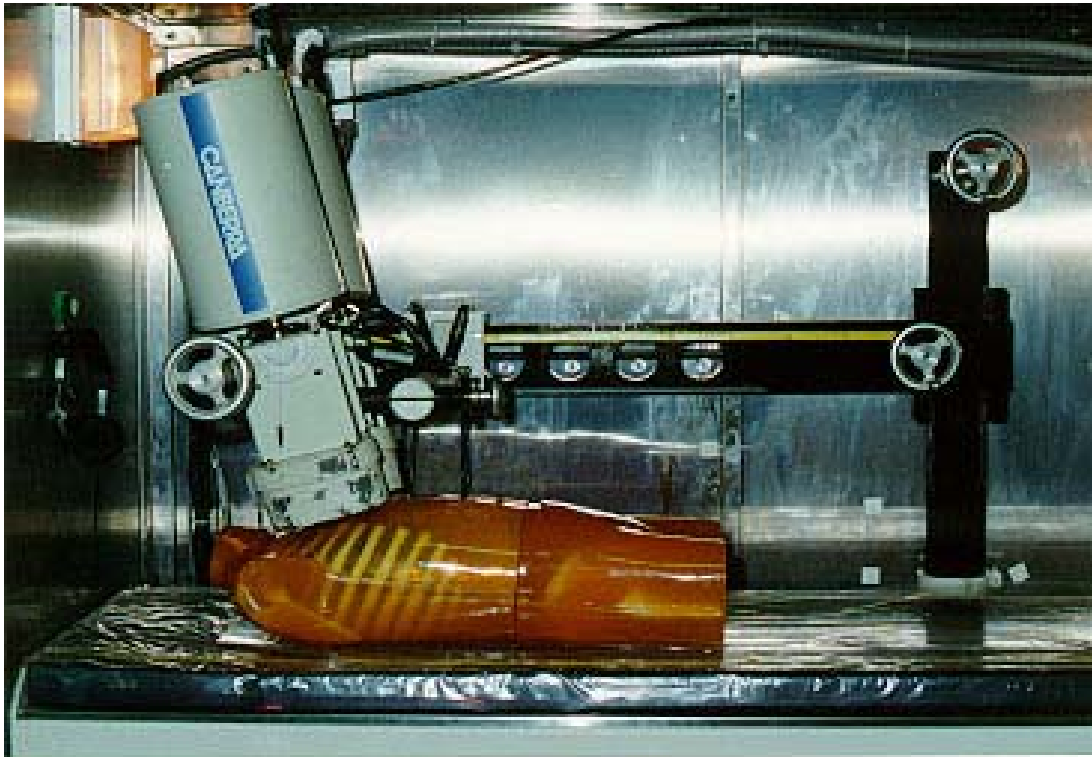
FIG. 1. KAERI detection system in place over JAERI torso phantom.
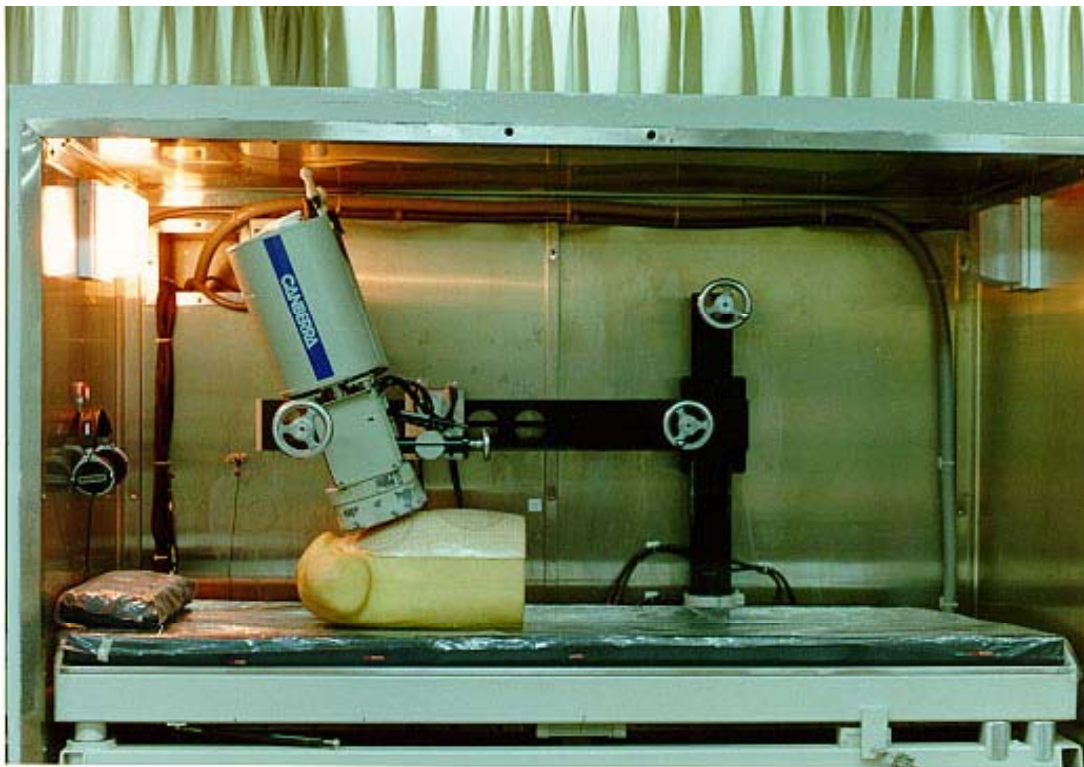
FIG. 2. KAERI detection system in place over LLNL torso phantom.
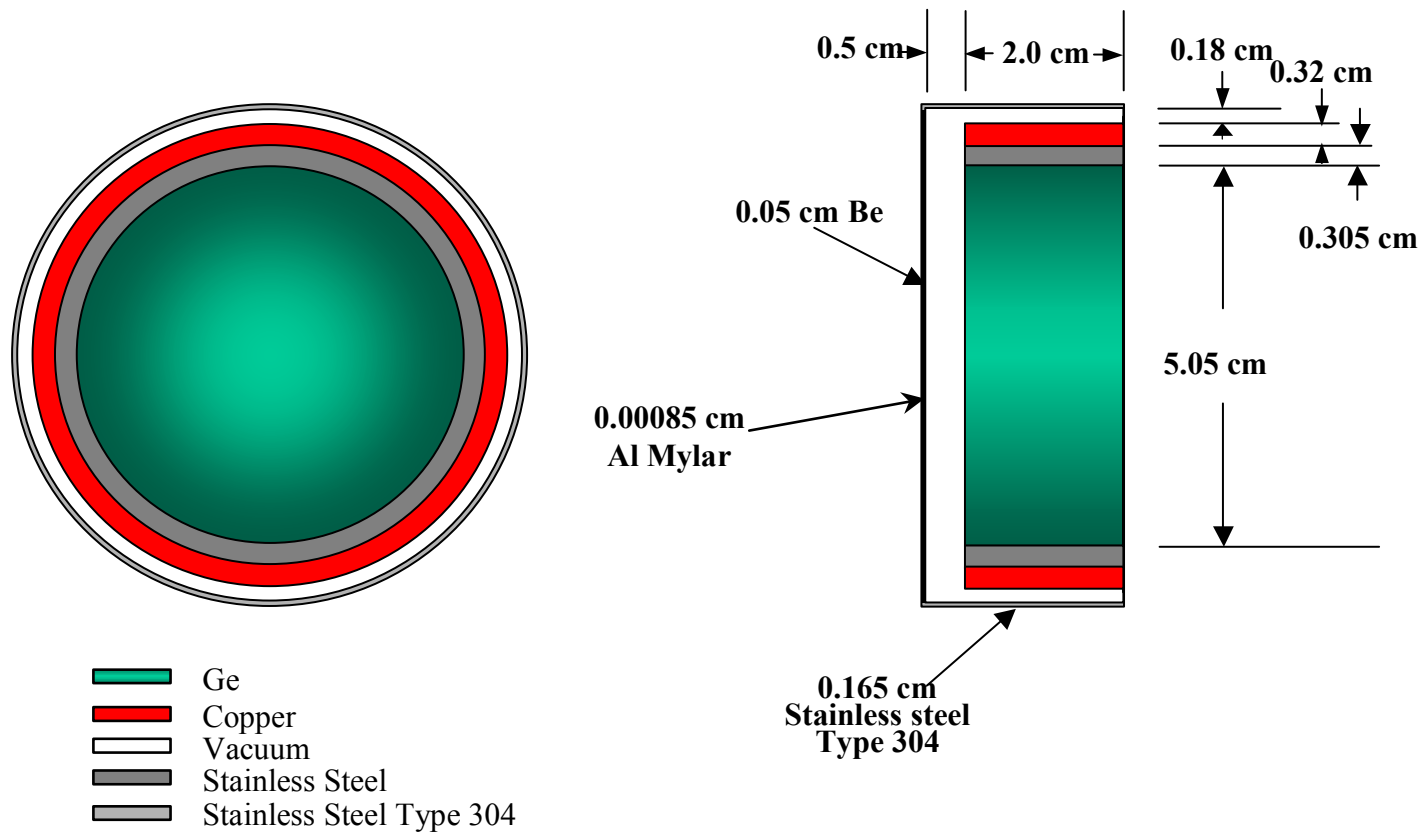
FIG. 3. KAERI LEGe Detector.
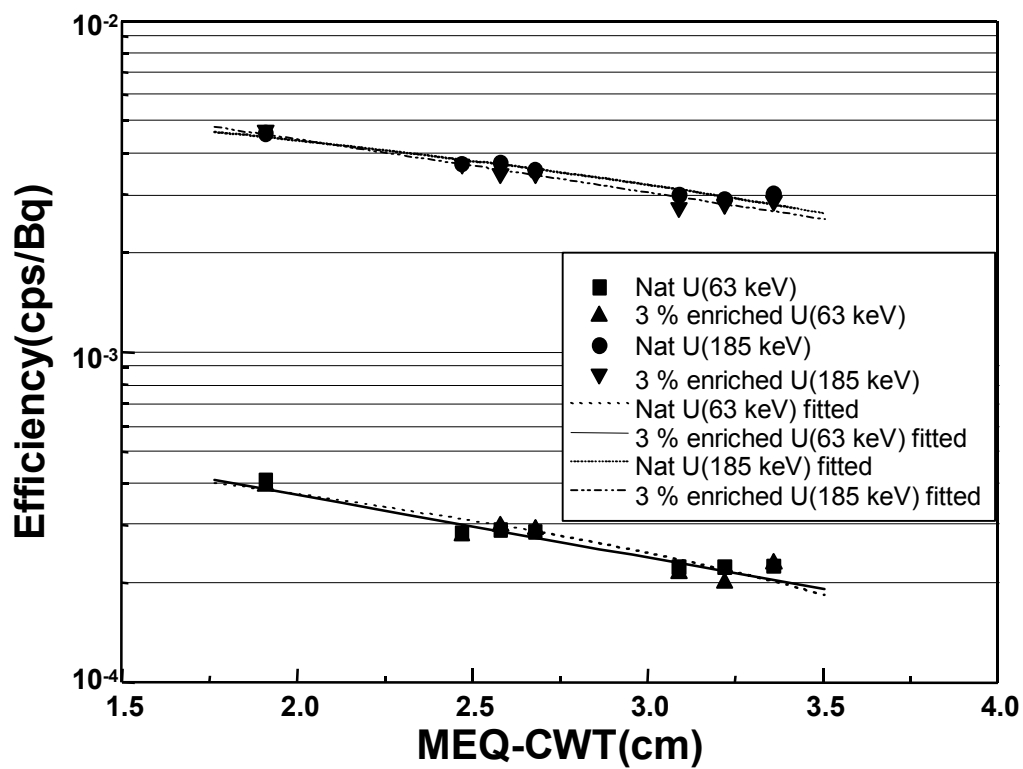
FIG. 4. Counting efficiency for uranium (natural and 3% enriched) with JAERI phantom.
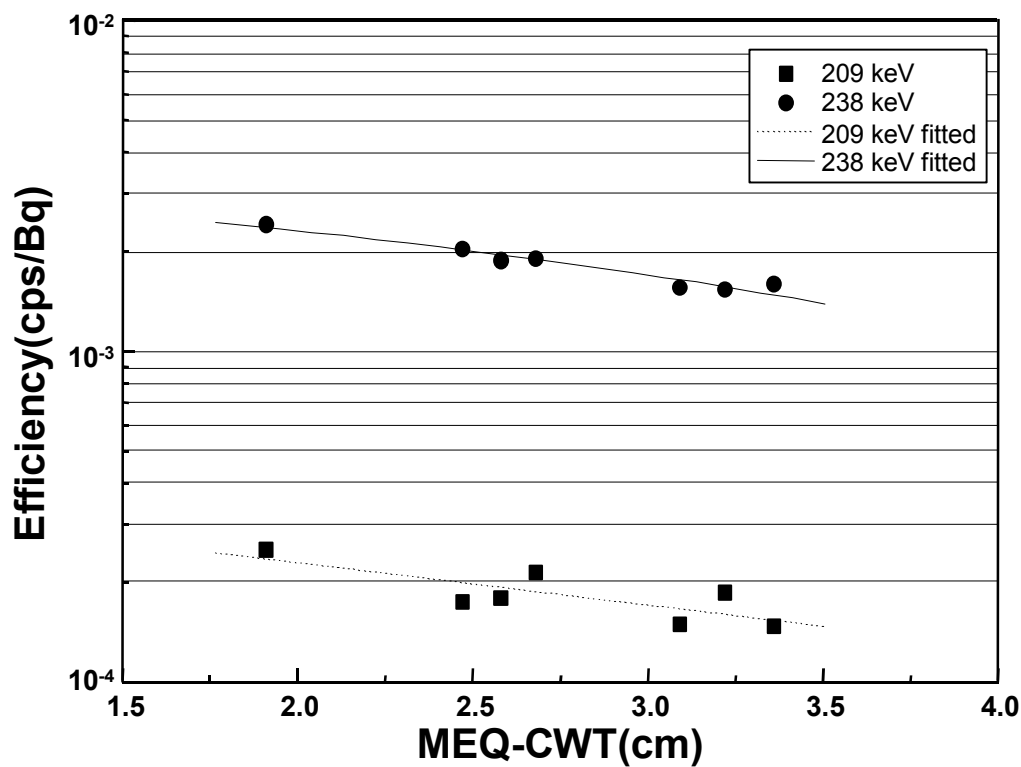
FIG. 5. Counting efficiency for thorium with JAERI phantom.
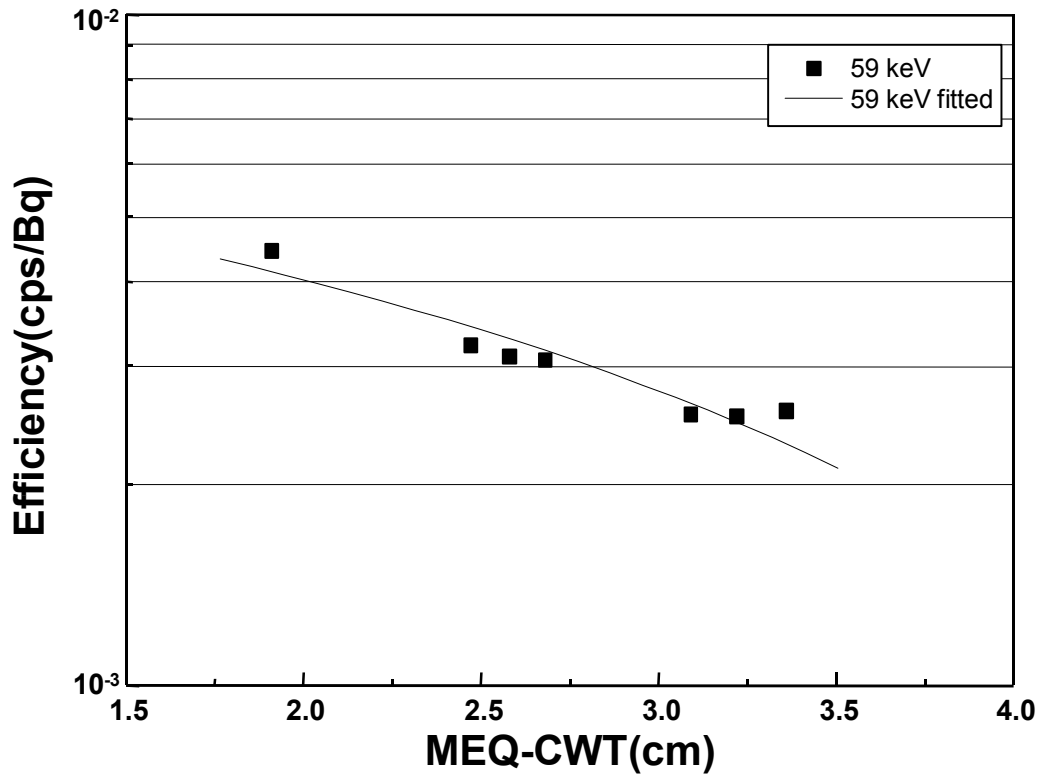
FIG. 6. Counting efficiency for ^{241}Am with JAERI phantom.
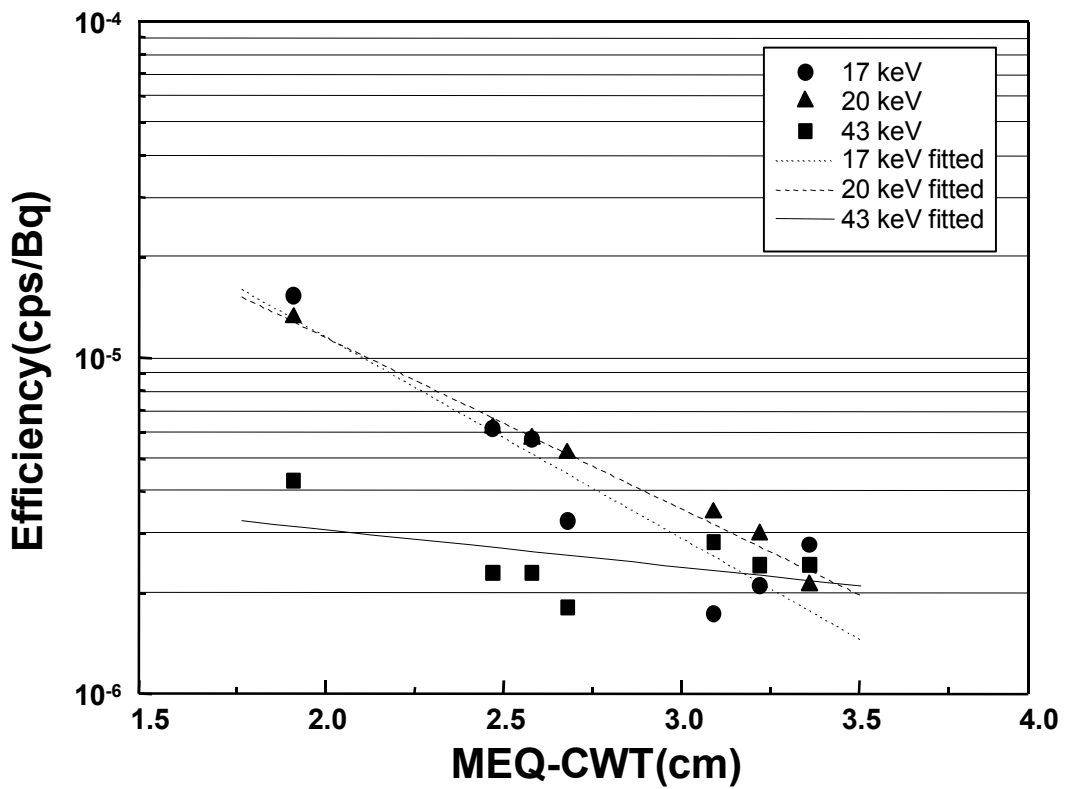
FIG. 7. Counting efficiency for ^{238}Pu with JAERI phantom.

114
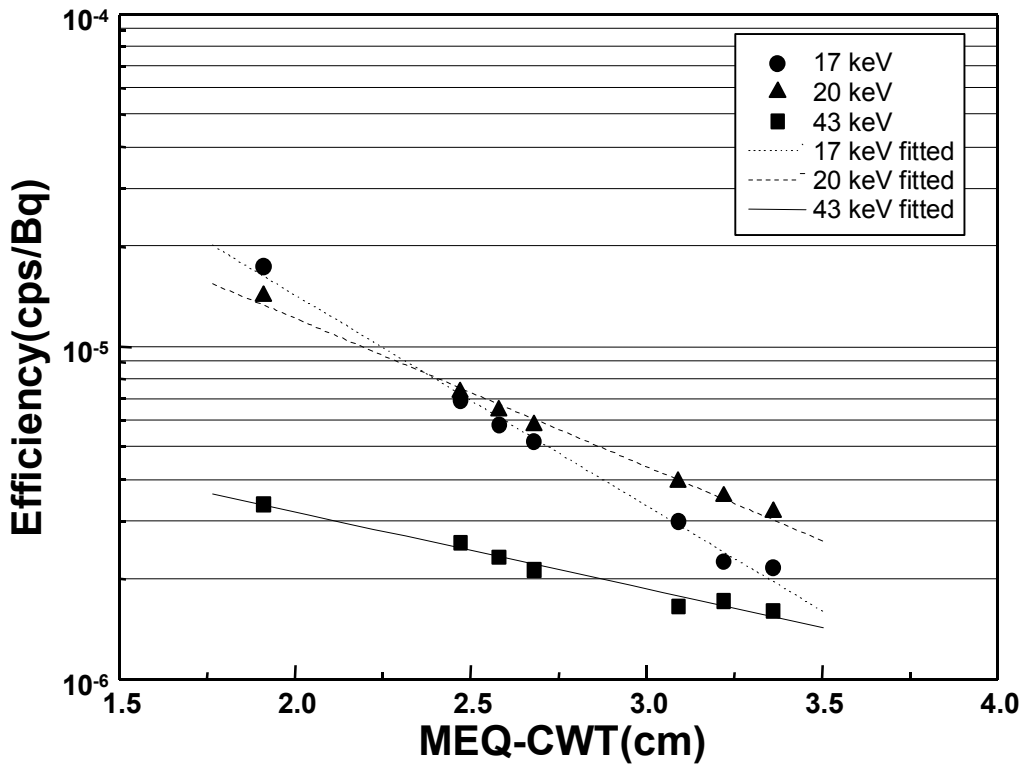
FIG. 8. Counting efficiency for ^{238}Pu with JAERI phantom.
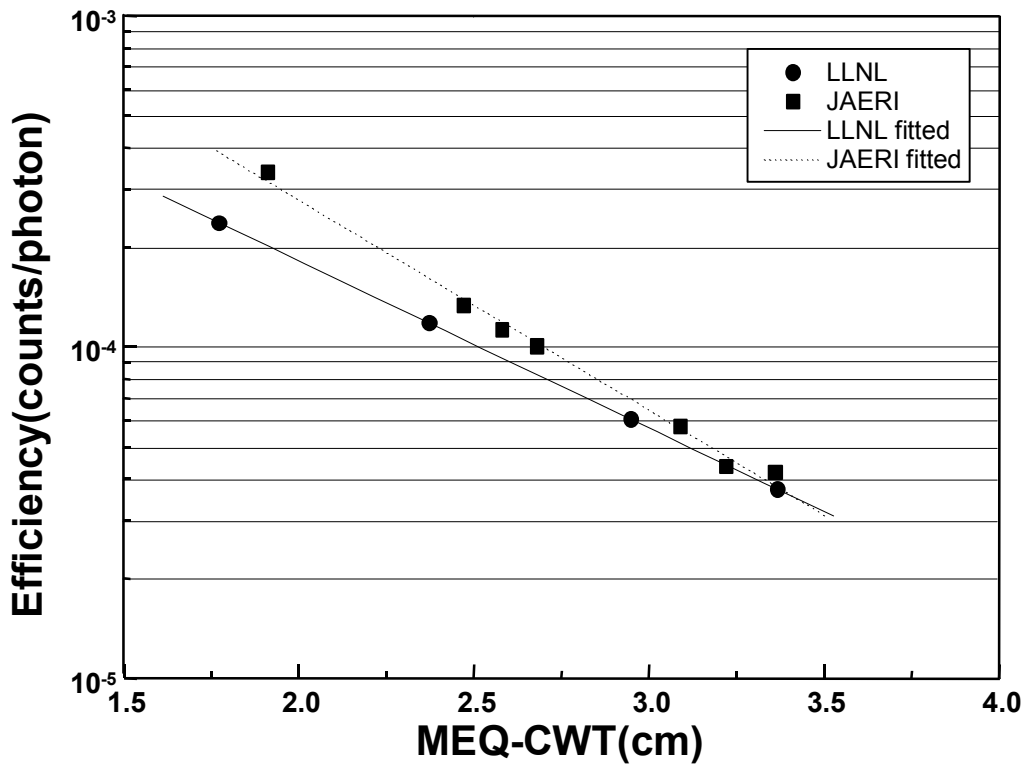
FIG. 9. Comparison of counting efficiencies for 17 keV photons using JAERI and LLNL phantoms.

115
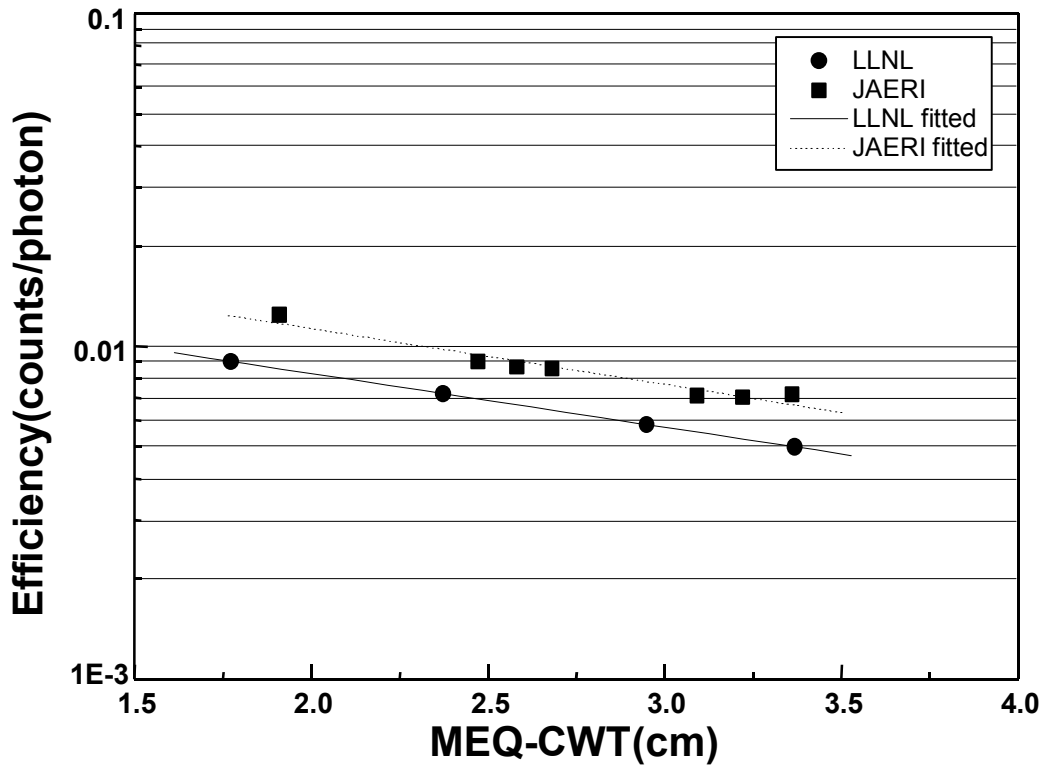
FIG. 10. Comparison of counting efficiencies for 60 keV photons using JAERI and LLNL phantoms.
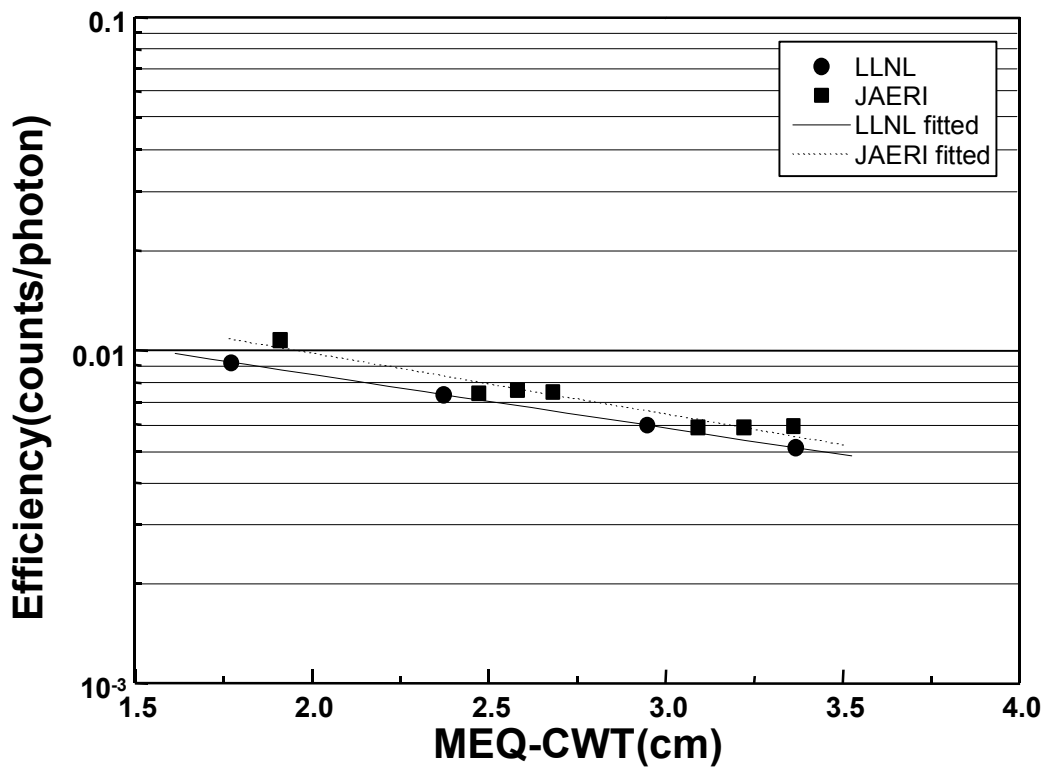
FIG. 11. Comparison of counting efficiencies for 63 keV photons using JAERI and LLNL phantoms.

116
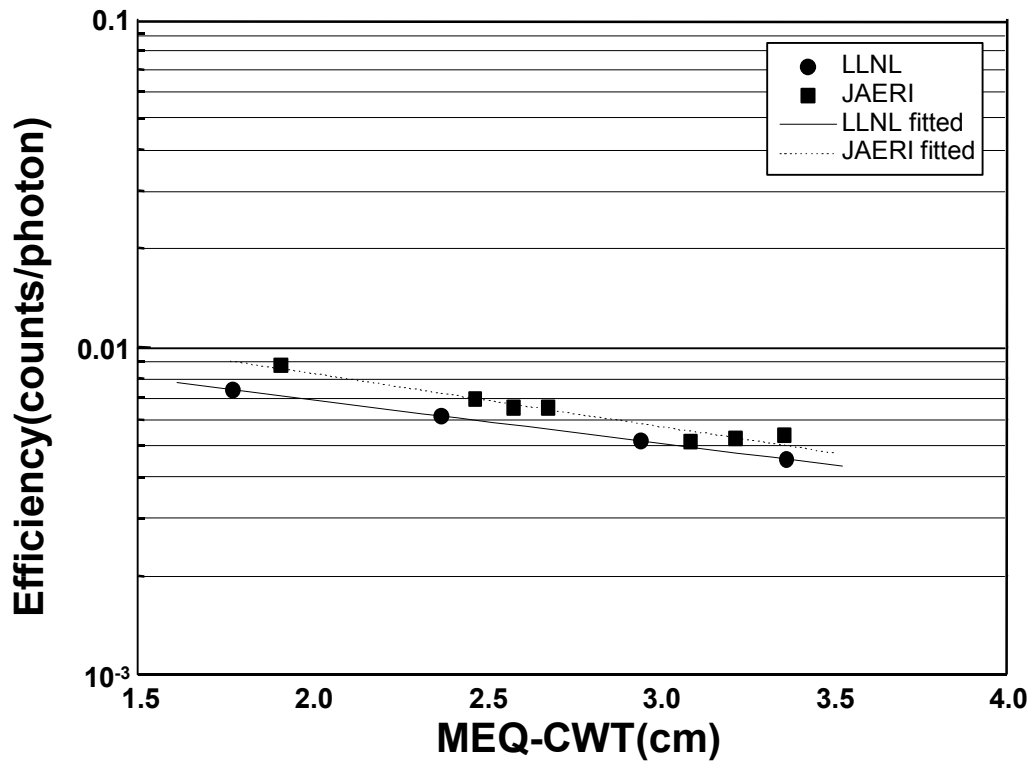
FIG. 12. Comparison of counting efficiencies for 185 keV photons using JAERI and LLNL phantoms.
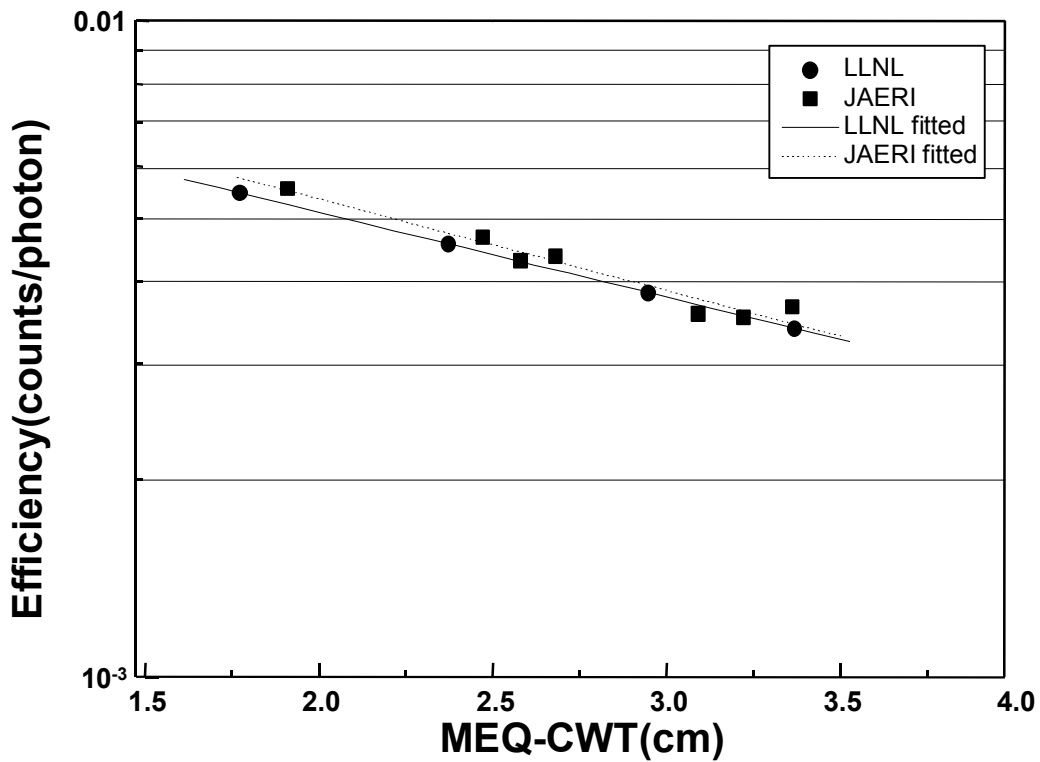
FIG. 13. Comparison of counting efficiencies for 238 keV photons using JAERI and LLNL phantoms.

117
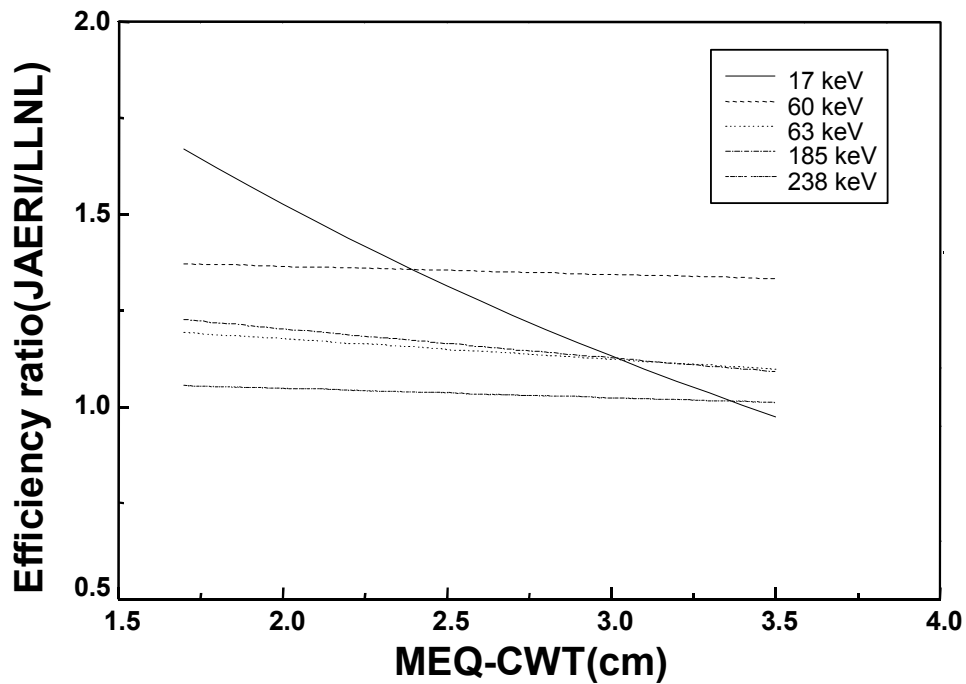
FIG. 14. Ratio of photon counting efficiencies for JAERI and LLNL phantoms

A difference in counting efficiencies obtained with the JAERI (Asian) and LLNL (Western) phantoms was a major reason for establishing this CRP. A Joint KAERI — Canadian HML project is aimed at comparison of the LLNL and JAERI torso phantoms. This cooperative project, funded by KAERI, was conceived because the LLNL phantom is very much larger than a typical Korean worker, whereas the JAERI phantom [3] supplied by the Human Monitoring Laboratory (HML) is based on Japanese Reference Man [4] and, therefore, is more typical of a Korean worker. KAERI wished to implement a new set of calibrations based on a phantom that was representative of an Asian man instead of the LLNL phantom, which is representative of a much larger person.

The comparison is illustrated in Figures 9 through 14. Figures 9 through 13 present the photon detection efficiencies for the 17.1 keV (^{238}Pu), 59.5 keV (^{241}Am), 63.3 keV (^{234}Th: ^{238}U), 185 keV (^{235}U), and 238 keV (^{212}Pb: ^{232}Th) photons in counts per emitted photon.

REFERENCES

[1]   International Commission on Radiological Protection, Report on Reference Man: Anatomical, Physiological and Metabolic Characteristics, New York, Pergammon Press; ICRP Publication 23 (1975).

[2]   ANSI, "American National Standard for performance criteria for radiobioassay," ANSI/N13.30 standard. American National Standard Institute, Inc, New York, NY (1996).

[3]   S Shirotani T., 1988. Realistic torso phantom for calibration of in vivo transuranic nuclide counting facilities, J. Nucl. Sci. Tech. 25:875–883 (1998).

[4]   Tanaka, G. Kawamura, H., Nakahara, Y., Reference Japanese Man-I. Mass of organs and other characteristics of normal Japanese, Health Phys. 36, 333–346 (1979).

MALAYSIA

How Mooi Lau
Malaysian Institute for Nuclear Technology Research (MINT)
Kajang, Malaysia

Introduction

The whole body counter was purchased in 1985, under a technical assistance project, from the Nuclear Data Corporation, which was subsequently bought by Canberra System Ltd Enterprise. After the system was purchased, an IAEA expert provided assistance with calibration and offered training on use of the system. It was put into operation in 1986. It was used to measure radiation workers from hospitals and MINT who worked with unsealed sources such as those involved in the production of ^{99m}Tc and ^{131}I.

Malaysia mines a lot of tin, and the tin tailings contain valuable rare earth elements. One company was extracting the rare earths and exporting them, mainly to Japan, for use in electronic industry. The Malaysian regulators were concerned that some workers may be exposed to unnecessarily high levels of uranium and thorium through intake of these nuclides, which are abundant in the tin tailing. MINT was instructed to measure the internal level of natural uranium and thorium in workers of concern to the regulatory agency. In addition, some people returning from Europe immediately after the Chernobyl Accident in 1986 were measured using this system.

The system became inoperative 1989 due to a problem with the electronics and difficulties encountered in obtaining replacement parts. Due to lack of budget for the high cost of repair, alternative measurement methods were used until 1995. At that time, with a change of staff, in-house repairs were made, a new set of electronic components was installed and the WBC is made operational again. At that time, it was mainly used to monitor isotope production workers, especially those working with ^{131}I.

However, the need to monitor the workers in the tin mining industry for the uranium and thorium intake, as requested by the regulatory agency, remained. Since this is the only operational whole body counter in the country, it has to be well maintained and ready to respond to any request from users. With the impending construction of a nuclear power station in Indonesia, it is expected that the regulatory authority will require more complicated analyses. The Malaysian Ministry of Health has another whole body counter in the Institute of Medical Research. It also has some technical problems, and it is expected that increased effort will be needed to make it operational, perhaps with the assistance on MINT staff.

Whole Body Counter System

The WBC was a Nuclear Data WBC-6000 system, with a chair type configuration. A number of problems were encountered when the system was first installed, mainly due to lack of calibration sources and phantom. Reliance was placed on the manufacturer's precalibration for the initial measurements. The manufacturer did not install the system or provide training on its use. Based on comments during the subsequent IEAE expert mission, it appears that the system was not installed properly.

Lack of a proper phantom proved to be a problem. The expert had been in Central Europe at the time of the Chernobyl accident and had some internal contamination. He used himself as a secondary standard to provide a rough check of the system. However, it was not sensitive enough to detect the fallout isotopes or even the ^{40}K.

Following proper adjustment of the system and optimization of the electronics and the peak search software, an improvised phantom roughly equivalent to standard man

dimensions, was constructed using 17 plastic bottles. Measurements were performed with ^{137}Cs and ^{40}K in solution. A whole body count of the expert was performed again and his ^{137}Cs content was found to be approximately correct. Also the ^{40}K levels of several staff were measured and found to be reasonable.

A number of measurements have been made and recorded since beginning of the use of this WBC system, even though the assessments may not have been very accurate. This provide at least an indication of the levels, if any, of the internal contamination for workers in unseal source areas. Monitoring was provided for staff working in the Isotope Production Laboratory, reactor operation staff and some staff from medical institutes and hospitals using unsealed sources. Most of the measurements made were at background levels. Only occasionally, some internally deposited ^{131}I was detected in Isotope Production staff. The production process has been upgraded to reduce the internal dose contribution. The routine measurement of workers using unsealed sources continues.

A personal computer with MCA emulation software has now been purchased and installed, and the WBC seems to work very well. The personal computer is an IBM compatible system with a Pentium processor. The data acquisition software was purchased from EG&G ORTEC from Oak Ridge, USA. The signals from the detector were fed into the MCA and displayed on the PC monitor. Manipulation of the spectrum and data processing is performed partially manually.

UNITED STATES OF AMERICA

D.P. Hickman
Lawrence Livermore National Laboratory
Livermore, California, United States of America

Introduction

The in vivo measurement facility at Lawrence Livermore National Laboratory (LLNL) provides services for the in vivo analysis of radioactivity in the whole body and specific organs. These tasks are performed as part of the overall Health and Safety Programme for LLNL employees. The Whole Body Counter services are in support of the Health Physics programme conducted by the LLNL Hazards Control Department. The in vivo measurement facility specializes in the application of improved instrumentation and/or analysis techniques and by participation in national and international intercomparison programmes and standards committees.

LLNL performs several types of in vivo measurements, including, whole body counting, in vivo organ counts such as lung, liver, and bone, thyroid measurement, and wound counting. LLNL also has an established mechanism for measuring non-LLNL personnel on an as-needed basis.

LLNL Whole Body Counting Facility

The WBC facility at LLNL consists of a shielded counting room [1]. This room is located underground approximately 20 feet and is surrounded by approximately 5 feet of low background serpentine rock fill. A cinderblock barrier and a thin steel retaining wall retain the fill. A graded lining of 0.125 inch lead, 0.020 inch cadmium, and 0.030 inch copper is located on the walls, ceiling, and floor. The graded lining is sealed with ethyl methacrylate spray and vinyl fabric wallpaper. In addition, a ventilation system consisting of two HEPA filters in series controls possible airborne radioactivity problems. The shielded facility reduces the background by a factor of 50 to 100 depending on the energy of the radiation. In order to maintain constant contact with those individuals in the shielded room, a communications system, consisting of a voice intercom system and a live video system, exists.

Whole body in-vivo measurements are performed in the underground counting room with the High Purity Germanium (HPGe) Scanning Bed System. This system consists of four 75% efficient P-type high purity germanium detectors in a 30 liter dewar (Figures 1and 2). Normally, the subject undergoing measurement is traversed over the detector system while supine on a moving bed. This system is used to determine whether detectable quantities of high-energy gamma-emitting radionuclides (such as ^{137}Cs and ^{60}Co) are present anywhere in the body. The detection level for this system is approximately 1 nCi for radionuclides with energies above 200 keV. In-vivo organ measurements focus on activity deposited in specific organs such as lungs and the respiratory system. The low-energy photons of radiation emitted from the organs are measured either by an array of six 1800 mm^2 low energy planar germanium detectors (LEGe) (Figure 3) or by two 15.2 cm square phoswich detectors. These detectors are placed over the subject's chest while he/she is laying down, usually at a 45° angle. The activity detected in the lung is affected by the chest wall thickness of the subject and any activity that may be emitted from the ribs and/or liver. To obtain an accurate measurement of activity, a chest wall thickness measurement (using ultrasound) or calculation is performed. To determine activity present in the bone, a head (skull) count is taken to measure skeletal activity. Liver activity is determined by a liver count. From these combined measurements and the lung count, a matrix computation method is performed to determine the activity and cross-over activity attributed to each of these organs.

Note: Detectors 5&6 and Detectors 2&3 are two fixed assemblies

Ge
Teflon
Copper
Vacuum
Stainless Steel Type 304

FIG. 1a. LLNL LEGe detector array.
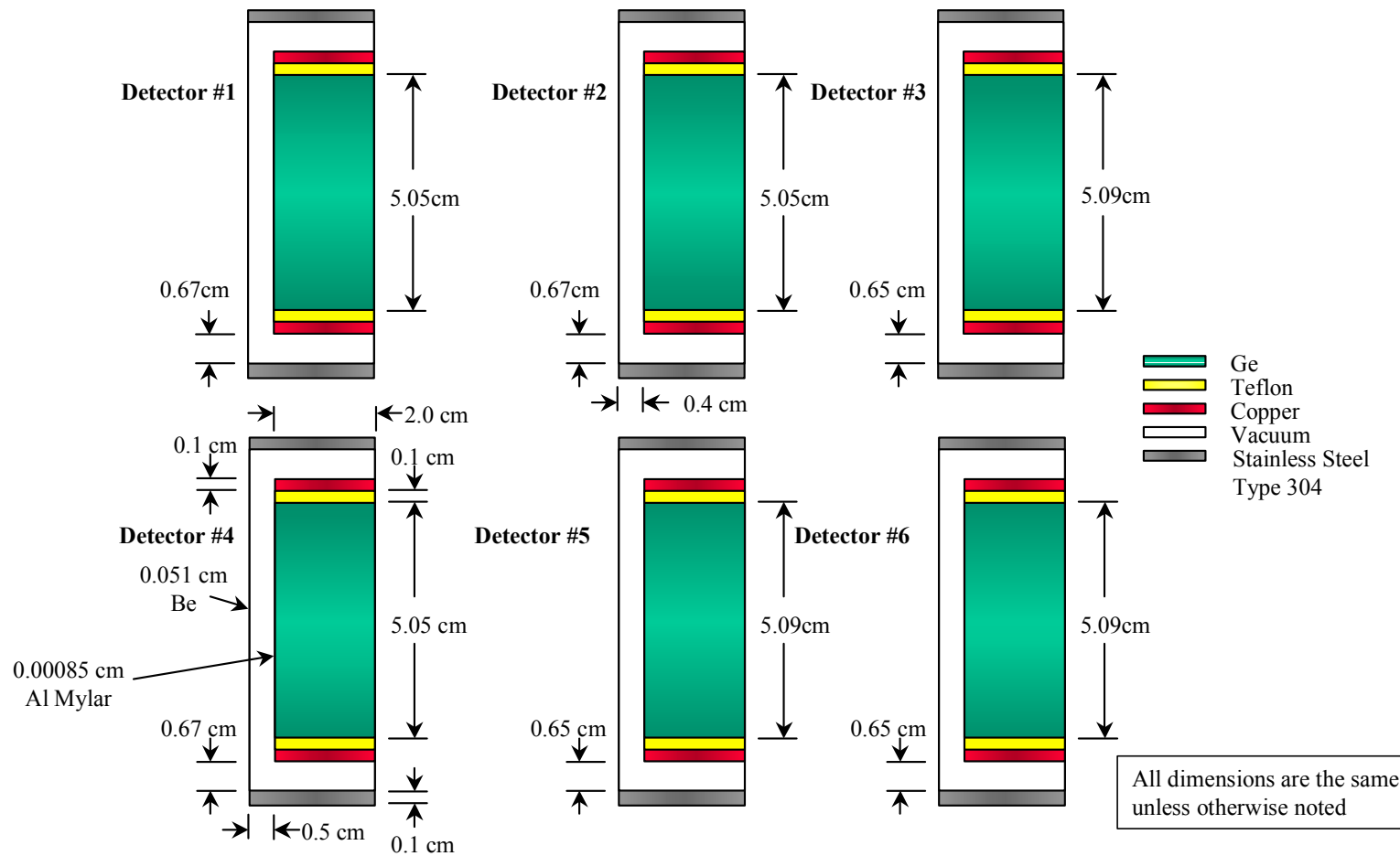
FIG. 1b. LLNL LEGe detector dimensions

FIG. 2. LLNL scanning bed whole body counter.
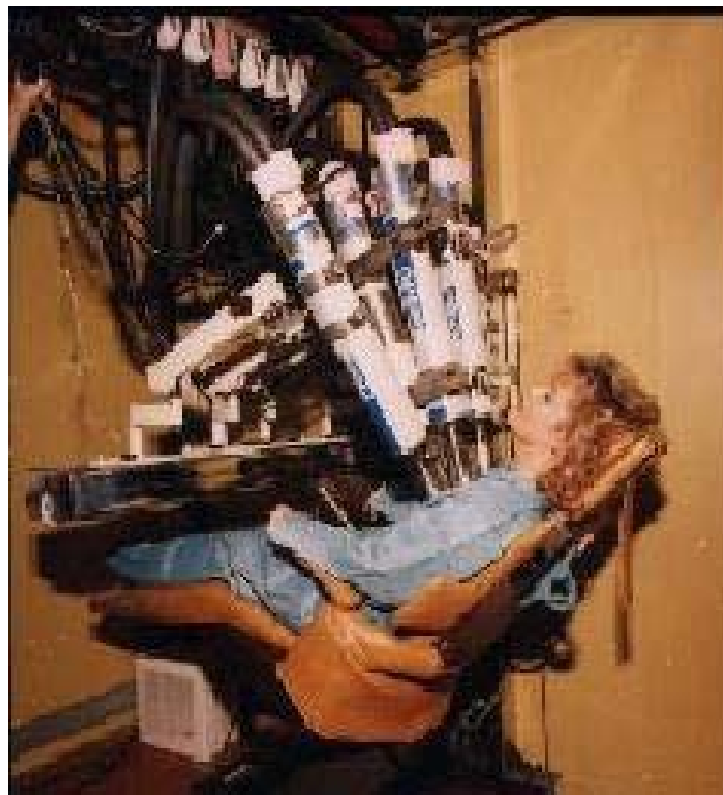
FIG. 3. LLNL organ counting system.

LLNL participates and assists in several intercomparison and the DOE Intercalibration Committee. By the end of year 2001, LLNL will be accredited by the Department of Energy for in vivo bioassay measurements in accordance with ANSI 13.30, Performance Criteria for Radiobioassay.

LLNL Phantom Library

Lawrence Livermore National Laboratory maintains a vast library of calibration organs and phantoms, many of which have historical significance in the establishment of phantoms that are currently world standards in calibration of in vivo measurement systems. Some of these organs and phantoms can be made available for loan to organizations and companies. These loans are subject to Laboratory and DOE monitoring requirements and are established for specified time periods.

The most utilized LLNL phantom is the LLNL realistic torso phantom, which is used to calibrate detectors for the measurement of photon emitting radionuclides that are internally deposited in organs contained within the human torso. The design criteria was established by the DOE (formally the Energy Research and Development Agency — ERDA) Intercalibration Committee for Low Energy Photon Measurements. The developmental approach of the committee was to model the phantom using a human cadaver that was consistent with anthropometric measurements of DOE workers augmented by reference man data.

The phantom is constructed of artificial tissue and bone equivalent material and contains a rib cage, removable organs, and chest plates with varying ratios of muscle and fat equivalent material to simulate a wide range of chest wall thickness. The tissue-equivalent torso phantom is specifically constructed for the calibration of counting systems used to measure transuranic nuclides in the lung, liver, and pulmonary lymph nodes. It is, however, also useful for high-energy gamma emitting radionuclides in the lung and liver. The lung, liver and lymph node sets used for calibration contain specified quantities and/or mixtures of homogeneously distributed radionuclides. There are several publications describing the development, construction, and verification of the LLNL torso phantom.

LLNL has also developed the seamless BOttle Manikin ABsorption (BOMAB) Phantom, which is used to calibrate whole body counters. The seamless BOMAB consists of ten bottles and is composed of polyethylene plastic and constructed without seams in any of the ten bottles. The 10 bottles are containers of varying sizes, which when appropriately assembled, are roughly equal to the size, weight, and shape of Reference Man (ICRP 1995). The containers can be filled with solution or materials of known density and quantities of radionuclides for calibration purposes. The volumes of the manufactured version simulate a 70 kg person with an overall tolerance of 10%. Each bottle has a recessed screw-type fill port.

REFERENCE

[1]   Griffith, R.V., Anderson, A.L., Lindeken, C.E., Construction of a Unique Underground Whole Body Counter, Lawrence Radiation Laboratory Report UCRL-72739 (1970).

PARTICIPANTS IN THE CO-ORDINATED RESEARCH PROJECT

P. Burns
Australian Radiation Laboratory,
Lower Plenty Road, Yallambie, Victoria 3085, Australia
Tel: +61 3 9433 2211
Fax: +61 3 9432 1835
Email: Peter.Burns@health.gov.au

T.K. Haridasan
Environmental Assessment Division, Internal Dosimetry Section,
Low Level Counting Laboratory, BARC Hospital,
Anushakti Nagar, Mumbai 400 094, India
Fax: +91 22 550 5151

D.P. Hickman
Special Projects Division, Hazards Control Department, LLNL,
P.O. Box 5505, L-379, Livermore, CA 94551,
United States of America
Tel: +1 510 422 8958
Fax: +1 510 422 5176
Email: dhickman@llnl.gov

R. Hochmann
International Atomic Energy Agency, IAEA Seibersdorf Laboratories,
A-2444 Seibersdorf, Austria
Tel: +43 1 2600 28504
Fax: +43 1 2600 2891
Email: R.Hochmann@iaea.org

Zunsu Hu
China Institute for Radiation Protection,
PO Box 120, Taiyuan 030006, Shanxi, China
Tel: +86 351 702 0266, Ext. 2232
Fax: +86 351 702 0407
Email: huzunsu@mh.ty.col.com.cn

N. Ishigure
Dosimetry of Internal Exposure Section, Division of Radiotoxicology
   and Protection, National Institute of Radiological Sciences,
9-1, Anagawa-4, Inageku, Chiba 263, Japan
Tel: +81 43 206 3097
Fax: +81 43 284 1389
Email: ishigure@nirs.go.jp

G.H. Kramer
Radiation Protection Bureau,
775 Brookfield Road, PL6302D1, Ottawa, Ontario K1A 1C1, Canada
Tel: +1 613 954 6668
Fax: +1 613 957 1089
Email: Gary_H_Kramer@hc-sc.gc.ca

How Mooi Lau
Malaysian Institute for Nuclear Technology Research (MINT),
Bangi, 43000 Kajang, Malaysia
Tel: +60 3 825 0510
Fax: +60 3 825 2588
Email: lau@mint.gov.my

Tae Young Lee   Korea Atomic Energy Research Institute,
P.O. Box 105, Yusong, Taejeon, 305-600, Republic of Korea
Tel: +82 42 868 8139
Fax: +82 42 868 8609
Email: tylee1@nanum.kaeri.re.kr

Abdus Sattar Mollah   Institute of Nuclear Science and Technology (INST),
Atomic Energy Research Establishment (AERE),
Ganakbari, Savar, GPO Box 3787, Dhaka-1000, Bangladesh
Tel: +880 2 419 1230
Fax: +880 2 863 051
Email: mollahas@hotmail.com

R.C. Sharma   Internal Dosimetry Section, Health Physics Division,
Bhabha Atomic Research Center (BARC), Trombay, Bombay 400 085,
India
Tel: +91 22 556 3060, Ext. 2265 and +91 22 551 2936
Fax: +91 22 556 0750

H. Spitz   Department of Mechanical, Industrial and Nuclear Engineering,
Center for Radiological Assessment, University of Cincinnati,
PO Box 210072,
Cincinnati, OH 45221-0072, United States of America
Tel: +1 513 556 2003
Fax: +1 513 556 3390
Email: Henry.Spitz@uc.edu

R.E. Toohey   Radiation Internal Dose Information Center,
Oak Ridge Associated Universities,
P.O. Box 117, Oak Ridge, TN 37831-0117, United States of America
Tel: +1 423 576 3448
Fax: +1 423 576 8673
Email: TooheyR@ORAU.GO